# Electrochemical Treatment of Problematic Water Recycle Waste Streams

Jelena Radjenovic[1], Arseto Bagastyo[1], Korneel Rabaey[1,2], Damien Batstone[1], Wolfgang Gernjak[1], Yang Mu[1], Rene A. Rozendal[1], Beate Escher[3], Yvan Poussade[4] and Jürg Keller[1]

September 2012

*A collaboration between the Urban Water Security Research Alliance, Veolia Water Australia, Seqwater, Queensland Health Forensic and Scientific Services and Magneto Special Anodes (Netherlands)*

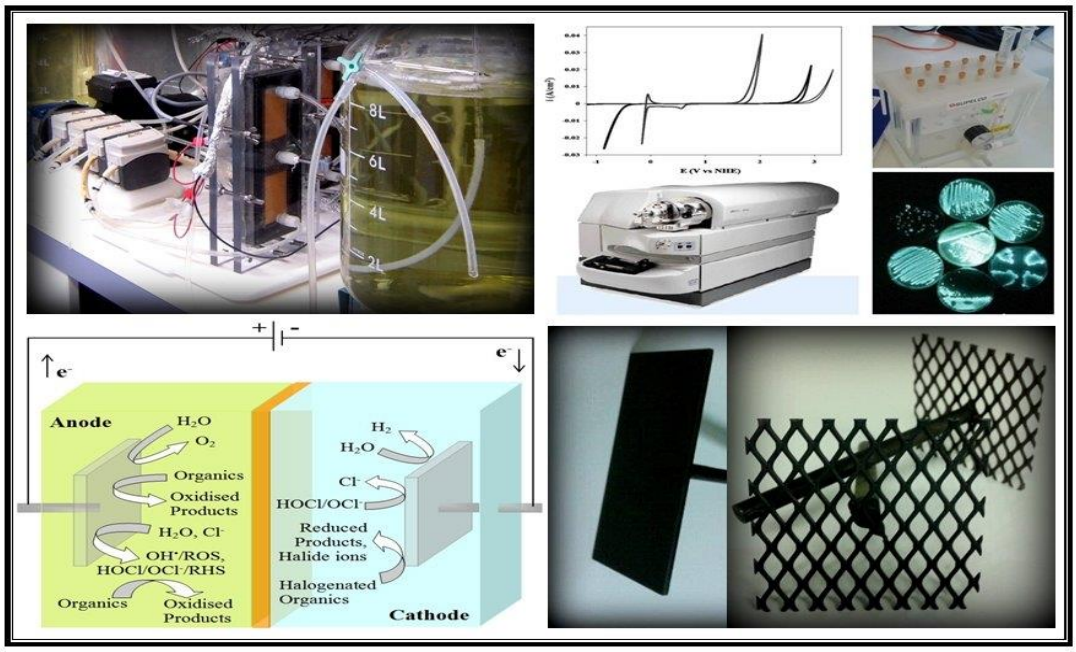


## Urban Water Security Research Alliance Technical Report No. 82

Urban Water Security Research Alliance

Urban Water Security Research Alliance Technical Report ISSN 1836-5566 (Online)
Urban Water Security Research Alliance Technical Report ISSN 1836-5558 (Print)

The UWSRA is a $50 million partnership over five years between the Queensland Government, CSIRO's Water for a Healthy Country Flagship, Griffith University and The University of Queensland. The Alliance has been formed to address South East Queensland's emerging urban water issues with a focus on water security and recycling. The program will bring new research capacity to South East Queensland tailored to tackling existing and anticipated future issues to inform the implementation of the Water Strategy.

This report has been produced by The University of Queensland for the Urban Water Security Research Alliance in collaboration with Veolia Water Australia, Seqwater, Queensland Health Forensic and Scientific Services and Magneto Special Anodes (Netherlands).

For more information about the:

UWSRA - visit http://www.urbanwateralliance.org.au/
Queensland Government - visit http://www.qld.gov.au/
CSIRO, Water for a Healthy Country Flagship - visit www.csiro.au/org/HealthyCountry.html
The University of Queensland - visit http://www.uq.edu.au/
Griffith University - visit http://www.griffith.edu.au/
Veolia Water - visit http://www.veoliawater.com.au
Seqwater - visit http://www.seqwater.com.au/
Magneto Special Anodes – visit: http://www.magneto.nl/
Queensland Health Forensic and Scientific Services – visit: http://www.health.qld.gov.au/
The Advanced Water Management Centre - visit http://www.awmc.uq.edu.au/
National Research Centre for Environmental Toxicology - visit http://www.entox.uq.edu.au/

Enquiries should be addressed to:

The Urban Water Security Research Alliance
PO Box 15087
CITY EAST QLD 4002

Ph: 07-3247 3005
Email: Sharon.Wakem@qwc.qld.gov.au

Project Leader – Jelena Radjenovic
The University of Queensland
ST LUCIA QLD 4072

Ph: 07-3346 3234
Email: j.radjenovic@awmc.uq.edu.au

Authors:
1 The University of Queensland, Advanced Water Management Centre (AWMC), QLD 4072, Australia.
2 Laboratory for Microbial Ecology and Technology (LabMET), Ghent University, Coupure Links 653, B-9000 Ghent, Belgium.
3 The University of Queensland, National Research Centre for Environmental Toxicology (EnTox), QLD 4108, Australia.
4 Veolia Water Australia, PO Box 10819, Adelaide St Post Office, Brisbane QLD 4000, Australia.

Radjenovic, J., Bagastyo, A., Rabaey, K., Batstone, D., Gernjak, W., Mu, Y., Rozendal, R.A., Escher, B., Poussade, Y. and Keller, J. (2012). *Electrochemical Treatment of Problematic Water Recycle Waste Streams*. Urban Water Security Research Alliance Technical Report No. 82.

## Copyright



## Disclaimer



## Cover Photograph:

Description: Electrochemical set-ups, techniques and instrumentation used in the project: electrolytic cell; cyclic voltammetry techniques; liquid chromatography-mass spectrometry instrumentation; solid phase extraction; *Vibrio fischeri* bioassays; scheme of electrochemical process; plate and mesh electrodes employed.

# ACKNOWLEDGEMENTS

The Urban Water Security Research Alliance is a scientific collaboration between the Queensland Government, CSIRO, The University of Queensland and Griffith University.

This research was undertaken by The University of Queensland in a collaboration between the Urban Water Security Research Alliance, Veolia Water Australia, Seqwater, Magneto Special Anodes (Netherlands) and Queensland Health Forensic and Scientific Services. The authors want to acknowledge the funding provided for this project through the Australian Research Council (ARC) Linkage Scheme, with the cash contributions from the partner organisations, and the in-kind contributions provided by the partners and Queensland Health Forensic and Scientific Services.

The authors also want to acknowledge the technical staff from Veolia Water Australia, Bundamba Advanced Water Treatment Plant (AWTP), and Magneto Special Anodes for their assistance.

Also, particular thanks go to Hanne Thoen and Miroslava Macova from National Research Centre for Environmental Toxicology, The University of Queensland, for performing the bioassays. The authors would like to thank to Benjamin Tan, Mary Hodge and Henry Olszowy from Queensland Health Forensic and Scientific Service (QHFSS) for performing the chemical analyses of oxidation by-products. Also, big thanks go to Pieter Hack and other staff from Magneto Special Anodes for providing the electrode materials and taking time to answer all our queries. We would also like to acknowledge Cedric Robillot from Seqwater, Dipl Ing and Yvan Poussade from Veolia Water Australia for their support to the project. Finally, the authors also thank Beatrice Keller-Lehmann and other staff at the Advanced Water Management Centre (AWMC) for their support.

# FOREWORD BY THE URBAN WATER SECURITY RESEARCH ALLIANCE

Water is fundamental to our quality of life, to economic growth and to the environment. With its booming economy and growing population, Australia's South East Queensland (SEQ) region faces increasing pressure on its water resources. These pressures are compounded by the impact of climate variability and accelerating climate change.

The Urban Water Security Research Alliance, through targeted, multidisciplinary research initiatives, has been formed to address the region's emerging urban water issues.

As the largest regionally focused urban water research program in Australia, the Alliance is focused on water security and recycling, but will align research where appropriate with other water research programs such as those of other SEQ water agencies, CSIRO's Water for a Healthy Country National Research Flagship, Water Quality Research Australia, eWater CRC and the Water Services Association of Australia (WSAA).

The Alliance is a partnership between the Queensland Government, CSIRO's Water for a Healthy Country National Research Flagship, The University of Queensland and Griffith University. It brings new research capacity to SEQ, tailored to tackling existing and anticipated future risks, assumptions and uncertainties facing water supply strategy. It is a $50 million partnership over five years.

Alliance research is examining fundamental issues necessary to deliver the region's water needs, including:

- ensuring the reliability and safety of recycled water systems.
- advising on infrastructure and technology for the recycling of wastewater and stormwater.
- building scientific knowledge into the management of health and safety risks in the water supply system.
- increasing community confidence in the future of water supply.

This report is part of a series summarising the output from the Urban Water Security Research Alliance. All reports and additional information about the Alliance can be found at http://www.urbanwateralliance.org.au/about.html.

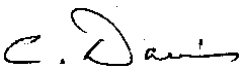

**Chris Davis**
Chair, Urban Water Security Research Alliance

# FOREWORD BY SEQWATER, VEOLIA WATER AUSTRALIA, MAGNETO SPECIAL ANODES AND QUEENSLAND HEALTH FORENSIC AND SCIENTIFIC SERVICES

The Western Corridor Recycled Water Scheme and the Gold Coast Desalination Plant are two major assets forming part of the South East Queensland (SEQ) Water Grid. These assets are owned by the Queensland Bulk Water Supply Authority, trading as Seqwater, with their operation and maintenance undertaken by Veolia Water Australia under a long term service agreement. They are designed to provide drought resilient high quality water for this fast growing area in years and decades to come.

This infrastructure relies on world class innovations and technologies and both Seqwater and Veolia Water Australia are committed to ensuring the Western Corridor Recycled Water Scheme and the Gold Coast Desalination Plant remain at the leading edge of the water purification industry. Seqwater, Veolia Water Australia and The University of Queensland have entered into a research collaboration in January 2008 in order to embrace the pace of change in technology and maintain the efficiency, reliability and sustainability of these assets.

Water quality management and monitoring are key elements of the strategy underpinning this collaboration, aiming at driving scientific research to inform decision making processes with regards to new potential contaminants in indirect potable reuse and desalination applications. In 2009, this partnership supported The University of Queensland (UQ) in obtaining a grant for the project *"Electrochemical treatment of problematic water recycle waste streams"* (LP0989159), under the Australian Research Council (ARC) Linkage Scheme. This report presents some significant outputs from this research supported by the cash contributions from the ARC and partner organisations - Veolia Water Australia, Magneto Special Anodes, Seqwater, and the Urban Water Security Research Alliance. In-kind contributions to the project were provided by the Veolia Water Australia, Magneto Special Anodes, Seqwater, and Queensland Health Forensic and Scientific Services.

# CONTENTS

# LIST OF FIGURES

# LIST OF TABLES

# EXECUTIVE SUMMARY

Urban water supply is one of the major challenges in Australia in the decades to come. To meet the growing demand for water, multi-billion dollar schemes have recently been set in motion to augment the water supply by a combination of: *i)* expansive reuse, particularly in South East Queensland (SEQ); and *ii)* sourcing of climate independent "new" water, e.g. from desalination. Desalination is still an expensive and energy–intensive option, and there is an increasing awareness of water recycling potential as an additional source of water.

As described in the South East Queensland Water Strategy (2008), regional growth and development need to be managed in a sustainable way, ensuring a reliable supply of water of acceptable quality, and for long term usage. Several projects were designed to achieve the goals of this strategy, the most important being the production of Purified Recycled Water (PRW) through the Western Corridor Recycled Water Project (WCRWP). To produce PRW, a multi–barrier process is used which includes: 1) source control; 2) wastewater treatment plants (WWTPs); 3) micro- or ultra-filtration (MF/UF); 4) reverse osmosis (RO); 5) advanced oxidation processes (AOPs); 6) blending in the natural environment; and 7) the water treatment plant (WTP) (www.qwc.qld.gov.au). Barriers 3), 4) and 5) are provided by the three Advanced Water Treatment Plants (AWTPs) at Luggage Point, Gibson Island and Bundamba. PRW will be added to Wivenhoe Dam when the combined levels of the major dams falls below 40%, becoming part of the drinking water supply through the SEQ Water Grid.

In the three AWTPs, RO treatment is the central unit operation, which produces the largest by–product stream, reverse osmosis concentrate (ROC). ROC generated in water recycling typically represents 15–20% of the feed stream. Due to the high concentrations of nutrients, metals and recalcitrant pollutants originating from the treated sewage effluent, disposal of these streams represents a major problem as they require on-site treatment. Pharmaceuticals, endocrine disruptors, recalcitrant nitrogen compounds and other anthropogenic contaminants pass to variable extents through tertiary wastewater treatment plants [1, 2]. In spite of the variable removals observed during conventional WWTP processes, many of these chemicals are routinely observed in secondary treated effluents at ng $L^{-1}$ concentration levels, and can be expected in ROC streams at even higher concentrations. Thus, ROC represents both a potential hazard and a unique opportunity to remove the risk associated with the discharge of these contaminants into the environment.

In the past 5-10 years, several options have been investigated for the treatment of ROC, such as coagulation, activated carbon, ozonation and AOPs [3-5]. Nevertheless, these strategies are considered energy intensive and imply expensive investments, since they generally require a large amount of chemicals and produce solid/liquid wastes (e.g. chemical sludge). The Australian Research Council (ARC) granted funding in 2009 to the Advanced Water Management Centre (AWMC), at The University of Queensland (UQ), for the ARC Linkage project *"Electrochemical treatment of problematic water recycle waste streams"*. The project was co-funded by Veolia Water Australia, the Urban Water Security Research Alliance (UWSRA), Seqwater, Magneto Special Anodes (Netherlands) and Queensland Health Forensic and Scientific Service (QHFSS). The project was focused on the development of electrochemical process for the treatment of ROC.

The unique ability of electrochemical processes to oxidise and reduce organic compounds at controlled electrode potentials, and using only electrons, as reagents represents a great advantage over AOPs and other technologies traditionally applied in (waste)water treatment; which are based on the use of chemicals. Electrochemical systems are chemical-free, environmentally compatible, versatile, robust and easily adapted to various types of treatment applications [6]. Electrochemical reduction was suggested in the 1970s as a promising method for the dehalogenation of chlorinated pesticides under mild experimental conditions, without using the highly reactive reducing agents [7]. It enables selective dehalogenation through controlled potential and selection of cathode material, without the need for waste disposal. Electrochemical oxidation has gained interest in recent years due to the

generation of a variety of oxidant species (e.g. $OH^{\bullet}$, $O_3$, $H_2O_2$) at the anode by the electrolysis of water. Another advantage of applying electrochemical process for the treatment of ROC was low energy investment, owing to its high conductivity.

In the first year of the project, several titanium-based electrode materials purchased from Magneto Special Anodes were tested for electrochemical oxidation of ROC. Since their oxidising power is determined by the type of mixed metal oxide (MMO) coating, five different anodes were investigated: Ti/$IrO_2$-$Ta_2O_5$, Ti/$RuO_2$-$IrO_2$, Ti/Pt-$IrO_2$, Ti/$PbO_2$ and Ti/$SnO_2$-Sb. The results showed excellent performance of nearly all materials in terms of chemical oxygen demand (COD) and colour removal (complete removal observed for 2-2.5 kWh $m^{-3}$ of energy consumption), with Ti/Pt-$IrO_2$ and Ti/$SnO_2$-Sb electrodes being the most efficient ones. However, this performance seemed to be linked to the production of active chlorine at the anode, and electro-chlorination of the organic matter, since the highest residual chlorine and formation of hazardous trihalomethanes (THMs) and haloacetic acids (HAAs) were observed precisely at Ti/Pt-$IrO_2$ and Ti/$SnO_2$-Sb anodes.

In our next study, we investigated the removal of trace organic contaminants in electrochemical oxidation of ROC using a Ti/$RuO_2$-$IrO_2$ anode. 28 target organic contaminants (pharmaceuticals and pesticides) were selected, based on their frequent occurrence in treated sewage effluents and diverse physico-chemical properties. Complete removal of nearly all contaminants was noted at higher current densities (i.e. $\geq$ 150 A $m^{-2}$), with triclopyr being the most persistent pollutant. Besides the current applied, removal efficiency seemed to depend on the accumulation of oxidants in the bulk liquid of the external reservoir. The results of the Microtox bioluminescence bioassay support the hypothesis that the main oxidant species was likely to be active chlorine, since the toxicity was drastically increased.

The Ti/$RuO_2$-$IrO_2$ anode has excellent chemical and mechanical stability, as well as electrocatalytic activity. It is classified as an anode of lower oxidising power, and the literature indicated an enhancement of the oxidising capabilities in the presence of chloride ions ($Cl^-$) [8, 9]. However, the results obtained in this project indicated that the electro-chlorination mechanisms led to a substantial increase in toxicity of the treated stream.

In our next study, we investigated and compared the mechanisms of electrochemical oxidation of a model contaminant using Ti/$RuO_2$-$IrO_2$ and a high oxidising power anode, Ti/$SnO_2$-Sb. The latter one is considered as the only MMO anode capable of generating quasi-free hydroxyl radicals ($OH^{\bullet}$). The results of the extensive analysis based on the use of advanced liquid chromatography-mass spectrometry (LC-MS) methods indicated that, irrespective of the MMO electrode coating, the target compound was transformed into (poly)chlorinated derivatives. Besides active chlorine, active bromine (Br) was found to play a significant role in the indirect oxidation of the organics. Although $Br^-$ ions are present in a ~1000 times lower concentration than the $Cl^-$ in the ROC, hypobromic acid (HOBr) generated by the oxidation of $Br^-$ to $Br_2$ at the anode and dissolution of $Br_2$ yielded several bromine-containing by-products. Although the degradation rates observed for the identified by-products were higher at the Ti/$SnO_2$-Sb anode, bioluminescence inhibition test with *Vibrio fischeri* and the combined algae test with *Pseudokirchneriella subcapitata* indicated a substantial increase in non-specific toxicity of the reaction mixture due to the formed halogenated by-products. In order to reduce the toxicity of the oxidised ROC, electrochemical reduction was studied as a post-treatment option. While the carbon-based cathode used seemed to efficiently adsorb the halogenated organic matter, it did not show satisfactory dehalogenation performance.

Boron-doped diamond (BDD) anodes are the latest technological leap in the area of technical electrode materials. They are considered to be capable of generating quasi-free $OH^{\bullet}$ of a similar oxidising potential to aqueous $OH^{\bullet}$ [10]. The high cost of the substrate onto which the BDD film is deposited (e.g. Nb, W, Ta) represents a major impediment to their large-scale application. Nevertheless, considering the poor performance observed for MMO electrodes in electrochemical oxidation of ROC, the next stage of the project was focused on investigation of the performance of BDD anodes for the oxidative electrochemical treatment of ROC. The results obtained indicated an outstanding performance of BDD in terms of COD and dissolved organic carbon (DOC) removal compared to

MMO electrodes. Furthermore, the formed THMs and HAAs seemed to be degraded by prolonged oxidation time. However, the analysis of adsorbable organic halogen (AOX) showed continuous formation of chlorinated and brominated organics, with the latter ones being formed to a much lesser extent due to a low initial $Br^-$ ions concentration. Moreover, considering the high energy required in the process (i.e. 104 kWh $m^{-3}$), it can be concluded that the formed polychlorinated and chloro-bromo derivatives might require impractical reactor residence times to be further degraded, even in the case of a BDD electrode.

In the last stage of the project, a novel strategy was investigated based on the use of electrodialysis to decrease the initial concentration of $Cl^-$ ions, and posterior electrochemical oxidation of this treated ROC stream. The performance of MMO electrodes was found to be worse in the absence of high Cl- ions concentration, implying that the oxidation at these electrodes was mainly relying on the generation of active chlorine. On the other hand, BDD was capable of efficiently removing COD and DOC, suggesting its capacity of $OH^{\bullet}$ production. Moreover, addition of sulphate ions seemed to enhance further its oxidising power, due to the generation of persulfate ion and, more importantly, sulphate radicals. At the same time, the formation of THMs and HAAs was minimised to concentrations below 1 μM.

In summary, electrochemical oxidation alone does not seem to be an adequate option for removing trace organic contaminants from the ROC stream, as high $Cl^-$ ion concentration leads to intense electro-chlorination of the organic matter, even in the case of highly oxidising BDD electrodes. It is likely that the $Cl^-$ ion concentration needs to be reduced prior to the oxidative treatment, in order to avoid the generation of chlorinated by-products. Electrodialysis of ROC may be an option to achieve this goal. However, further research is needed to explore the performance of different reactor configurations and lower the energy demand of a combined electrodialysis and electrochemical oxidation process.

# 1. INTRODUCTION: MANAGEMENT OF REVERSE OSMOSIS CONCENTRATE IN SOUTH EAST QUEENSLAND

The WCRWP is the largest advanced water treatment project in Australia, with the capacity to recycle 232 ML/d of water for industrial use, indirect potable use, and possibly irrigation [11]. Located in SEQ, WCRWP was completed in 2008 in response to a severe drought affecting the region in the period 2001-2008. The scheme consists of three AWTP - Bundamba, Luggage Point and Gibson Island. The three AWTPs employ pre-treatment (i.e. ferric chloride dosing, coagulation, clarifier solids separation), UF/MF, RO filtration, AOP, and chlorination to produce purified recycled water from secondary treated wastewater, sourced from six wastewater treatment plants [12].

The main barrier to a range of organic and inorganic contaminants present in the secondary treated wastewater effluents RO membrane filtration. RO is a physical separation process in which externally pressurised feed water flows through the membrane producing: *(i)* a clean stream (permeate) which represents water of very low mineral content that passes through the membrane; and *(ii)* a waste stream (concentrate or brine) that contains the rejected contaminants. Thus, using membrane filtration the pollutants are effectively transferred from the water supply to a lower volume waste stream. However, no pollutant destruction is achieved and the rejected contaminants may be concentrated up to 7 times in the ROC stream. Considering the elevated concentrations of nutrients, metals and pollutants of anthropogenic origin (e.g. pharmaceuticals, endocrine disruptors, personal care products and pesticides), direct discharge of brine may have negative impacts on the environment. Additional challenge to ROC disposal is posed by its high salinity, which may affect the ecosystems in the receiving water bodies [13].

The WCRW scheme produces in total 41 ML/d of brine at full capacity, divided between the three AWTPs [14]. The treatment of brine stream is currently implemented only at the AWTP Bundamba, and it consists of: *(i)* moving bed biofilm reactor (MBBR) nitrification process for ammonia conversion to nitrate; *(ii)* solids contact clarifiers; and *(iii)* denitrification filters for nitrate and solids reduction. The Bundamba ROC treatment train achieves around 35% of nitrogen reduction [14]. At present, no nitrogen reduction processes have been implemented for the Luggage Point and Gibson Island AWTPs. In the case of Gibson Island AWTP, this is due to feed nitrogen levels being lower than the Healthy Waterways target (1.8 mgN/L in the feed water vs 3 mgN/L target). For Luggage Point AWTP, uncertainty existed with the long-term total nitrogen levels in the treated wastewater feed, as the WWTP was undergoing nitrogen reduction optimisation in parallel with the Western Corridor project delivery phase.

The ROC waste streams generated at AWTPs Bundamba, Luggage Point and Gibson Island are discharged to nearby waterways and, ultimately, Moreton Bay. Although the characteristics of brine streams comply with the existing regulations of the Healthy Waterways Strategy for nutrient, and chlorine and ammonia limits [15], the release of contaminants such as pharmaceuticals, pesticides and others represents a matter of concern. Considering that these pollutants are derived from the secondary wastewater effluent and thus exert low biodegradability, their removal by the employed nitrification/denitrification treatment of ROC in AWTP Bundamba is unlikely. The E-screen ROC conducted on the ROC stream from AWTP Bundamba showed appreciable estrogenic activity [16].

The ROC offers an opportunity for reducing human and ecotoxicological risk by implementing on-site brine treatment prior to environmental discharge. Several treatment options were investigated in order to reduce the pollutant load in ROCs produced during water recycling: coagulation and activated carbon adsorption [3], UV/$H_2O_2$ [17], $TiO_2$ photocatalysis [3], ozonation and Fenton oxidation [18]. However, high cost of these technologies related to the use of chemicals may limit their application [19]. In recent years, there has been an increasing interest in applying electrochemical oxidation for the treatment of refractory and highly saline waste streams such as ROC [3, 20, 21]. The unique ability of electrochemical processes to oxidise and/or reduce organic compounds at controlled electrode potentials and using only electrons as reagents represents a great advantage over existing AOPs.

The ARC linkage project "*Electrochemical treatment of problematic water recycle waste streams"* (LP0989159, 2009-2012), co-funded by the UWSRA, Veolia Water Australia, Seqwater, and Magneto Special Anodes, and with Queensland Health Forensic and Scientific Services (QHFSS) as a partner organisation, aimed at investigating the performance of electrochemical oxidation and reduction for the treatment of ROC. The main project objectives were: *(i)* evaluate the oxidising power of different electrode materials applied in electrochemical oxidation of ROC; *(ii)* determine the toxicity of the treated ROC and the formation of oxidation by-products of concern (e.g. halogenated organics); *(iii)* investigate the performance of electrochemical reduction treatment for the removal of halogenated by-products; and *(iv)* develop treatment strategies to avoid the formation of oxidation by-products of increased toxicity.

# 2. LITERATURE REVIEW

## 2.1. Characteristics of Reverse Osmosis Concentrate from Wastewater Reclamation Plants

RO membrane filtration is recognised as an important barrier for a wide range of inorganic and organic contaminants. It is capable of achieving an outstanding quality of the product water, thus being a widespread technology in municipal wastewater reclamation. However, one of the major challenges of the RO treatment is sustainable and environmentally acceptable management of brine stream. The volume and composition of ROC stream depends on the membrane operation system, the feed water matrix and the quality of the product water [22-24]. Membrane percent recovery is defined as the flow rate of permeate yielded for every flow rate of the incoming feed during membrane separation. The lower salt concentrations of secondary wastewater effluents likely allow much greater membrane recovery, typically 75-85% for RO [25, 26]. Therefore, ROC generated from treated municipal effluents normally represents about 15-25% of the feed water flow, and may consist of a combination of concentrates produced in a multiple-stage membrane process, such as UF or nanofiltration (NF) as pre-treatment. This stream may also include small amount of any rejected chemicals which have been added for pre-treatment or maintenance/cleaning purposes, such as the coagulants/flocculants and chloramines which are used prior to the RO process to remove organic and inorganic foulants and/or for biofouling control, and the anti-scalant added for preventing the precipitation on the membrane [27-29]. Due to the high salt rejection at RO membrane, ROC typically has high salinity, i.e. total dissolved solids (TDS) content.

In addition, ROC from reclamation plants treating municipal wastewater is characterised by the elevated concentration of nutrients, recalcitrant chemical oxygen demand (COD) and low biodegradability. Bagastyo *et al.* [30] have determined that approximately half of the organics contributing to the measured COD in the ROC samples from AWTP Bundamba and AWTP Luggage Point was a fraction with molecular weight (MW) < 1 kDa. Since RO membranes have excellent performance in removing trace organic contaminants such as pharmaceuticals, endocrine disruptors and pesticides from the feed stream [31-33], they will be concentrated up to 7 times in the ROC [25, 34], along with other wastewater effluent residuals (e.g. metals, microbial products). Depending on the wastewater source, the organic pollutants in the ROC may be bioaccumulative and/or toxic [35]. However, it should be noted that some constituents may have lower concentration factor or even higher, depending on chemical characteristics of compounds and membrane properties, thus causing a variability in the ROC characteristics. Seasonal variations could also affect the nature of the ROC stream. Nevertheless, ROC is likely to exhibit an increased toxicity compared to the feed stream. In a recent study by Escher *et al.* [36], RO feed and concentrate stream from AWTP Bundamba were characterised by a test battery of six bioassays. While toxicity to Vibrio fischeri was increased for 36% relative to the toxicity of the RO feed stream, E-screen test, photosynthesis inhibition test and algal 24 h growth rate bioassay showed an increase of 424%, 457% and 487%, respectively.

## 2.2. Review of the Reverse Osmosis Concentrate Management Options

The common practice for brine management is direct or indirect disposal to surface waters, sewers and evaporation ponds [22-25, 37]. In coastal RO plants, direct disposal to marine environments may be technically and/or economically viable [37, 38]. Yet, this practice should be further scrutinised. Direct discharge of ROC into the environment may have adverse effects on aquatic ecosystem [39] [25]. Due to the elevated concentration of salts in the ROC, sewer discharge may cause inhibition of microorganisms in the WWTPs [22]. On the other hand, evaporation ponds are feasible only for small volumes of concentrate, and they require considerable land area and a warm and dry climate [22]. Deep well injection is another brine disposal option where the concentrated stream is injected into subsurface at hundred metres or more below the freshwater aquifer. Due to more stringent regulations, this method is being restrained, and may only be applied in the absence of another viable alternative [22, 23].

Zero liquid discharge (ZLD) refers to a class of developing technologies that process the concentrate stream to the point where there is no liquid discharge through one or combined of the following steps: *(i)* intermediate treatment in-between RO process (such as ion exchange and precipitation for foulant or scalant removal using lime soda); and *(ii)* post-treatment of ROC from the final RO process train, such as evaporators, brine concentrators and crystallisers to completely separate dissolved salts from the water [40-42]. Another process that approaches ZLD, which is particularly suitable for inland water reclamation facilities, is nutrient and salts recovery. Kumar *et al.* [43] investigated the application of polymer ligand exchange resins to recover phosphate from the ROC as struvite. In addition, it has been proved that electrodialysis (ED) applying ion exchange membrane and electric current is feasible to separate nutrient/salt ions and organic compounds contained in the ROC [44]. This ED method can be combined with other methods to improve water recovery, such as lime soda precipitation (to reduce scaling problem in ED system), evaporation (for ED downstream brine treatment) and/or ozonation (to reduce the accumulation of organic compounds) [45, 46]. Badruzzaman *et al.* [47] evaluated the use of bipolar membrane electrodialysis to convert the ROC into valuable products, i.e. mixed based and mixed acids, as well as onsite chlorine production from electrochlorination. However, both ZLD and ED approach are energy-intensive, need further handling of the solid salts/liquid wastes, and are therefore currently economically unfeasible [23, 41].

In the past 10 years, there has been a growing number of studies focusing on the evaluation of different physico-chemical treatment options for reducing the load of pollutants in the ROC (Table 1) [3-5, 17, 18, 48, 49]. These options ranged from classical separation methods (e.g. coagulation, carbon adsorption and ion exchange) to chemical oxidation including AOPs such as UV/$H_2O_2$, $TiO_2$ photocatalysis, ozonation, sonolysis and Fenton oxidation. Most of the studies report the removal of COD, dissolved organic carbon (DOC) and nitrogen, yet very few studies have focused on the removal of particular contaminants (e.g. pharmaceuticals) and/or toxicity. It should be noted that the ROC characteristics and treatment conditions were slightly different in each study.

Coagulation involves the addition of chemicals, mostly aluminium and ferric salts, to enhance a rapid settling of aggregates of organic matter. Dialynas *et al.* [3] observed a better performance of ferric chloride than aluminium sulfate when treating ROC, and 42% and 52% of DOC removal was achieved at optimum dosages of 2 mM $Al_2(SO_4)_3$ and 0.4 mM $FeCl_3$, respectively. However, coagulation has very low efficiency in removing the trace organic pollutants [50]. Variation in feed water composition and flow rate make the process control difficult since coagulation requires optimum conditions (e.g. coagulant dosage, pH). Finally, coagulation produces large amounts of chemical sludge, and is thus unsuitable for large-scale applications.

Magnetic ion exchange (MIEX®) resin combines traditional strong base anion exchange properties, like quaternary ammonia functional groups, a polyacrylic, macroporous structure, and medium pore size and porosity. The resin alone or in combination with coagulation has been investigated for the removal of NOM from different waste streams [51-54]. MIEX resin was reported to remove colour, $UV_{254}$, COD and DOC from highly saline landfill leachate, however the extent of the removal was strongly affected by the background water matrix that may lead to fast saturation due to the resin blocking [55]. Thus, frequent resin regeneration is required to maintain the treatment performance at high level. Also, the treatment generates liquid waste that needs to be further handled.

Several studies have reported high efficiency of granular activated carbon (GAC) [3] and powdered activated carbon (PAC) [48] in removing organic matter from the ROC stream. However, this treatment requires a large volume of adsorbent, which is impractical for large-scale applications. Ng *et al.* [56] studied the performance of biological activated carbon (BAC) treatment of ROC. The authors observed very low total organic carbon (TOC) and COD removals, 25% and 40%, respectively, indicating that the ROC contained a large fraction of non-biodegradable organic compounds derived from biologically treated secondary effluents. In another study [57], 3 to 10 mg of $O_3$/L and 10 and 20 min contact times in batch operation were found to increase the biodegradability of the ROC by 1.8–3.5 times, while the obtained TOC removal was 5.3–24.5%.

**Table 1. Summary of physico-chemical reverse osmosis concentrate treatment options.**

| Technology | Method and Material | Key Results | Ref. |
|---|---|---|---|
| **Coagulation** | Ferric chloride and alum in the standard jar tests. | More efficient DOC removal, i.e. 52% with ferric chloride (0.4 mM optimum dose), than with alum addition. | [3] |
| | | Ferric coagulation (1.5 mM optimum dose) effectively removed low to high MW organics, with DOC and COD removal up to 38% and 49%, respectively. | [30] |
| | | 26% DOC removal was achieved by 1 mM ferric chloride. | [49] |
| **Ion Exchange (MIEX®)** | MIEX resin in the jar tests. | 35% COD and 43% DOC removal were obtained with the dosing of 10 mL $L^{-1}$ MIEX and 10-20 min contact time. | [30] |
| **Adsorption (Activated Carbon – AC)** | Granular AC (GAC) or powdered AC (PAC) adsorbents studied at different carbon doses. | The highest DOC removal (91%) achieved at a dose of 5 g $L^{-1}$ GAC. | [3] |
| | | 88% and 95% of DOC were removed by 5 g $L^{-1}$ dose of GAC and PAC, respectively. | [49] |
| | | An application of combined PAC and microfiltration as accumulative counter current adsorption process obtained ~70% of both COD and DOC removal with 0.6 g $L^{-1}$ PAC. | [48] |
| **Chemical Oxidation and Advanced Oxidation Processes (AOPs)** | Ozonation and ozone-based AOPs | 64.9±11.3% of COD and 26.3±7.5% of TOC removal was achieved with average $O_3$ dose of 6 mg $L^{-1}$ (20 min contact time). | [57] |
| | | A combined $O_3/H_2O_2$ process achieved 75% DOC removal (1000 mg $L^{-1}$ $O_3$ and 0.7 mol $H_2O_2$/mol $O_3$). | [18] |
| | | A dose of 5-10 mg $O_3$ $L^{-1}$ showed an effective removal of ß-blockers, such as metoprolol and propranolol, from ROC. | [5] |
| | | 22% DOC and 14% COD removal were achieved using $O_3$ alone (1 L/min and 17.6±8.3mg/h). Combined with ferric coagulation, 41% DOC and 28% COD were removed. | [49] |
| | Fenton process | 50% DOC removal was obtained at pH ~ 3 with 10 mM $Fe^{2+}$ and 10 mM $H_2O_2$. | [18] |
| | Photocatalysis ($UV/TiO_2$) | DOC removal of up to 30% was achieved with 0.5 and 1 g $L^{-1}$ $TiO_2$ alone in dark room (1 h), and was increased up to 49% by using UVA with 1 g $L^{-1}$ $TiO_2$ (1h - 3 kWh $m^{-3}$). | [3] |
| | | A maximum of 19% DOC and 10% COD removal was achieved at UVA and UVC with 1 g $L^{-1}$ $TiO_2$ (1 h). Combined with ferric coagulation, 72-95% of DOC could be removed after 6 h. | [49] |
| | | 80% DOC removal required 2 g $TiO_2$ $L^{-1}$ and UV dose of 10 kWh $m^{-3}$. | [18] |
| | Photooxidation ($UV/H_2O_2$) | 40% DOC removal was obtained with UV dose of 12 kWh $m^{-3}$ and 10 mM $H_2O_2$. | [18] |
| | | 50-55% COD and 40% DOC removal were achieved with UVC dose of 3.1 kWh $m^{-3}$ and 12 mM $H_2O_2$. | [30] |
| | | 27% of DOC removal was achieved after 0.5 h of 10 kWh $m^{-3}$ UVC/3 mM $H_2O_2$. After subsequent biological activated carbon treatment, 63% of DOC was removed. Microtox assay performed at non-extracted samples showed no toxicity of raw and treated ROC. | [58] |
| | Sonolysis | Insignificant effects of sonolysis alone on DOC and COD removal (<5%) (1 h reaction time with 220 W energy). | [49] |
| | | 29% DOC was degraded after 1 h at 67.5 W energy input. At higher energy (135 W), DOC removal was increased to 34%. | [3] |

Ozonation and other AOPs are being actively investigated for the treatment of ROC, in order to degrade the organic contaminants and/or convert them into more easily biodegradable form [3, 5, 18, 30]. Ozonation at pH 7.0 was found to be very efficient for removing β-blockers from the RO brine stream [5], which was assigned to their high reactivity towards hydroxyl radicals ($OH^{\bullet}$). Westerhoff *et al.* [59] observed 75% of DOC removal in a combined $O_3/H_2O_2$ treatment of ROC (0.7 mol $H_2O_2$ $mol^{-1}$ $O_3$ dose), although extremely high $O_3$ dosages were required (1000 mg $L^{-1}$ of $O_3$). The authors also investigated Fenton oxidation of ROC (pH 3.3, 10 mM $Fe^{2+}$, 10 mM $H_2O_2$), which removed up to 50% of DOC, and $UV/TiO_2$ oxidation, which achieved the highest DOC removal (i.e. 80% DOC removal at a UV dose of 10.4 kWh $m^{-3}$). Moreover, as the majority of the ROC organics remaining after the $UV/TiO_2$ oxidation were found to be biodegradable, a combined AOP-biodegradation treatment of ROC was suggested.

On the contrary, Zhou *et al.* [49] found that combined AOP processes such as UV/$H_2O_2$ and UV/$TiO_2$ could remove only small fractions (<20%) of DOC from the raw ROC, due to strong scavenging effect of $OH^{\bullet}$ by the water matrix present in the raw RO concentrate. In the same study, ozonation at pH 7.0 achieved only around 22% of DOC removal, along with 90% of the colour removed. The authors suggested a coupled treatment of coagulation and subsequent AOP (e.g. $FeCl_3$ coagulation, UVC/$TiO_2$) for decreasing the toxicity of the brine stream and converting the organics into compounds that are more amenable to biodegradation.

Bagastyo *et al.* [30] observed around 40% DOC removal and complete colour removal in a UV/$H_2O_2$ treatment of ROC sampled at AWTP Bundamba and AWTP Luggage Point (3.1 kWh $m^{-3}$ UVC dose, 400 mg $L^{-1}$ $H_2O_2$). While most of the humic acids and soluble microbial products (SMPs) were well removed, lower MW organics (<0.5 kDa) were more recalcitrant in the employed AOP.

Although a combination of two or more AOP treatments can be applied to enhance the oxidation rate of contaminants, large amounts of chemicals and high energy input are typically required for the degradation of recalcitrant contaminants contained in the brine stream. As an alternative to AOPs, in electrochemical oxidation process $OH^{\bullet}$ as well as a variety of other oxidants (e.g. $O_3$, $H_2O_2$) are formed from the electrolysis of water at the anode.

## 2.3. Electrochemical Treatment of Reverse Osmosis Concentrate

The capability of electrochemical oxidation to generate oxidants in-situ without the need for regents is a compelling advantage over competing technologies. Electro-oxidation can overcome the limitations of AOPs not only in terms of chemical usage, but also in terms of the oxidising abilities, since a range of oxidant species can be generated at the anode poising different anode potentials. On the other hand, electrochemical reduction was suggested already in the 1970s as a promising method for the dechlorination of persistent contaminants under mild experimental conditions, without using the highly reactive reducing agents [7]. It enables selective dehalogenation through controlled potential and selection of cathode material, without the need for waste disposal.

Considering that electricity can now be produced from sustainable sources such as solar and wind, electrochemical techniques hold the potential of replacing chemicals by sustainable electrical energy. Several promising characteristics of the electrochemical processes for environmental applications are:

- No use of chemicals – the treatment uses electrons as the only reagent.
- Versatility – the process can be modified to suit different treatment requirements in terms of characteristics of wastewater (e.g. COD, colour) and contaminants present.
- Robustness – capable of dealing with variations in the influent composition and flow rate.
- Energy efficiency –operation at ambient temperature and pressure; energy requirements can be minimised by the appropriate cell design, as well as choice of electrode material (i.e. minimised side reactions).
- Amenability to automation – the electrical variables (current and potential) are particularly suited for facilitating data acquisition, process automation and control.
- Compact design – the process can be easily scaled-up and added to the existing treatment trains; it can be applied in small isolated communities, as it removes contaminants, but also in the oxidation step kills pathogens, and treated water can be safely discharged.

However, electrochemical treatment may have several associated limitations such as:

- The process suffers from mass transport limitations, and its efficiency is highly dependent on the reactor design (e.g. size of the electrode area).
- Contact of cell components with the aggressive media may lower the durability and long-term stability of electrode material.
- Electrode fouling may occur, i.e. anode passivation by the formed oxidation by-products, and/or cathode scaling.

- High operating cost is expected for heavily polluted waters and waters containing recalcitrant contaminants, due to high electric energy consumption.
- Elevated concentration of chloride ions may lead to intense electrochemical hypochlorination and formation of chlorinated by-products, expected to have increased toxicity and persistency.

### 2.3.1. Principles of Electrochemical Processes

In an electrochemical reactor, electric current or voltage is used to induce chemical reactions, i.e. oxidation at the anode and reduction at the cathode. By withdrawing electrons from the anode, this electrode becomes positive. Species in contact with the anode will be stripped of electrons and get oxidised. On the other hand, these electrons move towards the cathode which becomes negatively charged. Species in contact with the cathode will gain electrons and be reduced. The movement of electrons in the external electrical circuit is compensated with the movement of ions of the electrolyte, i.e. wastewater to be treated. The main reactions in electrochemical oxidation and reduction of aqueous electrolytes are oxidation of water to oxygen (Equation 1), and reduction of water to hydrogen (Equation 2), respectively:

**Equation 1** $2\ H_2O(\underline{l}) \rightarrow O_2(g) + 4\ H^+(aq) + 4e^-$

**Equation 2** $2\ H_2O(l) + 2e^- \rightarrow H_2(g) + 2\ OH^-(aq)$

Thus, electrolysis of water at the anode will lead to a local pH decrease, while electro-reduction of water to hydrogen and hydroxyl ions will lead to local pH increase at the cathode.

Electrolytic cell can have a non-divided or divided configuration (Figure 1). In the latter case, cation exchange membrane (CEM) or anion exchange membrane (AEM) is placed between the anode and the cathode in order to limit the movement of electrolyte species to cations and anions only, respectively. Non-divided cells have a lower energy demand due to the absence of a membrane separator, which contributes to the ohmic drop in the cell. On the other hand, divided electrolytic cells allow a separate investigation of electrochemical oxidation and reduction, as well as the use of different catholyte and anolyte. For example, the efficiency of electrochemical wastewater disinfection is enhanced by using a divided electrolytic cell because the generated chlorine is not reduced at the cathode. However, scaling of the membrane and electrode gap should be considered when applying the divided cell configuration [6].

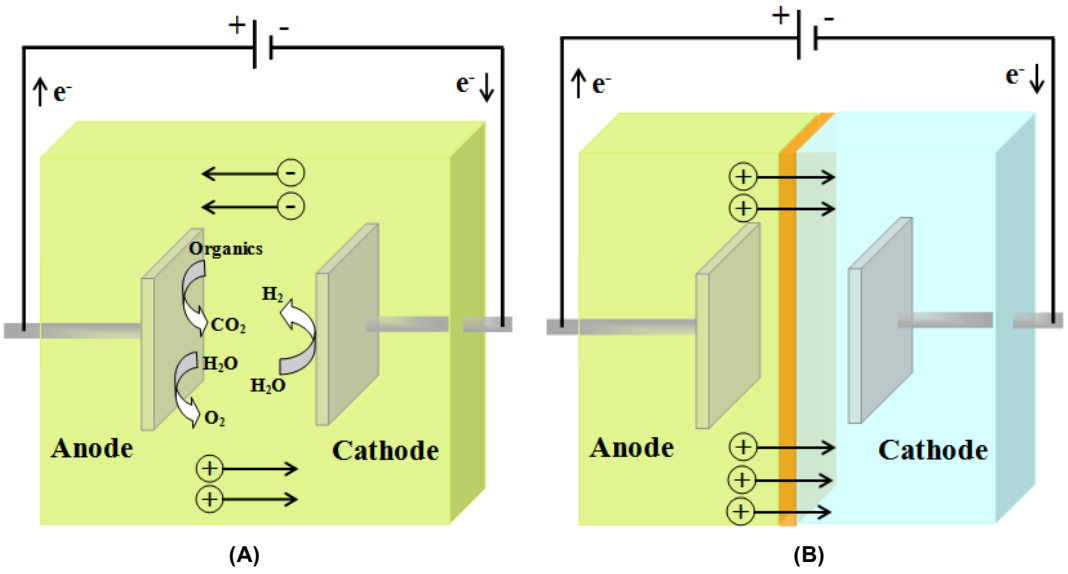


**Figure 1. Schematic representation of an electrolytic cell: A) non-divided cell, and B) divided cell, anode and cathode are separated by a cation exchange membrane (CEM).**

The performance of electrochemical oxidation and reduction in terms of removal efficiency and energy requirements depend on several parameters such as the electrode material (e.g. type, active surface), reactor design (e.g. inter-electrode gap, presence of ion exchange membrane), mass transport regime, applied current/potential, characteristics of electrolyte (e.g. presence of halide, sulphate and other ions, organic scavengers of $OH^{\bullet}$) [60]. To ease the maintenance, the cells should be constructed in a simple way so that the cell components can be easily removed and exchanged.

#### 2.3.1.1 Electrochemical Oxidation

Electrochemical oxidation can take place through two mechanisms: *(i)* direct oxidation, by direct electron transfer between the substrate and the anode; and *(ii)* indirect oxidation, by the oxidant species electrogenerated at the anode (e.g. $OH^{\bullet}$, $O_3$, $H_2O_2$, $HClO/ClO^-$) (Figure 2). In the indirect mechanism, oxidation of contaminants by short-lived species (e.g. $OH^{\bullet}$) may be restricted to the anode surface. Long-lived oxidants such as free chlorine ($HClO/ClO^-$) are able to diffuse away from the electrode surface and promote the bulk oxidation of the organics. Both oxidation mechanisms may coexist during the electrochemical oxidation.

Direct electrochemical oxidation will be the dominant mechanism only at low potentials, before the thermodynamic potential of oxygen evolution reaction (OER) is reached (Equation 1), i.e. at 1.23 V vs. Standard Hydrogen Electrode (SHE). The kinetics of direct electrochemical is often very slow, requires interaction of the substrate with the anode surface, and is thus mass transfer-limited and can be achieved only in very limited cases [61].

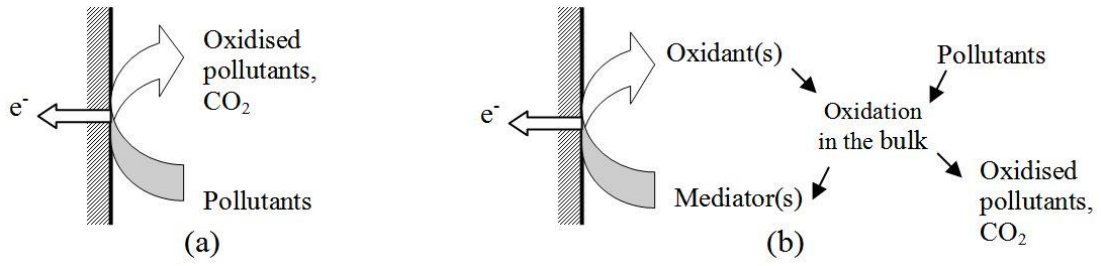


**Figure 2. Scheme of the electrochemical oxidation: A) direct, and B) indirect (mediated) oxidation [6].**

**Table 2. Oxidation potential of common oxidants at pH 0 [62, 63].**

| Oxidant Agents | Oxidation Potential Energy, $E^o$ (V) |
|---|---|
| Fluorine | 3.03 |
| Hydroxyl radical | 2.80 |
| Atomic oxygen | 2.42 |
| Ferrate (VI) | 2.20 |
| Ozone | 2.07 |
| Peroxodisulfate | 2.01 |
| Hydrogen peroxide | 1.78 |
| Permanganate ion | 1.77 |
| Perhydroxyl radical | 1.70 |
| Permanganate | 1.68 |
| Hypobromous acid | 1.59 |
| Chlorine dioxide | 1.57 |
| Silver (II) ion | 1.50 |
| Hypochlorous acid | 1.49 |
| Perchlorate | 1.39 |
| Chlorine | 1.36 |
| Dichromate | 1.23 |
| Dissolved oxygen | 1.23 |

It is generally considered that direct anodic oxidation has a minor contribution to the overall oxidation of organics at potentials higher than the threshold for water electrolysis. Application of higher anodic potentials leads to generation of oxidant species from the electrolysis of water (e.g. $OH^{\bullet}$, $O_3$, $H_2O_2$) and/or ion mediators (e.g. $HClO/ClO^-$). Table 2 summarises common oxidants and their oxidation potentials expressed vs SHE. Thus, the prevailing mechanism of electro-oxidation will be determined by the characteristics of the waste stream (i.e. presence of organic scavengers, $Cl^-$, $Br^-$, $CO_3^{2-}$, $SO4^{2-}$), as well as the type of the anode material used.

#### 2.3.1.2 Electrochemical Reduction

Similarly to the electro-oxidation mechanism, electrochemical reduction may proceed through: *(i)* direct reduction, by direct electron transfer from the cathode to the substrate; and *(ii)* indirect reduction, via redox mediators (e.g. $Fe^{3+}$-triethanolamine (TEA) complex, quinone derivatives). Direct electro-reduction is often in taking place simultaneously with the hydrogen evolution reaction (HER). In the case of cathodes activated with noble metal particles (e.g. palladium), indirect reduction via electrolytic production of atomic hydrogen represents another reduction mechanism, especially when operating in protonated solvents.

Electrochemical reduction, both direct and indirect, has been widely investigated for dehalogenation of brominated flame retardants [64], X-ray agents [65] and chlorinated pesticides [66], as well as for the remediation of nitroaromatic contaminants [67]. Considering that the reactivity of carbon-halogen (C-X) bond decreases in the order I>Br>Cl>F, reductive electrochemical treatment may become a low-current-yield process for the treatment of fluorinated and chlorinated contaminants [68]. Furthermore, the process will rely on the contact of the contaminant and/or mediator with the cathode surface, and will typically require large electrode active surface area. This drawback can be overcome by using three-dimensional (3-D) electrodes. In summary, the choice of electrode material is crucial for this process, as it determines the reaction pathway, selectivity and specific energy consumption.

### 2.3.2. Importance of Electrode Material in Electrochemical Treatment

The choice of electrode material affects efficiency and selectivity of electrochemical treatment [69]. One of the most commonly investigated electrodes for environmental applications of electrochemical oxidation are mixed metal oxide (MMO) electrodes, known under the trade name Dimensionally Stable Anode (DSA®). MMOs have been investigated for the treatment of pesticide contaminated water, landfill leachate, organic petroleum wastewater and other difficult to treat waste streams [69]. They consist of corrosion-resistant base materials such as titanium or tantalum, coated with a layer of transient metal oxides (e.g. $IrO_2$, $SnO_2$). The particular type of coating determines the electrocatalytic activity of the electrodes. According to their interaction with the electro-generated $OH^{\bullet}$, they are classified into “active” and “non-active” anodes.

At both active and non-active anodes, “active oxygen” (anode adsorbed hydroxyl radicals, $OH^{\bullet}$) is generated by the electrolysis of water (
Equation 3). At the active anodes with a strong interaction between the electrode (M) and the adsorbed $OH^{\bullet}$, so-called higher oxide, MO is formed (Equation 4). The redox couple M and MO, called chemisorbed active oxygen, selectively oxidises the organics (R), as shown in Equation 5, forming oxidation products ($RO^*$). However, this reaction is in competition with the side reaction of oxygen evolution, decreasing the efficiency of the anodic process due to the MO decomposition (Equation 6).

**Equation 3** $M + H_2O \rightarrow M(OH^{\bullet}) + H^+ + e^-$

**Equation 4** $M(OH^{\bullet}) \rightarrow MO + H^+ + e^-$

**Equation 5** $MO + R \rightarrow M + RO^*$

**Equation 6** $MO \rightarrow M + \frac{1}{2} O_2$

At the non-active anodes, where the MO does not form due to the weak interaction between the $OH^{\bullet}$ and the anode surface, the oxidation of organics is non-selective. This so-called physisorbed active oxygen (i.e. M ($OH^{\bullet}$)) may lead to complete combustion of R to $CO_2$. The non-active electrode participates in oxidation as an inert material, while the oxidation is mediated by $OH^{\bullet}$ as shown in Equation 7. This reaction is also in the competition with the oxygen evolution (Equation 8).

**Equation 7** $M(OH^{\bullet}) + R \rightarrow M + mCO_2 + nH_2O + H^+ + e^-$

**Equation 8** $M(OH^{\bullet}) \rightarrow M + \frac{1}{2} O_2 + H^+ + e^-$

For example, $IrO_2$ and $RuO_2$-based anodes are considered to be "active" due to their strong interaction with the electro-generated $OH^{\bullet}$, which results in a low over-potential for $O_2$ evolution [69]. High oxidation power anodes such as $Ti/PbO_2$ and $Ti/SnO_2$ are "non-active", characterised by a weak electrode - $OH^{\bullet}$ interaction and lower electrochemical activity for $O_2$ evolution, thus providing a higher current efficiency for organics oxidation. As postulated by Comninellis [70], non-active electrodes are theoretically capable of mineralising the organic compounds via $OH^{\bullet}$, in contrast to active anodes which only partially oxidise the organics by the adsorbed active oxygen species.

The latest technological leap in the area of technical electrode materials is the invention of boron-doped diamond (BDD). BDD electrodes are characterised by a much wider potential range in aqueous electrolytes compared to other electrode materials (ca. -1.25 to +2.3 V versus the Normal Hydrogen Electrode-NHE) [71]. The interaction between the surface of a BDD electrode and electro-generated $OH^{\bullet}$ is weak, allowing them to mineralise organic pollutants in the vicinity of the electrode surface. These quasi-free $OH^{\bullet}$ represent the main advantage of BDD electrodes over conventional materials, as they enhance the degradation rates of organic pollutants. The high cost of the substrate onto which the BDD film is deposited (e.g. Nb, W, Ta) represents a major impediment to their large-scale application. While relatively cheap Ti possesses all the necessary features of a good substrate material (i.e. good electrical conductivity, mechanical strength and electrochemical inertness), the deposition of BDD films on Ti with satisfactory stability is difficult to date [72]. On the contrary to MMO electrodes, BDDs are currently not available in practical mesh geometries.

The cathode materials typically used in aqueous solvents are silver, copper, nickel and carbon based cathodes. They can be fabricated in the form of a place, or foam, while the latter one is also available as carbon cloth, carbon mesh, carbon paper and carbon granules. Besides the choice of the cathode material which will largely influence the kinetics of electro-reduction, the main challenge in designing the reductive electrochemical remediation of organic contaminants is ensuring their efficient contact with the cathode surface. This can be achieved in most cases by changing the reactor's geometry from planar to column-type, employing 3-D electrodes (e.g. granular, mesh or foam cathode), and improving the stirring inside the reactor.

### 2.3.3. State-of-the-Art Review

Table 3 summarises the existing studies on the electrochemical treatment of ROC. Van Hege *et al.* [20, 21] proposed electrochemical oxidation as a promising method for the treatment of problematic waste streams such as ROC. Electrochemical remediation of ROC offers an obvious advantage of low energy consumption due to its high electric conductivity. In their first study, Van Hege *et al.* [20] observed complete removals of COD and total ammonium nitrogen (TAN) after supplying 1.5 and 2 Ah $dm^{-3}$ of specific electrical charge (Q) galvanostatically at 167 A $m^{-2}$, using an undivided cell. Nevertheless, although absorbency at visible wavelength was completely removed, decrease in absorbency at 254 nm was only less than 50%, implying incomplete degradation of the aromatic fraction of organic matter. When comparing the performance of MMO and BDD electrodes for electro-oxidation of ROC [21], the highest COD removal was noted for BDD and $Ti/SnO_2$, and TAN removal for BDD and $Ti/RuO_2$ anode. This was explained by the predominant mechanism of electrochlorination in TAN removal, as the highest concentration of active chlorine was measured for BDD electrode, followed by $Ti/RuO_2$. Also, removal of colour was complete, and as noted by Panniza

*et al.* [73] likely achieved through chlorine mediated indirect oxidation mechanisms. On the other hand, in the case of Ti/$PbO_2$ and Ti/$SnO_2$ electrodes, cathodic increase in pH was higher than the anodic pH decrease in a non-divided electrochemical cell, causing the precipitation of $Ca^{2+}$ and $Mg^{2+}$ ions present in the ROC, and electrode scaling.

Dialynas *et al.* [3] used a DiaCell® single compartment electrolytic flow-cell equipped with BDD electrodes to electrochemically oxidise 8 L of ROC in batch recirculation mode. At current density (J) of 514 A $m^{-2}$ only 30% of DOC was removed after 30 min of electrolysis, while further increase to 2543 A $m^{-2}$ did not result in any significant improvement. It should be noted that the electrolysis was able to oxidise the organic matter with absorbency below 250 nm, but it did not affect significantly the absorbance peak at 310 nm, often related to naphthalene-like compounds [74]. Chaplin *et al.* [75] investigated electrochemical destruction of N-nitrosodimethylamine (NDMA) in ROC using a rotating disk electrode (RDE) BDD and a flow-through Mini DiaCell® reactor. In the RDE experiments with decreased mass transfer limitations, NDMA oxidation was not affected by the DOC, $Cl^-$ and $HCO_3^-$. However, galvanostatic experiments performed at 20 A $m^{-2}$ in a flow-through reactor revealed five times lower NDMA removal rate constants. In the latter case, the estimated energy requirement for removing 75% of DOC was 6.9 kWh $m^{-3}$. It should be noted that the anode surface (i.e. 25 $cm^2$) versus active volume of the reactor (i.e. 15 mL) ratio of was high, thus creating strongly oxidising conditions inside the Mini DiaCell® reactor.

When comparing Ti/$IrO_2$-$Ta_2O_5$, BDD and Ti/$IrO_2$-$RuO_2$ electrodes in treating ROC, Zhou *et al.* [76] observed a complete COD removal at 250 A $m^{-2}$ after 1.5 h and 2 h for BDD and Ti/$IrO_2$-$RuO_2$, respectively, while partial removal was noted for Ti/$IrO_2$-$Ta_2O_5$. The Ti/$IrO_2$-$RuO_2$ electrode was suggested as the most suitable for full-scale application due to its lower cost and lower energy consumption compared to BDD (e.g. 66 vs 203 kWh $kgCOD^{-1}$ respectively for Ti/$IrO_2$-$RuO_2$ and BDD at 250 A $m^{-2}$).

High variety and complexity of brine streams makes overall evaluation of electrochemical treatment rather difficult. From the existing studies, it seems that complete COD and colour removal in electrochemical oxidation of ROC can be achieved in an economical and technically feasible way due to the presence of chloride ions. The energy consumption for the total removal from ROC was estimated at around 60 kWh $kgCOD^{-1}$ (i.e. ~6-6.5 kWh $m^{-3}$) in several studies [20, 21, 77]. However, ROC streams have very high concentrations $Cl^-$, typically from 1.4 up to even 8 g $L^{-1}$ [13], and besides their positive effect in terms of lowered ohmic resistance and thus decreased energy consumption, they can lead to prevalent electro-chlorination in the bulk liquid and generation of toxic chlorinated by-products.

For example, Perez *et al.* [77] have reported generation of trihalomethanes (THMs) and toxic chlorate ($ClO_3^-$) using a DiaCell set-up for the oxidation of ROC. While the authors determined 100 A $m^{-2}$ as the optimum current density for minimisation of THMs concentration, the generation of $ClO_3^-$ was continuously enhanced with the increase in the applied current. In addition, other studies have previously reported a risk of formation of toxic $ClO_3^-$, $ClO_4^-$ [78], $BrO_3^-$ and $BrO_4^-$ [79] at BDD electrodes. Thus, the increased toxicity of electrochemically treated effluent may diminish the beneficial effects of chloride ions. With a few exceptions, this aspect of application of electrochemical oxidation for the treatment of highly saline streams has been largely overlooked in the existing studies.

**Table 3. Summary of Studies on the Electrochemical Treatment of Reverse Osmosis Concentrate (modified from [80]).**

| Experiment | $A_{AN}$ ($cm^2$) | $V_{ACT}$ (L) | $V_{TOT}$ (L) | $d$ (mm) | $J$ ($A\ m^{-2}$) | $Q$ ($Ah\ L^{-1}$) | $q$ ($L\ h^{-1}$) | Key results | Ref. |
|---|---|---|---|---|---|---|---|---|---|
| [1]BDD, [2]Ti/$RuO_2$:<br>- undivided cell, batch mode. | 60 | 0.2 | 1 | 10 | 167 | 2 | 15 | [1]R(COD, TAN)=100% for 2 Ah $L^{-1}$<br>CE(COD)= [1]25%, [2]35%<br>CE(TAN)= [1]10%, [2]14%<br>[1]R=70-90% ($UV_{360}$, $UV_{455}$, $UV_{405}$)<br>R=40-50% ($UV_{254}$, $UV_{280}$)<br>[1]188 kWh $kg_{COD}^{-1}$, [2]780 kWh $kg_{TAN}^{-1}$<br>[1]$ClO_3^-$ formation | [20] |
| [1]BDD, [2]Ti/$RuO_2$,<br>[3]Ti/$PbO_2$, [4]Ti/$SnO_2$:<br>- undivided cell, batch mode. | 50 | 0.2 | 1 | 10 | 100-300 | 1-2 | 15 | [3,4]Ca and Mg precipitates (rise in pH)<br>R($UV_{455}$, 1Ah $L^{-1}$)= [1,2]74%<br>R(COD, 1Ah $L^{-1}$)= [1]56%, [2]12%, [3]19%, [4]22%<br>R(TAN, 1Ah $L^{-1}$)= [1]48%, [2]42%, [3]14%, [4]6%<br>[1]R(COD, TAN)=100% for 2 Ah $L^{-1}$.<br>Better performance of BDD over Ti/$RuO_2$<br>was assigned to higher formation of FAC | [21] |
| BDD (Diacell):<br>- undivided, batch mode. | 70 | 0.0078 | 8 | 10 | [a]514, [b]2543 | [a]0.23, [b]1.11 | 1200 | [a]R=30% (DOC)<br>[b]R=36% (DOC)<br>Oxidation of $UV_{\leq 250}$, but not $UV_{310}$. | [3] |
| BDD (Diacell):<br>- undivided, batch mode. | 25 | 0.015 | 0.25 | 3 | 20 | up to 2 | 6 | CE(DOC)=68-75%, 6.9 kWh $m^{-3}$ | [81] |
| BDD (Diacell):<br>- undivided, batch mode. | 70 | 0.0078 (min) | 2 | 5 | [1]50, [2]100, [3]200 | up to 4.9 | 600 | R(COD)= 100% ([1]0.5, [2]0.75, [3]1 Ah $L^{-1}$)<br>[1]59 kWh $kg_{COD}^{-1}$<br>$ClO_3^-$, $NO_3^-$ and THMs formation.<br>R(TrOCs)≥90%, not affected by $J$ | [77] |
| [1]BDD, [2]Ti/$IrRuO_2$,<br>[3]Ti/$IrO_2$-$Ta_2O_5$:<br>- undivided, batch mode. | 3 | 0.05 | 0.5 | 10 | 83, 167, 250 | 1, 2, 3 | - | R(COD, 250 A $m^{-2}$)=[1]100% (2.25 Ah $L^{-1}$)<br>[2]100% (30 Ah $L^{-1}$), [3]33% (3 Ah $L^{-1}$)<br>Ti/$IrRuO_2$ had the lowest energy consumption<br>e.g. for $J$=167 A $m^{-2}$: [1]203, [2]66 and [3]130 kWh kgCOD$^{-1}$ | {Zhou, 2011 #850} |

Note: $A_{AN}$-anode surface ($cm^2$), $V_{ACT}$-active volume, i.e. electrolytic cell volume (L), $V_{TOT}$-total volume (L), $d$-inter-electrode distance (mm), $J$-current density ($A\ m^{-2}$), $Q$-specific electrical charge ($Ah\ L^{-1}$), $q$-volumetric recirculation flow rate ($L\ h^{-1}$), R-removal (%), CE-current efficiency (%), FAC-free available chlorine, TAN-total ammonia nitrogen, UV-ultraviolet absorbance, $SUVA_{254}$-specific UV absorbance at 254 nm.

# 3. MATERIALS AND METHODS

## 3.1. Chemicals

All standards for pharmaceuticals and pesticides used were of analytical grade (≥99%). Chemical standards of carbamazepine (CBZ), trimethoprim (TMP), metoprolol (MTP) tartrate, ranitidine (RNT) hydrochloride, acetaminophen (ACTP), lincomycin (LNC) hydrochloride, diclofenac (DCF) sodium, diazinon (DZN), enrofloxacin (ENR), sertraline (SRL) hydrochloride, gemfibrozil (GMF), venlafaxine (VNF) hydrochloride, diuron (DIU), hydrochlorothiazide (HCT), caffeine (CAFF), roxythromycin (ROX), tramadol (TML) hydrochloride, ibuprofen (IBU), phenytoin (PNT) (5,5-diphenylhydantoin), metolachlor (MET), atrazine (ATZ), sulfadiazine (SDZ), norfloxacin (NFL), N,N-Diethyl-meta-toluamide (DEET) and triclopyr were purchased from Sigma–Aldrich (Steinheim, Germany), citalopram hydrobromide and 2,4-dichlorophenoxyacetic acid (2,4-D) were purchased from Toronto Research Chemicals (Ontario, Canada), and iopromide was purchased from U.S. Pharmacopeia (Rockville, U.S.A.). All chemical standards were of analytical grade (≥99%).

Isotopically labelled compounds used for the correction of matrix interferences GMF-d6, ACTP-d4, HCT-$^{13}$C,d2, TML-d6 hydrochloride, IBU-d3, SDZ-d4, VNF-d6, ENF-d5, sulfadiazine-d4, and RNT-d6 hydrochloride were purchased from Toronto Research Chemicals (Ontario, Canada), TMP-13C CBZ-d10, DEET-d6, CAFF-$^{13}$C, and DCF-d4 were purchased from Cambridge Isotope Laboratories (Andover, U.S.A.), and ATZ-d5 was purchased from Dr Ehrenstorfer GmbH (Augsburg, Germany).

Stock solutions of individual standards (1 g $L^{-1}$) and internal standards were prepared in methanol and stored at −20°C. Stock solutions of NFL and ENR were renewed monthly because of their limited stability. For the purpose of analyses, a standard mixture in methanol at approx. 20 mg $L^{-1}$ concentration was prepared from the individual stock solutions of the selected analytes. Further dilutions of this mixture were prepared in 25:75 (v/v) of methanol/water and were used as working standard solutions. A mixture of labelled standards at a concentration of 1 mg $L^{-1}$ was prepared by dilution of individual stock solutions in methanol, and was used for internal standard calibration. All solvents (methanol, acetonitrile and water) were high performance liquid chromatography (HPLC)-grade and were purchased from Merck (Germany), as well as hydrochloric acid (37%), ammonium acetate, sodium hydroxide and formic acid (98%).

## 3.2. Reverse Osmosis Concentrate Sampling

The ROC samples were obtained from AWTP Bundamba, prior to the nitrification stage. The sample was collected for all studies in a single sampling batch. To ensure homogeneity and ease of pumping in the laboratory, the ROC sample was filtered using a 0.20 µm Millipore membrane filter (Ø 45 mm STERITOP-GP) prior to the experiments, and stored in the dark at 4°C to minimise the microbial activity prior to the experiments. Since ROC sampling was performed in several instances during the project, its composition varied in each of the studies conducted. However, no considerable variation of COD, DOC, pH, conductivity and dissolved salts was observed. In order to avoid confounding results, ROC used in each study was from the same sampling batch. The minimum and maximum average concentrations/values of the untreated ROC sample used in the project are presented in Table 4. The additional information of ROC composition and its initial concentrations for each study are given in the respective appendices.

**Table 4. Characteristics of ROC studied.**

| Measures | Unit | Average concentration/value (min – max) |
|---|---|---|
| pH | | 7.6 – 8.1 |
| Conductivity | mS $cm^{-1}$ | 4.9 – 6.1 |
| Colour | mg Pt-Co $L^{-1}$ | 55 – 274 |
| SUVA | L $mg^{-1}$ $m^{-1}$ | 1.92 – 2.31 |
| COD | mg $L^{-1}$ | 136 – 175 |
| DOC | mg $L^{-1}$ | 42 – 58 |
| $Cl^-$ | mg $L^{-1}$ | 1018 – 1526 |
| $Br^-$ | mg $L^{-1}$ | 1.2 – 1.6 |
| $Ca^{2+}$ | mg $L^{-1}$ | 183 – 215 |
| $Mg^{2+}$ | mg $L^{-1}$ | 71 – 98 |
| $Na^+$ | mg $L^{-1}$ | 766 – 914 |

## 3.3. Experimental Set-Up

### 3.3.1. Reactor Configuration

Four types of electrochemical reactor configurations were used for the experiments performed in this project (Figure 3). The electrochemical cell was constructed by assembling equal rectangular frames made of polycarbonate or acrylic polymer (Perspex), with internal dimensions of 20 × 5 × 1.2 cm (active volume: 114 $cm^3$, with a headspace of 6 $cm^3$) and 20 × 5 × 2 $cm^3$ (active volume: 190 $cm^3$, with a headspace of 10 $cm^3$), respectively.

The frames were bolted together between the two side plates and sealed by rubber gaskets, creating anode and cathode compartments. While identical in the shape and material used, the four types of reactors varied in the electrode positioning, the number of compartments and ion exchange membranes used. Type-A reactor was comprised of two equal rectangular frames separated by a CEM (Ultrex CMI-7000, Membranes International Inc., USA). The frames were bolted together between two side plates and sealed by rubber gaskets, creating anode and cathode compartments. The frames and plates were made of acrylic polymer (Perspex) or polycarbonate polymer. The material used is described in detail in each study. The electrodes were placed inside the respective compartments, where the inter-electrode gap was 4 mm. Type-B reactor had the same frame set-up as Type-A reactor, the only difference being that the carbon plate cathode was placed between the side plate and the cathodic frame, thus resulting in the final volume of the cathodic compartment of 114 $cm^3$. Type-C reactor consisted of five compartments (i.e. two for anolyte and catholyte, two for the diluate/rinsing solutions and the central compartment for ROC) which were sequentially separated by CEM and AEM (CMI-7000 and AMI-7001, respectively, Membranes International, U.S.A.). Each compartment had an active surface of 100 $cm^2$ and active volume of 190 $cm^3$. The electrodes were placed in the terminal compartments, where the distance between anode and cathode was 6.5 cm. Finally, Type-D reactor was identical to Type-A reactor, but constructed in the absence of ion exchange membrane.

### 3.3.2. Electrode Materials

The materials used as anodes were either mesh Ti coated MMO electrodes (Magneto Special Anodes BV, Schiedam, The Netherlands) or plate Si-based BDD electrode (Adamant Tech., Switzerland.) as shown in Figure 4. The MMO coating materials include $IrO_2$-$Ta_2O_5$ (12 g $m^{-2}$ of Ir:Ta = 65:35), $RuO_2$-$IrO_2$ (12 g $m^{-2}$ of $RuO_2$:$IrO_2$ = 70:30), Pt-$IrO_2$ (12.5 g $m^{-2}$ of Pt:$IrO_2$ = 70:30), $PbO_2$ (3.75 g $m^{-2}$ $PbO_2$ coating) and $SnO_2$-Sb (15 g $m^{-2}$ Sn/$Sb_2O_5$ doped) which had a projected surface area of 24 $cm^2$, thickness of 1 mm, specific surface area of 1.0 $m^2$ $m^{-2}$ and current feeder of Ø 0.6 × 8 cm.

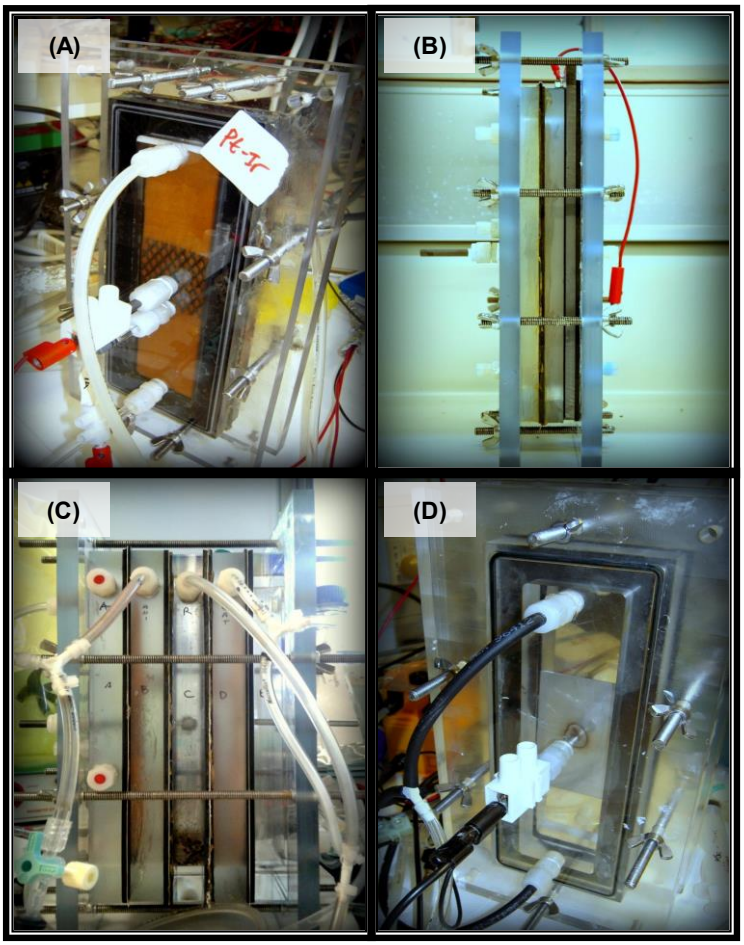


**Figure 3. Photographs of the electrochemical reactors used: A) CEM-divided reactor used for the electro-oxidation experiments, B) CEM-divided reactor used for the electro-reduction experiments, C) reactor used for the electrodialysis experiments, and D) non-divided cell reactor used for the electro-oxidation experiments.**

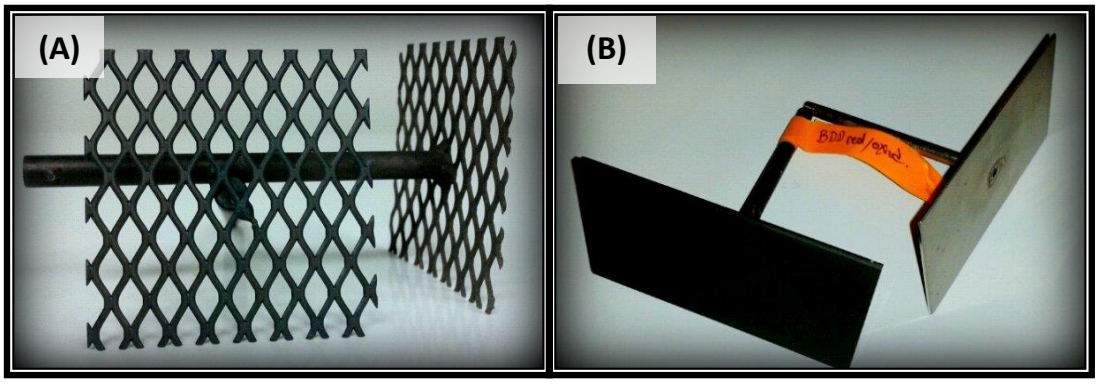


**Figure 4. Electrode materials: A) mixed metal oxide (MMO) mesh electrodes, B) plate boron doped diamond (BDD) electrodes.**

The monopolar plate Si/BDD anode (4.8 × 8.5 × 0.2 cm; 2-3 µm coating thickness of 500 ppm boron) had an active area of 40.8 $cm^2$. In all experiments the counter electrode (i.e. cathode) used was stainless steel of the same shape and surface dimensions as anode, except in the case of study in a non-divided cell, where both cathode and anode were BDD electrodes. For the electro-reduction study, a

resin-impregnated carbon electrode with dimensions 25 × 9 × 0.6 cm (active surface area: 20 × 5 $cm^2$) supplied by Morgan AM&T, Australia was used as a cathode.

### 3.3.3. Electrochemical Cell Control and Operation

Data was recorded every 60 s using either a VMP3 potentiostat (Princeton Applied Research, U.S.A) or a Wenking potentiostat (KP07, Bank Elektronik, GmbH, Pohlheim, Germany) and an Agilent 34970A data acquisition unit Agilent 34970A (Agilent Technologies, U.S.A.). The half-cell potentials were measured using Ag/AgCl (RE-5B, estimated at +0.205 V vs. SHE, supplied by Bio Analytical, U.S.A) as the reference electrode placed in the compartment close to the working electrode.

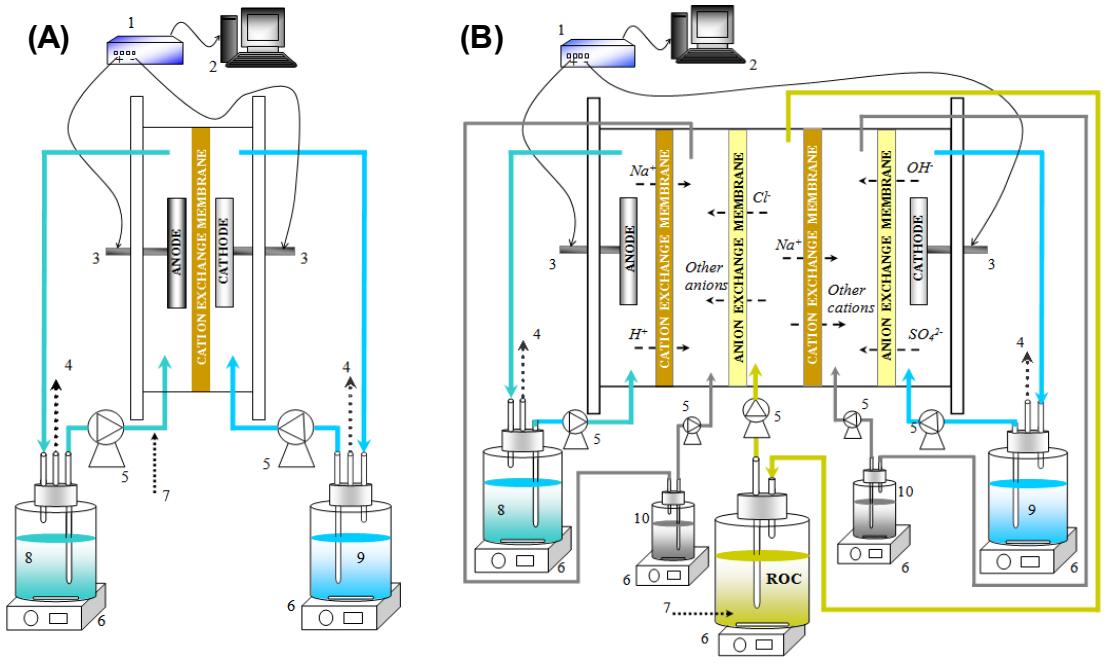


**Figure 5. Schematic diagram of the experimental set-ups used: A) two-compartment electrochemical reactor used for batch and continuous mode studies, and B) five-compartment electrodialysis reactor used for electrodialysis studies. (1) power supply, (2) data acquisition, (3) Ti-based current feeder, (4) gas ventilation, (5) Peristaltic pump, (6) stirrer, (7) pH monitoring and/or controlling system, (8) anolyte, (9) catholyte, (10) diluate/rinsing solution.**

All experiments were carried out using a chronovoltammetric technique (galvanostatic measurement) by controlling a fixed current across the working and the counter electrode. In addition to the chronovoltammetric technique, a linear sweep voltammetry technique was applied in order to obtain the onset potentials for $O_2$ and $Cl_2$ evolution at MMO and BDD anodes under specific experimental conditions, characterising their electrocatalytic properties. Details of the experiments are provided in the appendices of the respective studies.

The experiments reported in this project were conducted using set-ups illustrated in Figure 5, at high flow rate in order to increase the treatment efficiency and maintain well-mixed conditions, and in batch mode (set-up A was used in the continuous mode, too; details in Section 4.2). Unless stated otherwise, anolyte and catholyte solutions including rinsing solutions (i.e. in the case of electrodialysis) were continuously recirculated using a peristaltic pump (Watson Marlow, UK) at a flow rate of 120 mL $min^{-1}$ or 162 mL $min^{-1}$, i.e. depending on the particular experimental set-up with sufficient magnetic stirring in each electrolyte vessel. The experiments were carried out at room temperature (22±1°C).

### 3.3.4. Estimation of Electrochemical Process Performance

The changes in concentration of particular parameters (e.g. COD, DOC) are typically represented as a function of the specific electrical charge ($Q$, Ah $L^{-1}$) applied, as determined by Equation 9 [6]:

**Equation 9** $$Q = \frac{J.A.t}{V}$$

where $J$ is the applied current density (A $m^{-2}$), $A$ is the surface area of electrode ($m^2$), $V$ is the electrolyte volume (L), and $t$ is time (hour). It is important to note that plotting the data against $Q$ will take several factors into consideration for the overall treatment efficiency, i.e. electrode surface, and applied current per treated unit volume. Then, the specific energy consumption ($W$, kWh $m^{-3}$) was calculated as:

**Equation 10** $$W = Q.E_C$$

where $E_C$ = total applied cell potential (V), which equals $E_{anode}$ ($E_{AN}$, V) minus $E_{cathode}$ ($E_{CA}$, V).

The efficiency of electrochemical oxidation of organics can also be expressed as a Coulombic efficiency (CE). This efficiency, also known as instantaneous current efficiency (ICE), represents the ratio of the amount of electrons used for the desired reaction (in this case, oxidation of organic compounds in ROC measured as COD) and the total amount of electrons supplied. For electrochemical oxidation and reduction experiments operated in batch mode, CE was calculated using the following equation [60]:

**Equation 11** $$CE_{COD},\% = 100 * nFV\frac{(COD_t - COD_{t+\Delta t})}{MI\Delta t}$$

where $COD_t$ and $COD_{t+\Delta t}$ are the $COD$ concentrations ($gO_2$ $L^{-1}$) measured at times t and t+Δt, respectively, $F$ is Faraday's constant (96,487 C $mol^{-1}$), $V$ is the electrolyte volume (L), $I$ is the applied current (A), $n$ is the number of electrons involved in the reaction ($O_2$, $n$ = 4) and $M$ is the molar mass of oxygen ($M$ = 32 g $mol^{-1}$). A CE = 100% or ICE = 1 indicates a complete oxidation of organics by means of 100% supplied current. The decrease of the CE or ICE value is caused in the first place by the occurrence of side reactions of oxygen evolution in oxidation and hydrogen evolution in reduction.

Analogues equation was used to calculate the CE of chloride ions oxidation ($CE_{Cl^-}$):

**Equation 12** $$CE_{Cl^-},\% = 100 * nFV\frac{(Cl^-_{(t)} - Cl^-_{(t+\Delta t)})}{MI\Delta t}$$

where $n$ = 1 for chloride ion oxidation and M = 35.5 g $mol^{-1}$. The calculation of CE for total $Cl_2$ formation ($CE_{Cl2}$) is shown in the equation below [82]:

**Equation 13** $$CE_{Cl_2},\% = 100 * nFV\frac{(Cl_{2(t)} - Cl_{2(t+\Delta t)})}{MI\Delta t}$$

where $n$ = 2 for $Cl_2$ formation (2 $Cl^- \rightarrow Cl_2 + 2\ e^-$) and $M$ = 70.9 g $mol^{-1}$.

## 3.4. Chemical Analysis

### 3.4.1. Analysis of Global Parameters

All the samples collected from the reactors were immediately filtered by 0.22 µm syringe driven filter (33 mm diameter of MILLEX-GP Millipore, U.S.A) prior the analyses of global parameters such as COD, DOC, free chlorine and other parameters mentioned below. Samples were diluted when necessary, in order to stay within the calibration range of the measurement. The pH, temperature, and conductivity were measured using a hand-held multimeter (Cyberscan PC 300, Eutech Instruments). COD and residual chlorine concentration were measured directly after sampling. COD concentrations (mg $L^{-1}$) were determined with COD tube tests range 10-150 mg $L^{-1}$ (Merck, 1.14540.0001) by a spectrophotometric method at 445 nm wavelength [83].

Residual chlorine was analysed as free available chlorine (FAC) and total chlorine (i.e. sum of FAC and combined chlorine) using the *N*,*N*-diethyl-*p*-phenylenediamine (DPD) ferrous titrimetric method [83]. It is important to emphasise that oxidants other than FAC present in the solution (e.g. $H_2O_2$, $ClO_2$, $O_3$, $Br_2$) may react with DPD in a similar way to chlorine to form a red dye, thus interfering with the measurement. Unless reported otherwise, the remaining amount of subsamples was then quenched by adding specific amounts of $Na_2SO_3$ solutions, i.e. 120% of the molar concentration of FAC, i.e. 1.2 mol of sulphite per mol of HClO (assuming all FAC was in HOCl form), in order to eliminate further reaction of FAC before the chemical analysis.

DOC was analysed using an Analytik Jena multi N/C®-series instrument, and expressed as non-purgeable organic carbon (NPOC) which indicates the remaining acidified organic carbon after purging with an inert gas such as He, $N_2$, or $CO_2$ [83]. Since all the samples were pre-filtered, NPOC expresses the total DOC. In some studies, dissolved organic nitrogen (DON) was reported. DON was calculated by subtracting the concentration of $NH_4^+$-N from the Total Kjeldahl Nitrogen (TKN).

A Lachat Quickchem8000 flow injection analyser (FIA) was used to determine $NH_4^+$-N, $NO_x$-N, and $NO_2^-$-N, according to the Method 31-107-06-1-A, while TKN was measured using Lachat QuickChem Method 10-107-06-2-D.

The metal ions were determined using inductively coupled plasma optical emission spectroscopy (ICP-OES) method [83].

The halide ions ($Cl^-$, $Br^-$, and $I^-$) were measured by ion chromatography (IC, Dionex 2010i system).

### 3.4.2. Analysis of Trihalomethanes and Haloacetic Acids

Trihalomethanes (THMs), haloacetic acids (HAAs) and oxychloride ions (i.e. $ClO_2^-$, $ClO_3^-$, and $ClO_4^-$) were analysed at the QHFSS laboratories. 100 mL samples for the analyses of oxychlorides ions were collected in plastic bottles wrapped by aluminium foil, and analysed using ion chromatography (IC, Dionex). For the analyses of THMs and HAAs, 120 mL samples were collected in three 40-mL sterile vials containing 40 mg of $NH_4Cl$. The concentration of THMs, i.e. trichloromethane (TCM) ~ (chloroform, $CHCl_3$), bromodichloromethane, $CHCl_2Br$ (BDCM), dibromochloromethane, $CHClBr_2$ (DBCM), and tribromomethane (TBM) ~ (bromoform, $CHBr_3$), were determined by gas chromatography-mass spectrometry (GC-MS) with a purge and trap method, while HAAs, i.e. monochloroacetic acid (MCAA), dichloroacetic acid (DCAA), trichloroacetic acid (TCAA), bromochloroacetic acid (BCAA), monobromoacetic acid (MBAA), and dibromoacetic acid (DBAA), were derivatised to their methyl esters and subjected to solvent extraction prior to GC-electron capture detection (GC-ECD) analysis and confirmation by GC-MS.

### 3.4.3. Analysis of Adsorbable Organic Halogen

Halogen-specific adsorbable organic halogen (AOX) was analysed in the laboratories of the Curtin Water Quality Research Centre, Curtin University using a modified method by Kristiana *et al.* [84].

The method involved acidification of the sample to pH 2, followed by adsorption of adsorbable organic compounds (including halogenated organic compounds) onto activated carbon, which was then combusted and the hydrogen halide gases produced were trapped in MilliQ water in an absorber chamber. The dissolved halide ions in the absorber ($Cl^-$, $Br^-$, and $I^-$) were then analysed by on-line ion chromatography (Dionex ICS 3000). These halide ions correspond to the concentrations of halogen-specific AOX, namely adsorbable organic chlorine (AOCl), bromine (AOBr) and iodine (AOI), and are expressed in molar concentrations. Calibration of the system was done using trichlorophenol, tribromophenol and iodophenol standards. Application of the AOX analysis in this project is described in Appendix B and C.

### 3.4.4. Spectrophotometric Measurements

The 1 cm path length of acryl and quartz cuvettes were used for colour and UV absorbance (UVA) measurements, respectively. A Varian Cary50 UV-Vis spectrophotometer was used to measure the absorbance of UVA at 254 nm ($UV_{254}$) and colour intensity (at 475 nm absorbance). The colour concentration (expressed as mg $L^{-1}$ unit of Pt-Co) was then determined against the standard calibration of Platinum-Cobalt [83]. Specific UVA (SUVA, presented as L $mg^{-1}$ $m^{-1}$ unit) at 254 nm ($SUVA_{254}$) was calculated by dividing UVA 254 nm with DOC value.

### 3.4.5. Toxicity Tests

The Microtox non-specific toxicity bioassays were performed as described in detail in Escher *et al.* [85] with sample pH adjustment to pH 7 by adding an appropriate amount of 0.1 M NaOH or 0.1 M $HNO_3$. The Microtox assay measures the relative decrease in light output from the naturally bioluminescent marine bacteria, *Vibrio fischeri*, following its exposure to a toxicant. Since the samples were extracted by the solid phase extraction (SPE) procedure on the cartridges (Oasis HLB, Ireland) as described in the Appendix A, the generated oxidants, salts and particulates were removed by the SPE sample pre-treatment. The results of the Microtox test were expressed as baseline toxicity equivalent concentration (TEQ) derived from baseline toxicity quantitative structure-activity relationship (QSAR) relative to a virtual reference compound with $\log K_{OW} = 3$ and MW = 300 g $mol^{-1}$, which equates to an $EC_{50}$ of 12.2 mg $L^{-1}$. TEQ represents the non-specific toxicity of complex mixtures of compounds, where the contribution of each chemical is weighted by its hydrophobicity.

In the *Pseudokirchneriella subcapitata* bioassay (i.e. combined algae test) three endpoints were assessedhe: the direct inhibition of photosynthesis after 2 h and 24 h incubation via measurement of the quantum yield of photosystem II using Imaging pulse-amplitude modulated fluorometry (2 h IPAM and 24 h IPAM) and the inhibition of growth rate (24 h growth rate). The effect concentrations causing 50% of maximum effect ($EC_{50}$) were derived for all endpoints from full concentration-response curves and were expressed in units of relative enrichment factor (REF). The results of the endpoint of 24 h algal growth rate inhibition were additionally converted to baseline-TEQ relative to a virtual reference compound with an $EC_{50}$ of 18.75 mg/L [85].

### 3.4.6. Fluorescence Scan Analysis

Fluorescence spectra were measured using fluorometer Perkin Elmer LS-55. The filtered samples (3 mL) were scanned in a 1 cm quartz cell at excitation and emission ranges from 200 nm to 400 nm and from 280 nm to 500 nm, respectively. The excitation slit was 5 nm and 0.5 nm for emission. Excitation-emission matrix (EEM) plots were used to identify compounds based on specific peaks Chen *et al.* [86]. The sample was diluted to DOC < 1 mg $L^{-1}$ to avoid errors associated with inner filter effect [87]. Each analysis was performed against a blank, i.e. MilliQ water (18MΩ) to minimise both Raman and Rayleigh scatters, and normalised to their initial in each experiment.

### 3.4.7. Quantitative and Qualitative Analysis of Trace Organic Contaminants

Liquid chromatography-mass spectrometry (LC-MS) analyses were performed using a Shimadzu Prominence ultra-fast liquid chromatography (UFLC) system (Shimadzu, Japan) coupled with a 4000

QTRAP hybrid triple quadrupole-linear ion trap mass spectrometer (QqLIT-MS) equipped with a Turbo Ion Spray source (Applied Biosystems-Sciex, U.S.A.). Chromatographic separation was achieved with an Alltima C18 Column (250 × 4.6 mm, particle size 5 μm) run at 40°C, supplied by Alltech Associates Inc (U.S.A.). Details of the multi-residue, i.e. quantitative method used are described in the Appendix A.

The structure of electrochemical oxidation by-products of a model compound was elucidated by isolating the protonated molecular ions, collision induced dissociation (CID) $MS^2$ and $MS^3$ experiments in (+)ESI mode and mass spectral comparison with the parent compound. Additional confirmation of the identity was obtained by the retention time ($t_R$) and isotope abundance and distribution that enabled confirmation of halogenated intermediates. Details of the qualitative analysis are described in the Appendix D.

# 4. ELETROCHEMICAL TREATMENT OF REVERSE OSMOSIS CONCENTRATE

## 4.1. Impact of Mixed Metal Oxide (MMO) coating on the Performance of Electrochemical Oxidation

### 4.1.1. Experimental Set-Up

In the first stage of the project, concerns were raised about the comparability of the experimental results when working with real ROC stream during the three years of the project, due to the variability in its characteristics (e.g. COD, colour, chloride ion concentration). Thus, attempts were made to produce a synthetic ROC which would simulate the characteristics of a real ROC stream. However, trial electrochemical oxidation experiments with several synthetic ROCs showed a significantly different performance compared to the electrochemical oxidation of real ROC stream (Appendix B). Therefore, during the project real ROC stream from the AWTP Bundamba was used. The individual studies were always performed with the same batch sample of ROC.

The performance of electrochemical oxidation of ROC was investigated using Ti/$IrO_2$-$Ta_2O_5$, Ti/$RuO_2$-$IrO_2$, Ti/Pt-$IrO_2$, Ti/$PbO_2$ and Ti/$SnO_2$-Sb anodes in a batch recirculation mode. The reactor configuration used is type-A (Figure 3). Preliminary experiments in a non-divided cell (i.e. no ion exchange membrane between the cathode and the anode) showed fast passivation of the stainless steel cathode surface due to the local pH increase and formation of Ca precipitates. Thus, all further experiments were performed in a divided cell, using acid as a catholyte to prevent the cathode passivation and increase in the total cell potential ($E_{cell}$). The experiments were performed galvanostatically at a current, $I = 240$ mA, i.e. $J = 100$ A m$^{-2}$. In all experiments, stable performance of the reactor was observed, with constant potential of anode ($E_{anode}$) and cathode ($E_{cathode}$), as well as $E_{cell}$ (Appendix B). For example, in electrochemical oxidation of ROC at $J = 100$ A m$^{-2}$, the $E_{anode}$ and $E_{cell}$ were maintained at 1.7 ± 0.2 and 3.7 ± 0.3 V vs. Ag/AgCl, respectively.

### 4.1.2. Results and Discussion

Among the five MMO electrodes tested, Ti/$PbO_2$ and Ti/$SnO_2$-Sb exhibited the highest anodic potentials, i.e. 2.2 ± 0.3 and 2.1 ± 0.1 V vs. Ag/AgCl, respectively. This is in accordance with the higher $O_2$ evolution overpotential of the $PbO_2$ and $SnO_2$-Sb coatings [69].

**Table 5. Summary of the results of the electrochemical oxidation of ROC at five MMO electrodes after supplied specific electrical charge, Q = 0.55 Ah L$^{-1}$. The results are presented as mean values (n = 2) with their mean deviations.**

| Measured Parameter | MMO Electrode | | | | |
|---|---|---|---|---|---|
| | Ti/$IrO_2$-$Ta_2O_5$ | Ti/$RuO_2$-$IrO_2$ | Ti/Pt-$IrO_2$ | Ti/$PbO_2$ | Ti/$SnO_2$-Sb |
| COD (% removal) | 14.9 ± 0.6 | 17.0 ± 4.3 | 44.2 ± 21.5 | 23.3 ± 4.6 | 30.9 ± 4.1 |
| DOC (% removal) | 6.8 ± 2.8 | 7.5 ± 1.0 | 15.9 ± 1.2 | 8.6 ± 1.1 | 15.9 ± 0.5 |
| DON (% removal) | 10.9 ± 2.7 | 9.3 ± 4.1 | 57.4 ± 14.6 | 10.4 ± 7.3 | 56.9 ± 3.2 |
| Colour (% removal) | 81.3 ± 2.7 | 88.8 ± 1.3 | 96.3 ± 4.7 | 90.7 ± 0.7 | 97.9 ± 0.6 |
| $SUVA_{254}$ (% removal) | 25.1 ± 6.0 | 27.7 ± 5.3 | 39.9 ± 3.0 | 31.2 ± 1.1 | 43.2 ± 0.1 |
| FAC (mg L$^{-1}$) | 3.4 ± 0.4 | 6.1 ± 0.5 | 319.4 ± 22.3 | 7.2 ± 2.6 | 109.9 ± 7.1 |
| Total THMs (mg L$^{-1}$)* | 0.08 | 0.22 | 0.31 | 0.19 | 0.19 |
| Total HAAs (mg L$^{-1}$)* | 0.64 | 1.41 | 2.26 | 1.49 | 2.79 |
| Specific energy consumption (kWh m$^{-3}$) | 1.95 ± 0.15 | 2.06 ± 0.19 | 2.23 ± 0.06 | 2.25 ± 0.13 | 2.44 ± 0.07 |

Note: * n = 1

The best oxidation performance in terms of COD, DOC, DON, colour and $SUVA_{254}$ removal was achieved by Ti/Pt-$IrO_2$ and Ti/$SnO_2$-Sb anodes (Table 5). The oxidation of organics increased with the increase in active chlorine concentration, especially for Ti/Pt-$IrO_2$. The overall performance of electrochemical oxidation was similar for Ti/Pt-$IrO_2$ and Ti/$SnO_2$-Sb, although the highest concentration of electrogenerated chlorine was observed at Ti/Pt-$IrO_2$ anode, i.e. 319 mg $L^{-1}$ at $Q$ = 0.55 Ah $L^{-1}$. This suggests that the enhanced oxidation performance of the Ti/Pt-$IrO_2$ may be due to the dominant mechanism of chlorine-mediated electrolysis.

The current efficiencies obtained by the Ti/Pt-$IrO_2$ anode for chlorine generation ($CE_{Cl2}$) and COD removal ($CE_{COD}$) were 42% and 45%, respectively. On the other hand, 14% and 32% of $CE_{Cl2}$ and $CE_{COD}$, respectively, was calculated for Ti/$SnO_2$-Sb anode. The lower value of $CE$ implied that the electrode was starting to generate oxidation species other than chlorine which were responsible for the enhanced oxidation performance of the Ti/$SnO_2$-Sb anode, e.g. $OH^{\bullet}$, $O_3$, $H_2O_2$ [88]. In addition, while only 3% of $CE_{Cl2}$ was obtained at the same $Q$, the Ti/$PbO_2$ showed higher $CE_{COD}$ than Ti/$RuO_2$-$IrO_2$ and Ti/$IrO_2$-$Ta_2O_5$ anodes (i.e. 25% vs. 16% and 12%, respectively). When comparing the "non-active" anodes Ti/$SnO_2$-Sb and Ti/$PbO_2$, the latter was less effective in the treatment of ROC. Similar results were previously reported by Szpyrkowicz *et al.* [82].

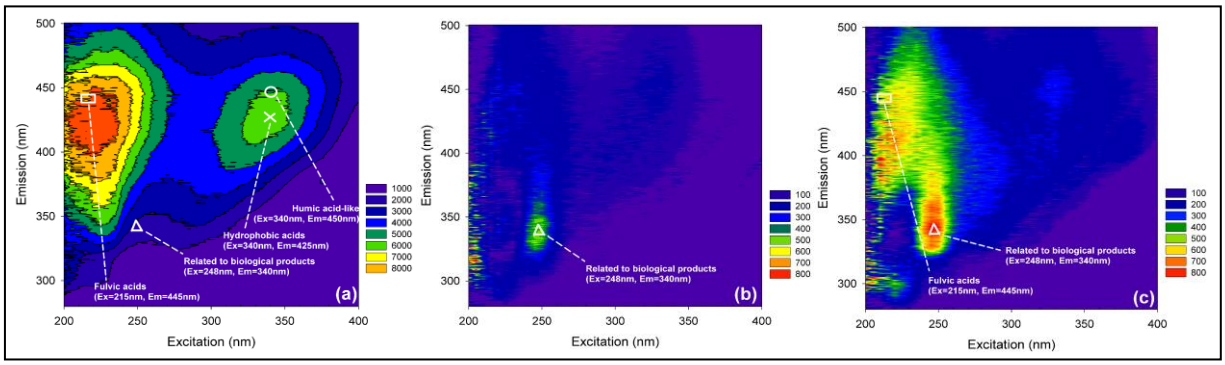


**Figure 6. The EEM of A) initial untreated ROC, and electrochemically oxidised ROC using B) Ti/Pt-IrO2, and C) Ti/SnO2-Sb anode at Q = 0.55 Ah L-1. The EEM of ROC oxidised at Ti/Pt-IrO2 and Ti/SnO2-Sb electrodes was plotted in higher resolution than the initial ROC (800 vs. 8000 fluorescent intensity).**

Figure 6 depicts plots of fluorescence EEM of the untreated ROC and ROC electro-oxidised at Ti/Pt-$IrO_2$ and Ti/$SnO_2$-Sb anodes. The EEM plots of the ROC electro-oxidised at all five MMO anodes are presented in the Appendix B. The Ti/Pt-$IrO_2$ and Ti/$SnO_2$-Sb were observed as the most effective anodes in removing the excitable fluorescent compounds. Although the quantitative performance of the five tested MMO electrodes was different, all anodes oxidised similar organic fractions, identified as fulvic acids and humic acid like compounds. Their removal increased with the enhanced formation of oxidants, which converted them into intermediates which either had a non-fluorescent nature of exhibited fluorescence to a limited extent (e.g. simpler non-aromatic compounds, halogenated organics) [89]. Thus, the observed decrease in the intensities of the EEM spectra did not necessarily imply a degradation of the organic compounds, which was confirmed by the relatively poor removal of COD and DOC. In the case of Ti/Pt-$IrO_2$ and Ti/$SnO_2$-Sb anodes, the remaining compounds were detected in the fulvic acid region and organics related to biological products.

As mentioned previously, chlorine-mediated electrolysis may lead to the formation of chlorinated by-products. In this study, since the oxidation performance was correlated to the production of active chlorine, the highest formation of THMs and HAAs, was inevitably observed for the best performing anodes, Ti/Pt-$IrO_2$ and Ti/$SnO_2$-Sb (Figure 7). While the highest total THMs (tTHMs) concentration at the end of electrolysis was measured for Ti/Pt-$IrO_2$, i.e. 0.31 mg $L^{-1}$, the highest total HAAs (tHAAs) concentration was observed for Ti/$SnO_2$-Sb, i.e. 2.79 mg $L^{-1}$. On the other hand, the lowest concentration of tTHMs and tHAAs was noted for the worst performing anodes, Ti/$IrO_2$-$Ta_2O_5$, i.e. 0.08 mg $L^{-1}$ and 0.64 mg $L^{-1}$, respectively. Both THMs and HAAs represented chlorinated and brominated derivatives. Although the measured concentration of $Br^-$ in the ROC was approximately

three orders of magnitude lower than $Cl^-$ (i.e. ~1.5 mg $L^{-1}$ vs. ~1220 mg $L^{-1}$), HBrO/$BrO^-$ is a more reactive oxidant than HClO/$ClO^-$, particularly with phenolic compounds [90], and it will participate in the bulk oxidation reactions. For example, among the tested anodes Ti/Pt-$IrO_2$ and Ti/$SnO_2$-Sb generated the highest MBAA and DBAA concentrations, i.e. ~ 0.01 mg $L^{-1}$ and ~ 0.03 mg $L^{-1}$. Higher formation of DBAA than MBAA as well as TCAA than DCAA and MCAA indicates consecutive attacks by active chlorine and/or bromine. $Cl_2$ and $Br_2$ could be generated not only at the surface of electrode but also by the bulk oxidation of $Cl^-$ and $Br^-$ by reactive oxygen species [91]. In addition, chlorate was the only inorganic chloro-species detected in all the tested anodes, and was likely formed through stepwise electrochemical oxidation of hypochlorite with chlorite as the intermediate [78]. The Ti/$SnO_2$-Sb anode yielded the highest concentration of chlorate, i.e. 70 mg $L^{-1}$, followed by Ti/Pt-$IrO_2$ and Ti/$PbO_2$. The lowest concentration of chlorate was observed for Ti/$RuO_2$-$IrO_2$ and Ti/$IrO_2$-$Ta_2O_5$, i.e. < 10 mg $L^{-1}$.

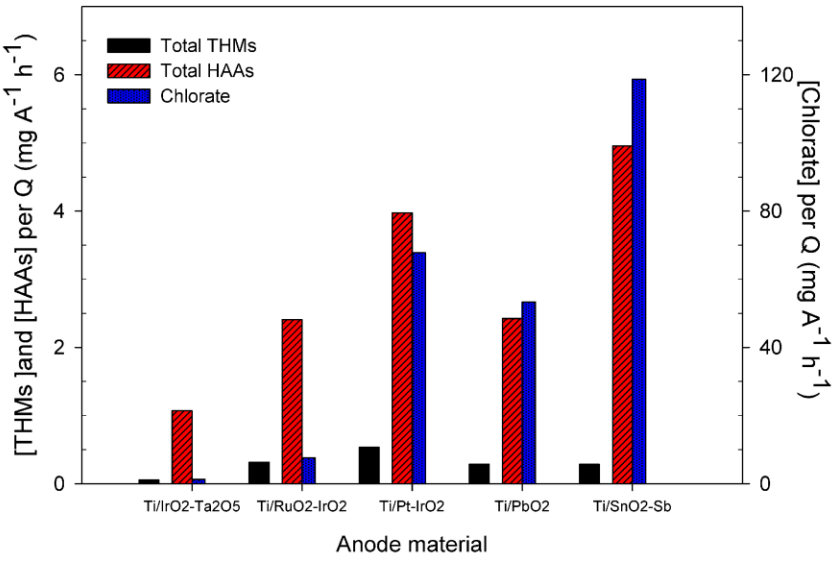


**Figure 7. Overview of the total THMs, HAAs and chlorate observed for the electrode materials investigated, formed after supplying Q = 0.55 Ah $L^{-1}$.**

### 4.1.3. Conclusions

In electrochemical oxidation of ROC considerable differences were observed between so-called "active" and "non-active" materials, and within these groups. Ti/Pt–$IrO_2$ and Ti/$SnO_2$–Sb outperformed the other electrodes tested in our study in terms of COD, DOC, $SUVA_{254}$, colour, $NH_3$–N and DON removal. This higher removal of organics, nitrogen and colour appeared to be associated with the high chlorine formation, and the highest formation of hazardous THMs and HAAs was noted for the abovementioned anodes. Furthermore, EEMs of the oxidised ROC indicated that the main oxidative transformation reactions involved humic and fulvic-like organic matter.

Since Ti/$SnO_2$-Sb anode exhibited the highest $E_C$ and therefore the highest energy investment, i.e. 2.44 ± 0.07 kWh $m^{-3}$, the Ti/Pt-$IrO_2$ electrode would be more attractive for full-scale applications if the formation of halogenated by-products could be avoided. Very high concentration of free chlorine determined at Ti/Pt-$IrO_2$ raised concerns about the increased toxicity of the electrochemically oxidised ROC. In our next study, we investigated the performance of electrochemical oxidation in terms of the removal of trace organic contaminants and toxicity as determined by the Microtox bioassay.

## 4.2. Electrochemical Oxidation at $RuIrO_2$–coated Titanium Electrode

### 4.2.1. Experimental Set-Up

The performance of electrochemical oxidation of ROC was estimated for the removal of target trace organic contaminants, i.e. pharmaceuticals and pesticides. The target analytes were selected based on their consumption data, ubiquity in treated sewage effluent and detected concentrations in the analysed ROC from the AWTP Bundamba, and with the intention of enclosing the compounds with varying physio-chemical properties and belonging to different therapeutic groups (Appendix A). The method developed will be based on the simultaneous extraction of all analytes, thus simplifying considerably sample preparation, and consecutive analysis in positive and negative ionisation mode by the $LC/MS^2$ method described in the Appendix A. The target trace organic contaminants were 21 pharmaceuticals: anti-inflammatory drugs ACTP, IBP and DCF, analgesic drug TML, stimulant drug CAFF, diuretic HCT, antibiotics ENR, NFL, ROX, LNC, TMP and SDZ, anticonvulsant drugs PNT and CBZ, antidepressants SRL, CTP and VNF, lipid regulator GMF, antihistamine drug RNT, X-ray agent IPM, and β-blocker MTP; also, 7 frequently encountered pesticides were included in the method: DIU, DZN, TPR, ATZ, 2,4-D, DEET and MET.

Target analytes were spiked in the ROC samples to final concentrations in the range of 7.8 (CBZ) to 37.4 $\mu g\ L^{-1}$ (IPM) (Appendix C). The influence of operational mode, current density, and applied electrical charge on the oxidation efficiency was investigated. The baseline toxicity of electrochemically oxidised ROC was evaluated in the bioluminescence inhibition tests (Microtox) using the marine bacterium *Vibrio fischeri*. When operating in continuous mode, two different ROC samples were used, marked as ROC-1 and ROC-2, both from the AWTP Bundamba but originating from different sample batches, in order to test the effect of ROC matrix on the removal of trace organic contaminants.

### 4.2.2. Results and Discussion

Figure 8 illustrates the observed removal of DOC and $SUVA_{254}$, and measured free and total chlorine during continuous oxidation of ROC-1 and ROC-2. Oxidative degradation of the organics in ROC was achieved only when the current density was increased, i.e. $J \geq 100$ A $m^{-2}$. Removal of DOC was observed to be more efficient for ROC-2 than ROC-1, i.e. 8.9 ± 1.4% and 26.5 ± 2.3% removal at J=250 A $m^{-2}$. Considering that the initial chloride ion concentrations as well as residual chlorine concentrations measured for the ROC-1 and ROC-2 were similar, more efficient mineralisation in the latter case is possibly a consequence of the higher initial specific aromaticity of ROC-2 as expressed by its $SUVA_{254}$ value (Appendix C). The enhanced formation of putative electron shuttles (e.g. porphyrins, quinones) from the aromatic fraction could be responsible for the higher NPOC removal observed for ROC-2, as these species accelerate the electron transfer between the organic matter and oxidants [92]. The removal of $SUVA_{254}$ was also enhanced with increasing the supplied charge, and 28.7 ± 1.8% and 42 ± 2.4% removal was observed J=250 A $m^{-2}$ for ROC-1 and ROC-2, respectively.

On the other hand, when oxidising the ROC in batch mode, more complete removal of DOC was achieved for ROC-1, i.e. (30.7 ± 1.8% at 250 A $m^{-2}$, and 1.45 kA h $m^{-3}$ of supplied electrical charge) (Figure 9). When comparing the oxidation of ROC-1 in the two operational modes tested, the same values of $Q_{sp}$ (~770 Ah $m^{-3}$) and $J$ (250 A $m^{-2}$) in batch and continuous and oxidation of ROC-1 rendered DOC removal of ~27 and 8.9 ± 1.4%, and $SUVA_{254}$ was ≥1 and 0.71 (i.e. 28.7 ± 1.8% of $SUVA_{254}$ removal), respectively. Thus, the removal of organic carbon depended on the accumulation of long lived oxidants (e.g. $HClO/ClO^-$, HOBr and $H_2O_2$) in the bulk liquid.

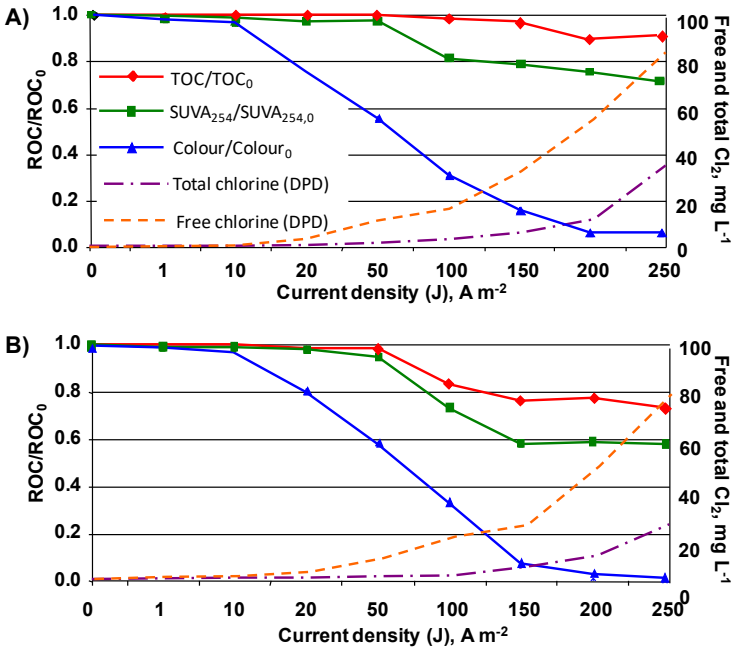


**Figure 8. Removal of DOC, $SUVA_{254}$ and generation of free and total chlorine during anodic oxidation in continuous mode of: A) ROC-1 and B) ROC-2 spiked with the trace organic contaminants, vs *J* (in A $m^{-2}$).**

For the final DOC removal achieved in continuous (8.9 ± 1.4%) and batch mode (30.7 ± 1.8%) oxidation of ROC-1 at 250 A $m^{-2}$, energy consumption was 0.704 kWh $g_{DOC}^{-1}$ and 0.350 kWh $g_{DOC}^{-1}$, respectively. Thus, more efficient removal of organic matter is achieved in batch mode, and the energy input per mass unit of DOC removed is lower compared to the continuously operated reactor. Nevertheless, lower throughput of batch mode compared to a continuous mode may increase significantly the total cost of the treatment.

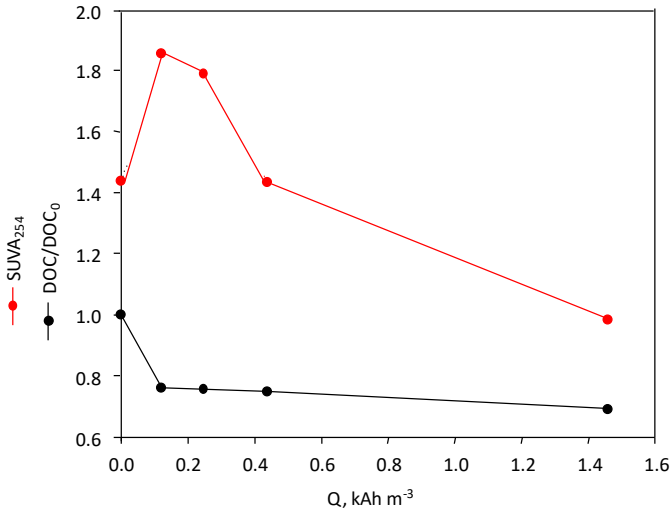


**Figure 9. DOC removal and $SUVA_{254}$ vs specific electrical charge (*Q*) in anodic oxidation in batch mode at 574 *J* = 250 A $m^{-2}$ of ROC-1 spiked with the trace organic contaminants.**

At the lowest current densities applied, i.e. J=1 and 10 A $m^{-2}$, the concentrations of target contaminants remained relatively constant, with more significant decreases observed for only three compounds, i.e. RNT (30 and 60% removal, respectively), DZN (30% removal) and SRL (~70% removal) (Appendix C). At these current densities, the anode potentials were very low, 0.95 and

1.15 V vs Ag/AgCl, respectively. Thus, there was no chlorine production and very little molecular oxygen production, and the most likely mechanism of removal of the abovementioned contaminants was direct oxidation. In the case of positively charged RNT, and negatively charged DZN, it is possible that these two compounds adsorbed onto the MMO anode surface using sulfur atom with two and three lone electron pairs as a ligands, respectively. Considering the adsorption properties of $RuO_2/IrO_2$ anodes, very high removal of SRL even at $J = 1$ A m$^{-2}$ can be explained by its hydrophobic nature, as this compound has the highest log $K_{OW}$ value (5.29) among the selected analytes. For the rest of the compounds, no direct oxidation was observed.

It is generally considered that direct anodic oxidation has a minor contribution to the overall oxidation of organics at potentials higher than the threshold for water electrolysis, i.e. 1.23 vs SHE (pH=0) [69]. Above this potential, direct electron transfer between the adsorbed organic compound and the electrode is less likely due to evolution of $O_2$, as well as mass transfer limitations. Thus, electrochemical oxidation will mainly rely on oxidation via the indirect mechanisms, e.g. reactive oxygen species (ROS). In the presence of $Cl^-$ ions indirect oxidation of organic contaminants via $Cl_2/HClO/ClO^-$ will be promoted. $HClO/ClO^-$ is a long-lived oxidant able to diffuse away into the bulk liquid and react chemically with the organics [93].

The increase in current density to 30 and 50 A m$^{-2}$ led to a significant improvement in the removal of ACTP (40% and 90%), DCF (40% and 88%), SDZ (44% and 88%), DZN (40% and 70%) and NFL (65% and 90%), and led to a complete removal of RNT (100%) and LNC (>90% and 100%, respectively) (Appendix C). At $J = 30$ A m$^{-2}$ the concentration of combined chlorine was 3.0 mg L$^{-1}$, indicating that oxidation of chloride ions to chlorine had occurred and that chloride had already reacted to form organic and inorganic chloramines. A previous study [94] identified that the activity of $RuO_2/IrO_2$ electrode increases at potentials higher than 1.3 V vs SHE, due to the evolution of $Cl_2$. Considering the activity of the abovementioned compounds towards chlorine [95-98], their removal could be explained by the reaction with $HOCl/ClO^-$. However, under the same conditions other compounds known to have high affinity towards free chlorine were removed to a much less extent, e.g. TMP (25% and 46%), GMF (11% and 43%), CAFF (14% and 26%), DIU (14% and 33%), MTP (10% and 30%) at $J = 30$ and 50 A m$^{-2}$, respectively [95-97, 99-102].

Furthermore, at $J = 100$ A m$^{-2}$ only 60% of CAFF was oxidised in both ROC-1 and ROC-2, despite its reported high reactivity with free chlorine in the pH range found in our experiments (Figure 10) [102]. At the same time, ENR completely disappeared although it is known to react very slowly with chlorine [98]. Also, 100% removal of CBZ at 150 A m$^{-2}$ was probably achieved by oxidants other than chlorine, since this compound is recalcitrant even towards the much stronger oxidant $ClO_2$ [103]. The largely incomplete oxidation of chlorine-oxidisable compounds and unexpectedly rapid disappearance of others known to react slowly with chlorine suggest that other oxidants in the bulk and/or surface reactions may play an important role. Besides reacting in the bulk, chlorine can react electrochemically at the anode forming adsorbed chloro- and oxychloro-radicals, which mediate the degradation of adsorbed organics [94]. Also, in the presence of $Fe^{2+}$ and $Mn^{2+}$ ions in ROC and electrogenerated $H_2O_2$, contribution of Fenton reaction to bulk oxidation can be expected.

Compounds that were more recalcitrant during electrochemical oxidation were characterised by either the absence of nucleophilic substituents that have an activating effect on the aromatic ring (e.g. IBU, PNT, MET, DEET), or by the decreased electron density on the aromatic ring due to the presence of electrophilic halogen groups (e.g. 2,4-D), ATZ, TPR and IPM). Further increasing the applied current density up to 250 A m$^{-2}$ ($Q_{sp}$ = 769.2 A h m$^{-3}$) led to an enhanced oxidation of ATZ (92%), MET (57% and 84%), IBU (46% and 67%) and PNT (61% and 67%) in the ROC-1 and ROC-2, respectively. On the other hand, only around 30–40% of 2,4-D, TPR and IPM removal was observed under these conditions, while DEET could not be oxidised. For most of the target contaminants, similar removals of were observed in ROC-1 and ROC-2. For some compounds, e.g. CTP, VNF, HCT, IBU, MTP and DIU significantly higher removals were observed in ROC-1.

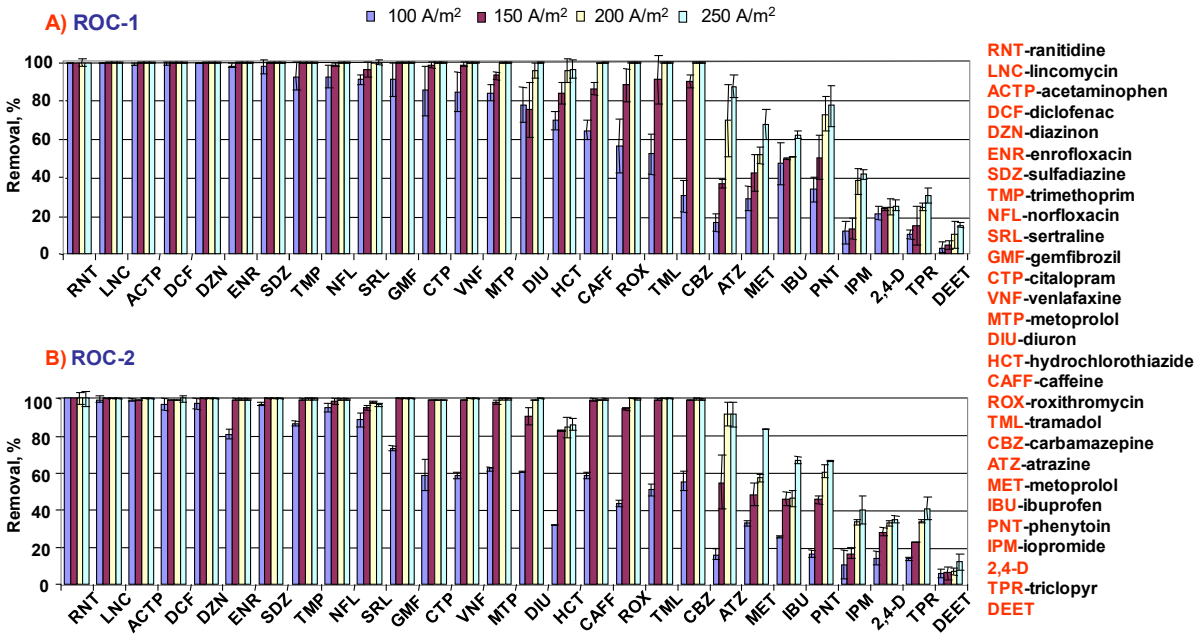


**Figure 10. Removals of target analytes during anodic oxidation in continuous mode of: A) ROC-1, and B) ROC-2 spiked with the trace organic contaminants, for the tested *J* in the range 100–250 A m$^{-2}$.**

When ROC was oxidised in batch mode at $J = 250$ A m$^{-2}$, significantly faster removal of all target contaminants was observed. Similar to continuous mode, TPR, 2,4-D, IBU, IPM, MET, PNT, ATZ, and DEET were again more persistent than the other analysed compounds (Figure 11). The oxidation of all target compounds was more efficient in batch mode due to the accumulation of oxidants in the bulk liquid, and consequently more intense indirect oxidation. With triclopyr as exception, all persistent trace compounds were completely oxidised in batch mode after applying 1.45 kA h m$^{-3}$. Therefore, these compounds require considerably higher electrical charge supplied per anolyte unit volume and longer residence times in order for indirect oxidation to occur.

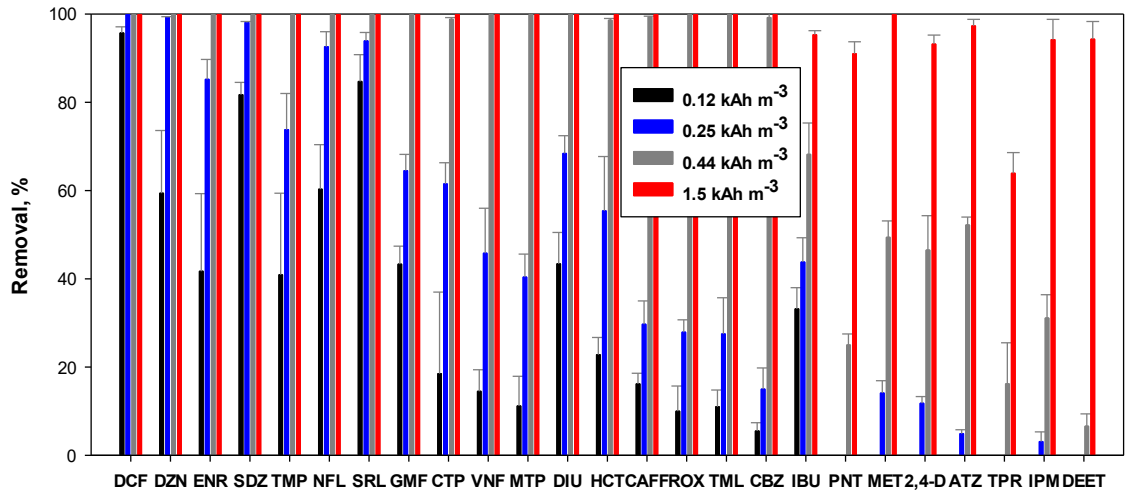


**Figure 11. Removals of target analytes during anodic oxidation in batch mode, *J*=250 A m$^{-2}$.**

In the case of MMO electrodes, particularly active anodes such as Ti/RuIrO$_2$ with low capability for OH$^{\bullet}$ generation, addition of Cl$^-$ has been reported to enhance the removal of a range of organic compounds, including dyes, pesticides, endocrine-disrupting compounds (EDCs) and other persistent contaminants [104-110]. Several studies have indicated that the superiority of non-active MMO electrodes (capable of generating OH$^{\bullet}$) over active MMOs such as RuO$_2$ practically vanishes in the

presence of chloride ions due to the promotion of chlorine-mediated electrolysis [76, 111, 112]. However, most of these studies were performed with supporting electrolyte solutions, and concerns have been raised about the increase in toxicity in chlorine-mediated electrolysis of real waste streams [113-116].

In order to investigate the toxicity of a mixture of trace organic contaminants and their oxidation byproducts, *Vibrio fischeri* bioassays were performed on the extracted samples of ROC oxidised in both batch and continuous mode. The majority of matrix components such as salts, particulates, and generated oxidants were removed by the SPE sample pre-treatment. The baseline toxicity determined in this bioassay provides an integrative measure of the combination of chemicals, whereas the contribution of each chemical is weighted only by its hydrophobicity.

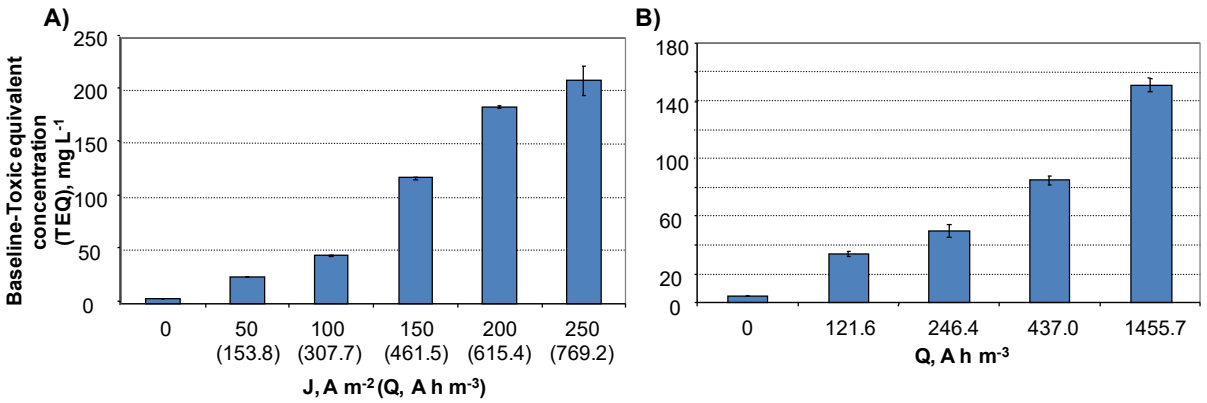


**Figure 12. Bioluminescence inhibition of ROC-1 spiked with target contaminants on *Vibrio fischeri* at 30 min expressed as baseline – TEQ in mg $L^{-1}$ in: A) continuous experiment conducted at $J$ = 50, 100, 150, 200 and 250 A $m^{-2}$, B) batch experiment conducted at $J$ = 250 A $m^{-2}$. Each replicate of the sample was tested in duplicates, at eight different concentrations. Results are expressed as average of duplicates ± standard deviation.**

While the sample extracts of the untreated ROC-1 spiked with target analytes exhibited a TEQ value of 3.7 ± 0.02 mg $L^{-1}$, the toxicity of sample extracts of ROC-1 oxidised in continuous mode drastically increased with increased current density (209.1 ± 14.4 mg $L^{-1}$ at $J$ = 250 A $m^{-2}$) (Figure 12). Similarly, batch mode oxidation increased the toxic response of *V. fischeri* from the initial 4.3 ± 0.1 mg $L^{-1}$ to 151.0 ± 4.9 mg $L^{-1}$ after applying 1.45 kA h $m^{-3}$. It is important to note that the Microtox bioassay cannot distinguish between the effects of the SPE enriched trace organic pollutants and the co-extracted organic matter. The hydrophobic (i.e. peptides and protein fragments) and/or aromatic fraction of the organic matter (fulvic- and humic-like substances) might have contributed to the observed increase in the toxicity, although this fraction is only partially retained on the SPE cartridge. Nevertheless, TEQ values determined for the ROC oxidised in batch and continuous mode are significantly higher than the values that could be expected owing to any potential by-products of the selected micropollutants.

### 4.2.3. Conclusions

In electrochemical of ROC spiked with a mixture of pharmaceuticals and pesticides at Ti/$RuIrO_2$ electrode, the removal of DOC depended on the accumulation of oxidants in the bulk liquid. Based on the changes in specific aromaticity, expressed as $SUVA_{254}$, it appears that the formation of chloro-, bromo- and hydroxyl-substituted aromatic intermediates was enhanced due to the prolonged indirect oxidation. Furthermore, the employed electrode was capable of oxidising most of the selected compounds. The most persistent contaminants had electrophilic substituents at the aromatic ring (2,4-D, ATZ, TPR, IPM), or an aromatic ring insufficiently activated towards nucleophilic attack (IBU, PNT, MET, DEET). Nevertheless, the results of the bioluminescence bioassay imply the formation of toxic by-products during both continuous and batch electrochemical oxidation of ROC. It seems that the participation of oxidants such as active chlorine and bromine in indirect oxidation at active Ti/$RuIrO_2$ anode causes transformation of the organic compounds into their halogenated derivatives.

## 4.3. Comparison of Electrochemical Oxidation Pathways and By-products at Ti/RuIrO$_2$ and Ti/SnO$_2$-Sb Electrodes

### 4.3.1. Experimental Set-Up

Electrochemical oxidation pathways of a model organic micropollutant, the β-blocker metoprolol (MTP), were investigated in a real ROC matrix. MTP is used for the treatment of a range of cardiac conditions such as hypertension, angina and arrhythmias, and it is commonly found in wastewater effluents and surface water [117]. In the previous experiments, MTP exhibited medium removal efficiency at Ti/RuIrO$_2$ electrodes (e.g. 100% removal in continuous oxidation at 100 A m$^{-2}$, Figure 10). We investigated the electrochemical oxidation pathways of MTP using titanium anodes coated with active layer $Ru_{0.7}Ir_{0.3}O_2$, and non-active SnO$_2$-Sb metal oxide layers. Two current densities were investigated, $J = 100$ and 250 A m$^{-2}$. The ability of a hybrid QqLIT-MS mass spectrometer to establish fragmentation pathways in MS$^3$ sequential product ion spectra experiments enabled elucidation of electrochemical oxidation pathways and identification of metoprolol by-products. Given that not all by-products can be readily quantified by chemical analysis, we additionally evaluated the toxicity of the reaction mixture using the marine bacterium *Vibrio fischeri*, and a combined algae test with *Pseudokirchneriella subcapitata*, respectively.

### 4.3.2. Results and Discussion

In total 25 by-products were identified in electrochemical oxidation of MTP. Some of the products such as P253 and P237 were formed by the cleavage of bonds in the MTP molecule (e.g. methyl and methoxy group, respectively), possibly by the action of radical and non-radical reactive oxygen species (ROS). Most of these products were previously identified as products of MTP oxidation by OH$^{\bullet}$ formed in radiolytic oxidation [118, 119] and ozonation [120].

However, several chlorine- and bromine-containing by-products were recorded at both anodes and current densities tested (Figure 13). For example, the parent compound underwent chlorination and bromination of the benzene ring. Active oxidants HOCl/OCl$^-$ and HOBr/OBr$^-$ are formed at the anodes by the oxidation of Cl$^-$ and Br$^-$ ions present in the ROC. In spite of occurring in much lower concentrations than Cl$^-$, Br$^-$ (1.48 mg L$^{-1}$ in ROC) is an important scavenger of OH$^{\bullet}$ [121], and HOBr is usually more reactive than active chlorine, especially with phenolic compounds [122]. This is especially concerning considering that brominated by-products are suspected to be more toxic, carcinogenic and mutagenic to humans than their chlorinated analogues [123]. Here, MTP and its primary oxidation by-products were further transformed into (poly)chlorinated and chloro-bromo derivatives. For example, fast formation of MTP-Cl (P301), MTP-Cl$_2$ (P335), MTP-Br (P345) and MTP-BrCl (P379) was observed at the beginning of the experiment at both Ti/RuIrO$_2$ and Ti/SnO$_2$-Sb anode.

Generally, the formation of chlorinated by-products in electrochemical oxidation is assigned to active chlorine (i.e. HClO/ClO$^-$) dissolved in the bulk liquid, although radical reactive halogen species (RHS) formed in reactions of Cl$^-$ and Br$^-$ ions with OH$^{\bullet}$ (e.g. Br$^{\bullet}$, $Br_2^{\bullet-}$, Cl$^{\bullet}$, $Cl_2^{\bullet-}$, and $ClBr^{\bullet-}$) are likely play an important role [124]. Preferential chlorination of the benzene ring is likely a consequence of protonated amine group, which is less reactive toward active chloro-species. Nevertheless, differences between the electrochemical treatment in the presence of Cl$^-$ and aqueous chlorination could also be caused by surface electrochemical reactions, in particular adsorbed chloro and oxychloro radicals [125]. As postulated by Comninellis [70], the type of anode coating is expected to influence the electrochemical reaction pathways and by-products distribution due to different formation rates of non-selective OH$^{\bullet}$ formed by water discharge. When comparing the degradation of phenol on Ti/SnO$_2$-Sb and Ti/RuO$_2$ anodes, Li *et al.* [126] explained poor performance of the latter by the shortened lifetime of OH$^{\bullet}$ that hindered a more complete oxidation. On the other hand, Panizza and Cerisola [88] demonstrated that in practice OH$^{\bullet}$ accumulate only in the vicinity of a SnO$_2$-coated anode.

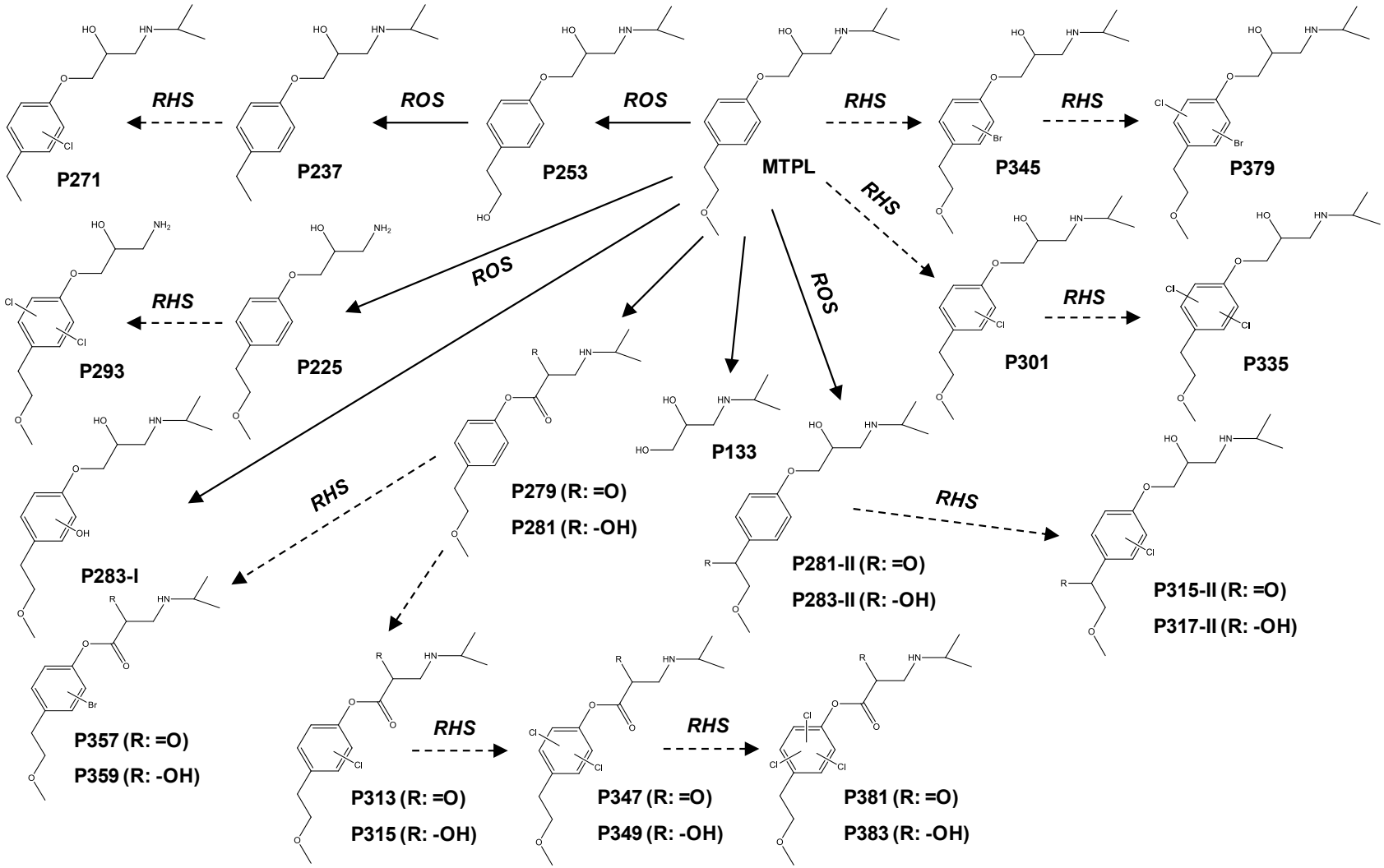


**Figure 13. Proposed electrochemical oxidation pathways of metoprolol (MTP) in ROC. ROS-reactive oxygen species, RHS-reactive halogen species.**

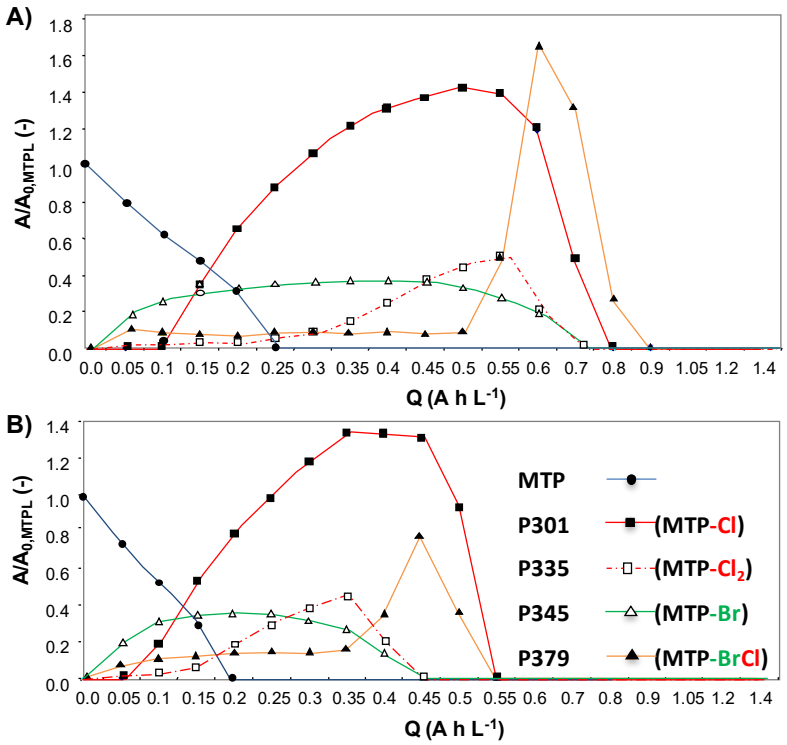


**Figure 14. The peak areas of MTP and its halogenated derivatives P301, P335, P345 and P379, formed during electrochemical oxidation, normalised to the initial value of the peak area of MTP ($t = 0$) presented vs. Q (A h $L^{-1}$): A) Ti/$RuIrO_2$, $J$ = 250 A $m^{-2}$, and B) Ti/$SnO_2$-$Sb_2O_5$, $J$ = 250 A $m^{-2}$.**

Although a more significant contribution of $OH^{\bullet}$ was expected for the Ti/$SnO_2$-Sb anode, near identical electrochemical oxidation pathways were observed for both anodes. When comparing Ti/$RuIrO_2$ and Ti/$SnO_2$-Sb anodes under the same conditions of flow rate, pH and temperature, the generation of both halogenated and non-halogenated by-products of MTP was enhanced on the active, $RuIrO_2$-coated electrodes. The rate of formation and disappearance of by-products was observed to be significantly faster for Ti/$SnO_2$-Sb anode (Figure 14). Similar effect was observed with the increase in current density for each anode, as illustrated for Ti/$RuIrO_2$ in Figure 15. Similar results were obtained for using Ti/$PbO_2$ anodes. Panizza *et al.* [127] observed faster formation of oxidation intermediates and in higher amounts, as well as their faster degradation with the increase in current density. Here, increase in current density lowered the accumulation of intermediates at both electrodes.

As the Ti/$SnO_2$ anode provided the fastest degradation, an additional experiment was performed with this anode at $J = 250$ A $m^{-2}$ to test the toxicity of the ROC after treatment. The non-specific toxicity, expressed as baseline-TEQ increased substantially in both ROC alone and ROC spiked with 50 µM MTP for the tested toxicity endpoints. MTP at 50 µM did not contribute to the mixture toxicity at all. Thus all increase in toxicity could be attributed to the transformation products, be it from MTP degradation or from the oxidation of natural organic matter (NOM). Toxicity increased linearly with the applied charge for both the spiked and unspiked samples (Figure 16). Baseline-TEQ are concentration additive in mixtures, therefore it was possible to subtract the contribution of the products formed during the electrochemical oxidation from the high background of increasing toxicity in the non-spiked ROC sample.

Introduction of –Cl and –Br substituents in the organic molecule are expected to augment significantly its biological activity and toxicological properties. While the transformation products were not quantified due to lack of standards, the sum of the peak areas weighted by their relative hydrophobicity relative to MTPL ($\mathbf{t}_R/t_{R,MTPL}$) can be used as a proxy for the prediction of mixture toxicity of the identified transformation products as is explained in more detail in the Appendix D. This measure (sum($A/A_{0,MTPL} * \mathbf{t}_R/t_{R,MTPL}$)) correlates linearly with applied charge, and thus the formed

by-products correlate linearly with the increase in mixture toxicity. Given the good agreement of the experimental and calculated increase in toxicity, we can safely conclude that the formed products are very problematic as they cause the toxicity to increase by a factor of 40–60 times depending on the toxicity endpoint.

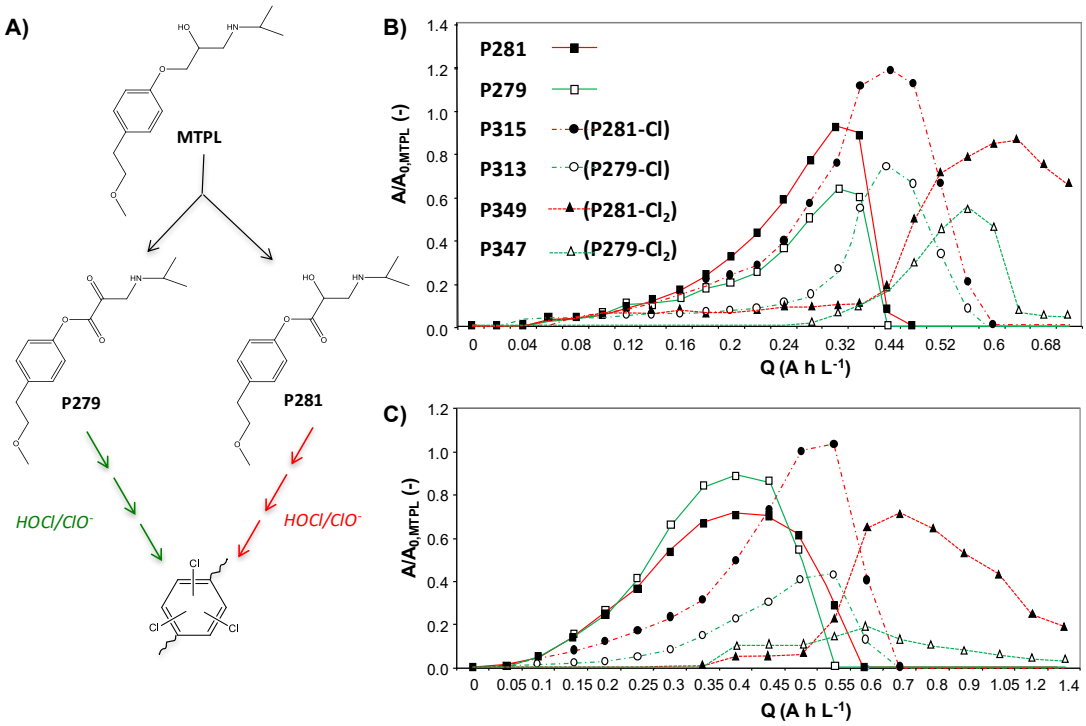


**Figure 15. The peak areas of by-products of MTP P279 and P281, and its halogenated derivatives P313, P315, P347 and P349, formed during electrochemical oxidation, normalised to the initial value of the peak area of MTP ($t$ = 0) presented vs. Q (A h L$^{-1}$): A) scheme of the formation of P279 and P281, and further electro-chlorination of their aromatic moieties, B) Ti/RuIrO$_2$, $J$ = 100 A m$^{-2}$, and C) Ti/RuIrO$_2$, $J$ = 250 A m$^{-2}$.**

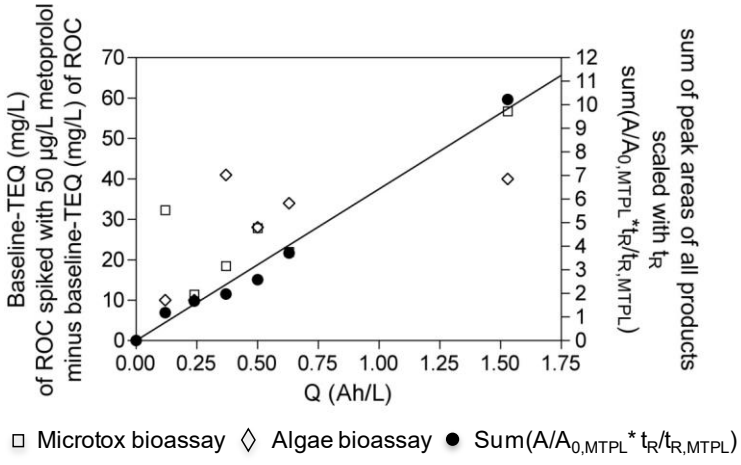


**Figure 16. Increase in toxicity, expressed as baseline-TEQ of spiked ROC minus ROC, and sum of peak areas of the identified products, scaled with the retention times in the HPLC to account for toxicity differences due to hydrophobicity as a function of the applied charge during the electrochemical oxidation experiment.**

### 4.3.3. Conclusions

The results of the LC-MS analysis indicated that irrespective of the electrode coating the same oxidant species participated in electrochemical transformation of MTP in ROC. Although Ti/$SnO_2$-Sb exhibited higher oxidising power for the same applied specific electrical charge, detrimental effect of $Cl^-$ and $Br^-$ and generation of large fractions of chloro-, chloro-bromo- and bromo derivatives was observed for both electrode coatings. Degradation rates of MTP and its degradation products were generally higher for the Ti/$SnO_2$-Sb anode. Nevertheless, the formed polychlorinated and chloro-bromo derivatives can be expected to be more persistent and might require impractical reactor residence times to be further degraded. Furthermore, results of the bioluminescence inhibition test with *Vibrio fischeri* and the combined algae test with *Pseudokirchneriella subcapitata* indicated a substantial increase in non-specific toxicity of the reaction mixture due to the formed halogenated by-products.

## 4.4. Reductive Electrochemical Post-Treatment of the Electro-Oxidised Reverse Osmosis Concentrate

### 4.4.1. Experimental Set-Up

In the present work, we have investigated the efficiency of electrochemical reduction in dehalogenating the chlorinated and brominated by-products formed during electrochemical oxidation of ROC. The analysis of halogen-specific AOX was employed for evaluating the efficiency of electro-reduction in dehalogenating the by-products formed during the electrochemical oxidation of ROC. In addition, THMs and HAAs were also analysed, by-products which represent small fractions of AOX. The toxicity of ROC at various points was determined using *Vibrio fischeri* bioassays (Microtox) [85].

The reduction experiments were performed galvanostatically in a divided electrolytic cell (Type B, Figure 3) using a single pass recirculation of both catholyte and anolyte. Resin-impregnated graphite supplied by Morgan AM&T (Revesby, Australia) was used as a cathode at a fixed current of -240 mA, which resulted in $E_{CA}$= (-2.1)-(-1.9) V vs. SHE. The carbon-based electrodes are robust, mechanically stable, have a high surface area, low cost, and a reasonably high over-potential for $H_2$ evolution [128, 129].

### 4.4.2. Results and Discussion

Figure 17 depicts changes in the concentration of AOCl, AOBr and AOI and toxicity to *Vibrio fischeri* expressed as TEQ of the initial ROC, electrochemically oxidised ROC ($ROC_{ox}$), electrochemically reduced $ROC_{ox}$ and recirculated $ROC_{ox}$ in open circuit. The obtained results showed partial removal of low MW by-products THMs and HAAs. While all the concentration of THMs was substantially decreased (i.e. the removal of tTHMs at 4.8 Ah $L^{-1}$ was 92%), the degradation of polychlorinated HAAs was accompanied by the formation of its monochlorinated derivatives, which seemed to be persistent to further dechlorination and were accumulated throughout the experiments. However, although the concentration of tHAAs remained constant during the open circuit experiments (i.e. no applied current), a decrease in the concentration of tTHMs was observed. After 72 h recirculation of $ROC_{ox}$, the obtained removal was 81%. This suggests that another mechanism of loss of THMs was their adsorption onto the cathode, besides volatilisation which occurred in both open circuit and galvanostatic experiments. The decrease in the THMs and HAAs concentrations was clearly enhanced by supplying the current to the cathode in the reduction experiments. However, it is uncertain whether this enhancement was due to their reductive dehalogenation or changed adsorption properties of cathodically polarised carbon.

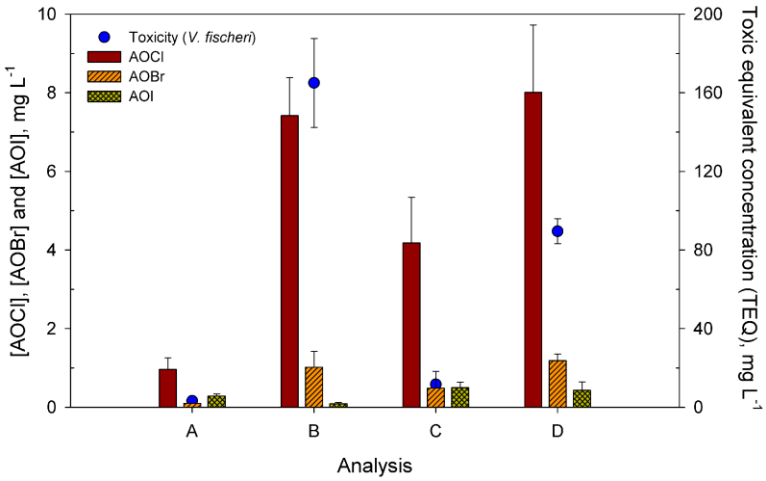


**Figure 17. Concentration of halogen-specific AOX (i.e. AOCl, AOBr and AOI) and baseline non-specific toxicity measured on four different sample conditions: A) initial untreated ROC, B) anodically pre-oxidised ROC ($ROC_{ox}$) as initial sample for reduction process, C) cathodically reduced $ROC_{ox}$ ($t$ = 72 h, $I$ = 240 mA), and D) recirculated $ROC_{ox}$ without applying current ($t$ = 72 h).**

The decrease of TEQ was then observed in both electrochemical cathodic reduction and open circuit experiments. As shown in Figure 17, i.e. TEQ was decreased from 165 ± 23 mg $L^{-1}$ to 12 ± 1 mg $L^{-1}$ and 90 ± 6 mg $L^{-1}$ when cathodic current was -240 mA and 0 mA, respectively. On the other hand, while in the reduction experiments the concentration of AOCl and AOBr was decreased, an increase of both AOCl and AOBr was observed in the open circuit experiments. This was interpreted as a consequence of the presence of residual chlorine and bromine in the electrochemically oxidised ROC which, in the absence of reductive current, continued to react further in the bulk solution since the samples were not quenched after oxidation. When current was applied to the cathode, active chlorine and bromine are rapidly reduced and thus their bulk oxidation reactions with the organic matter are significantly lowered. As increase in AOCl an AOBr can be expected to increase the baseline-TEQ value, the discrepancy in the results for AOCl/AOBr and TEQ in the open circuit experiments could be explained by the fact that TEQ decrease was caused by the adsorption of more hydrophobic fraction of AOCl/AOBr. More hydrophobic halogenated organics formed during electrochemical oxidation of ROC are likely to be well retained in the SPE cartridge during sample extraction, and they were likely responsible for the elevated TEQ of the $ROC_{ox}$. Consequently, adsorption of this more hydrophobic AOCl and AOBr onto the carbon cathode in open circuit experiments may have been the reason for a drastic reduction of TEQ. A slight increase in the AOCl and AOBr measured in the same open circuit experiments may represent the remaining, more hydrophilic fraction, and halogenated organics that were not contributing as much to the TEQ determined upon the SPE treatment of ROC samples. In the case of AOI, a slight increase of its concentration observed in both reduction and open circuit experiments. This could be explained by the faster reaction of residual HOI with the organic matter in the bulk, even when the cathodic current was applied. Nevertheless, since the concentration of AOI was lower than AOCl and AOBr, their contribution to the overall AOX was negligible.

The efficiency of overall reductive dehalogenation, i.e. cleavage of C-X bonds in THMs, HAAs and other halogenated organics, was estimated based on the release of $Cl^-$, $Br^-$ and $I^-$ ions. Increase in $Cl^-$ ion concentration to up to 375 mg $L^{-1}$ at 4.8 Ah $L^{-1}$ suggested partial dechlorination of the organics in $ROC_{ox}$. However, estimated release of chloride ions from the reduction of active chlorine determined as FAC (FAC> 300 mg $L^{-1}$, measured by the DPD method) was at least 600 mg $L^{-1}$. Thus, the efficiency of C-Cl bond cleavage in the determined AOCl compounds was expected to be low. As for bromide and iodide ions, their concentrations were only slightly increased, i.e. from 0.4 and 0.05 mg $L^{-1}$ to 1.2 and 0.83 mg $L^{-1}$, respectively, measured at 4.8 Ah $L^{-1}$.

### 4.4.3. Conclusions

Although a decrease in AOCl/AOBr and toxicity was observed during reductive electrochemical treatment of the $ROC_{ox}$, this decrease seems to be a consequence of the adsorption of AOX onto the carbon cathode, rather than its dehalogenation. The measured release of chloride ions seemed to correspond to the reduction of active chlorine determined as FAC by the DPD method. Nevertheless, the percentage of the measured increase in $Cl^-$ concentration assigned to FAC reduction, and to the reduction of chlorinated organics could not be determined. Overall, considering the amount of supplied electrical charge (4.8 Ah $L^{-1}$) and concentration of remaining AOX, electrochemical reduction at carbon cathode does not seem to be a promising option for the post-treatment of the electrochemically oxidised ROC.

## 4.5. Electrochemical Oxidation at Boron Doped Diamond Electrodes

In electrochemical oxidation, two reaction zones of an anode can be distinguished: *i)* electrochemical reaction zone (i.e. anodic surface and diffusion layer) where direct oxidation by electron transfer and/or $OH^{\bullet}$ occurs; and *ii)* chemical reaction zone (i.e. bulk liquid) where compounds are oxidised by electrogenerated oxidant species (i.e. indirect oxidation). It is very hard to distinguish between the contribution of direct and indirect oxidation as they will be influenced by multiple factors (e.g. anode coating, current density, flow dynamic regime, waste stream matrix, reactor design). It is generally assumed that the contribution of direct electron transfer between organic matter and anode is insignificant under the conditions of high current density [70, 130].

Among the existing materials, the highest formation of $OH^{\bullet}$ has been reported for novel BDD electrode, characterised by the high $O_2$ overpotential electrode. However, although BDD electrodes are expected to generate more $OH^{\bullet}$ than conventional MMO electrodes, competition between electro-chlorination and advanced oxidation by $OH^{\bullet}$ can be expected [131]. Generation of undesired chlorinated by-products such as THMs and haloacetic acids HAAs has also been reported in electrochemical oxidation of ROC at BDD electrodes [77]. The authors have concluded that at the optimum current density of 100 A $m^{-2}$, their formation can be minimised to concentrations lower than the standards for drinking water established in European and EPA regulations.

### 4.5.1. Experimental Set-Up

In this study, electrochemical oxidation at BDD electrode was evaluated for the removal of COD and DOC, as well as the formation of THMs and HAAs. Additionally, extent of electro-halogenation of the organic matter was investigated by measuring the AOX. The experiments were performed at two pH values, controlled pH 6–7 and at pH 1–2 (i.e. no pH adjustment). Details of the experimental set-up are described in the Appendix E. To determine the potentials of OER and $Cl_2$ evolution at the two pH values investigated, linear sweep voltammetry (LSV) was performed. LSV is a technique where the current at a working electrode (i.e. BDD anode) is measured while its potential is swept linearly in time, and oxidation (or reduction) of species is registered as a peak or trough in the current signal at the potential at which the species begins to be oxidised or reduced.

### 4.5.2. Results and Discussion

The LSVs of $Cl_2$ and $O_2$ evolution obtained for ROC at acidic and neutral pH confirmed that these two reactions are in competition at both pH values, with acidic pH increasing the difference between their onset potentials from 0.1 V to 0.2 V. Lower pH is expected to favour the chlorine evolution reaction [132]. High concentrations of active chlorine (i.e. $HClO/ClO^-$) were observed at both pH values (Appendix E), although the increase in free and total chlorine concentrations was less pronounced at pH 1–2 than at pH 6–7 due to $Cl_2$ stripping into the gas phase from the bulk water under the acidic pH conditions [133].

Under galvanostatic condition ($I$ = 510 mA), constant $E_{AN}$ was observed (i.e. 3.4 - 3.7 V vs. SHE), and thus electro-generation of $OH^{\bullet}$ was ensured at both pH 2 and pH 6-7. Figure 18 depicts the profile of COD and DOC removal during the electrochemical oxidation in both pH conditions. An enhanced COD removal was observed at pH 2 compared to pH 6-7, resulting its faster complete removal, i.e. after 5.2 Ah $L^{-1}$. This was likely a consequence of more intense electro-chlorination and HOCl being the dominant species at pH 2, since the chemical reactivity of chlorine species decreases with the pH increase due to the dissociation of HOCl to less reactive $OCl^-$ [133]. However, although complete removal was already observed at 5.2 and 6.6 Ah $L^{-1}$, the corresponding DOC removal was only 48% and 59% at acidic and circumneutral pH, respectively. At the final point ($Q$ = 10.9 Ah $L^{-1}$), the remaining DOC was 15 and 13 mg $L^{-1}$ which was not oxidisable by the dichromates ($K_2Cr_2O_7$) in the COD test kit. While more intense electro-chlorination at acidic pH results in the enhanced overall oxidation of organics, it does not improve the mineralisation of the organic matter. A complex scenario of oxidation mechanisms can be expected since the participation of $OH^{\bullet}$ in the oxidation of organic matter is lowered, particularly at acidic pH. The formed HOCl/OCl- and halide ions (mostly $Cl^-$) present in the bulk act as efficient scavengers of $OH^{\bullet}$ generated at the BDD anode, yielding $Cl_2^{\bullet-}$ species with $HOCl^{\bullet-}$ and $Cl^{\bullet}$ as intermediates [121, 134]. Therefore, the less reactive radical and non-radical RHS were responsible for the higher COD removal, but were less capable of breaking the organic bonds than $OH^{\bullet}$. On the other hand, participation of other oxidants, e.g. $S_2O_8^{2-}$ can also be expected to enhance DOC removal in circumneutral pH [135].

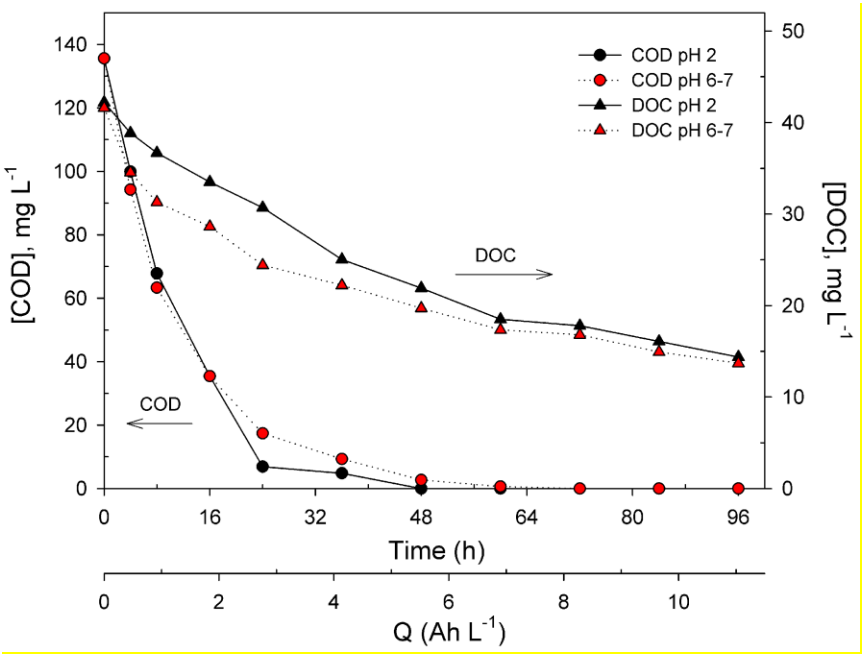


**Figure 18. Removal of: (●●) COD and (▲▲) DOC vs. supplied specific electrical charge (*Q*, Ah $L^{-1}$) during electrochemical oxidation of ROC at pH 2 (*black*) and pH 6-7 (*red*).**

The formation of AOCl and AOBr is shown in Figure 19. AOCl was a major species contributing 80% to the AOX. AOCl was increased from the initial 0.9 mg $L^{-1}$ to 30.7 and 28.7 mg $L^{-1}$ at the end of electrolysis at acidic and circumneutral pH, respectively. Considering the ratio between the remaining DOC and formed AOCl, increased toxicity of organic matter can be expected by the presence of (poly)chlorinated by-products. Further degradation is possible by prolonging the oxidation time until no residual chlorine is present. Nevertheless, such operation would not be economically viable due to the very high electrical charge applied. On the other hand, although $[Br^-]$ and $[I^-]$ in the initial ROC were much lower than $[Cl^-]$ (i.e. 1.6 and 0.6 vs 1386 mg $L^{-1}$, respectively), AOBr formation was still observed since electro-generated $HOBr/OBr^-$ or $HOI/OI^-$ species are usually more reactive than chlorine, especially with phenolic compounds [136]. However, brominated organics are more susceptible to oxidation than their chlorinated analogues, and although AOBr was increased from the initial 0.2 to 1.9-2 mg $L^{-1}$ after 0.8 Ah $L^{-1}$, it was further decreased to 1.2 mg $L^{-1}$ at the end of

oxidation (i.e. $Q = 10.9$ Ah $L^{-1}$). In the case of AOI, their formation was only detected in the first two samples, i.e. 0.3 mg $L^{-1}$.

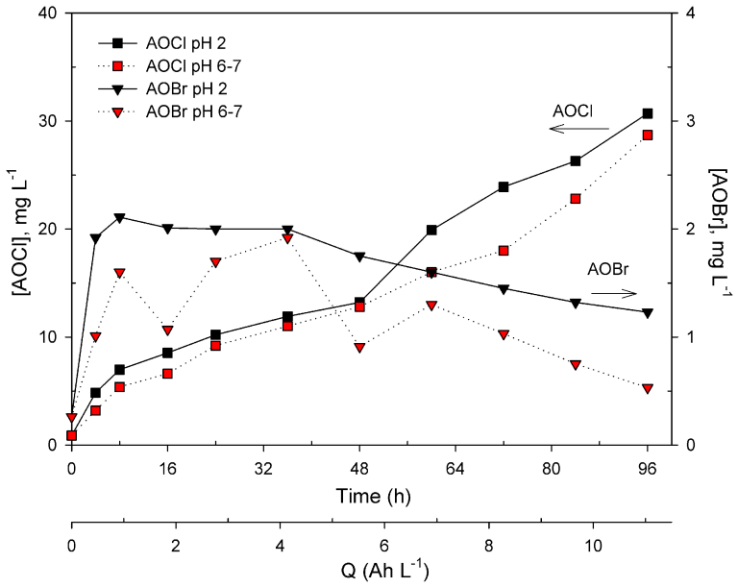


**Figure 19. Formation of: (■■) AOCl and (▼▼) AOBr vs. passed specific electrical charge (*Q*, Ah $L^{-1}$) during electrochemical oxidation of ROC at pH 2 (*black*) and pH 6-7 (*red*).**

Figure 20 shows the formation of THMs and HAAs with their corresponding individual species after $Q$ = 5.2 and 10.9 Ah $L^{-1}$ at acidic and circumneutral pH. In the untreated ROC, the measured concentration of tTHMs and tHAAs was already 0.13 and 0.16 mg $L^{-1}$, respectively. At pH 2, their concentrations were further increased to 0.4 and 3.2 mg $L^{-1}$, respectively after 48 h, and then degraded to 0.14 and 1.8 mg $L^{-1}$ after 96 h of electro-oxidation. Similarly, at pH 6-7, their concentrations were measured at 1.6 and 4.1 mg $L^{-1}$ for THMs and HAAs, respectively. The higher concentration of THMs and HAAs at pH 6-7 is due to their increased formation by base-catalysed hydrolysis of other DBPs which were not measured in this study, e.g. haloacetonitriles (HANs) and haloacetaldehydes (HAs) [137].

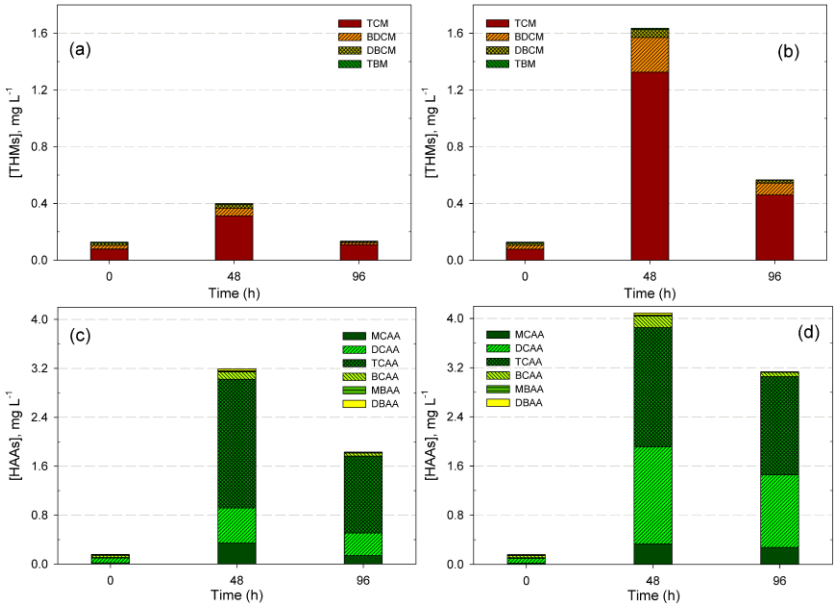


**Figure 20. Formation of: A) THMs at pH 2, B) THMs at pH 6-7, C) HAAs at pH 2, D) HAAs at pH 6-7 vs. passed specific electrical charge (*Q*, Ah $L^{-1}$) during electrochemical oxidation of ROC.**

Further degradation of these by-products was observed, reaching 0.5 and 3.1 mg $L^{-1}$ at the final point. In all cases, TCM was a dominant species (> 70% of tTHMs), followed by BDCM, DBCM, and TBM. Similarly, polychlorinated HAAs (i.e. TCAA and DCAA – comprising of 60-80% of tHAAs) were prominent among the HAAs measured in this study, while brominated HAAs, i.e. BCAA, MBAA and DBAA were detected in lower concentrations. Previously, a continued formation of THMs and HANs in electro-oxidation of ROC at BDD electrode was reported [116]. However, degradation of THMs and HAAs was eventually obtained in this study after 96 h ($Q$ = 10.9 Ah $L^{-1}$) at both pH. The oxidative degradation of brominated compounds will be faster than the chlorinated species [138]. Nevertheless, the enhanced degradation by volatilisation is possible for both chlorine and bromine species, particularly at acidic pH.

### 4.5.3. Conclusions

Complete decolourisation and COD removal during BDD oxidation of ROC were achieved at 5.2 and 6.6 Ah $L^{-1}$ at pH 1–2 and pH 6–7, respectively, corresponding to the energy consumption of 43 and 50 kWh $m^{-3}$, respectively. In terms of energy invested per unit of COD removed, the values obtained at pH 1-2 and pH 6-7, i.e. to 0.29 and 0.34 kWh g $COD^{-1}$), respectively, are similar to the ones reported in previous studies for electro-oxidation of ROC [21, 49]. DOC removal seemed to be initially faster at neutral pH, i.e. 48% and 59% of the initial DOC was degraded at the acidic and circumneutral pH, respectively, at 6.6 Ah $L^{-1}$.

Nevertheless, it is important to note that although the COD removal was complete, at the same time points in the experiments the remaining organic fraction exhibited a DOC:AOCl ratio of 1.83:0.37 and 1.44:0.45 at acidic and neutral pH, respectively, suggesting an increased toxicity of the treated effluent. Although the enhanced participation of $Cl_2$/HClO species led to a faster oxidation of organic matter at acidic pH, it also led to further electrochlorination. Varying the pH had no significant impact on the amount of AOCl formed. The formation of AOBr and AOI was limited by low initial concentrations of $Br^-$ and $I^-$ ions. On the other hand, THMs and HAAs were degraded at higher specific electrical charge to final concentrations of 1 and 4 μM (tTHMs), and 12 and 22 μM (tHAAs), at pH 1–2 and pH 6–7, respectively. Similar to the results obtained for active and non-active MMO anodes, BDD was not capable of suppressing the action of free chlorine in the bulk liquid. The removal of halide ions, particularly chloride, prior to electro-oxidation may overcome the issue of halogenation by-products formation.

## 4.6. Electrochemical oxidation of Electrodialysed Reverse Osmosis Concentrate

### 4.6.1. Experimental Set-Up

In order to study the performance of electro-oxidation of ROC at different electrode materials, and in the presence of significantly lower concentration of chloride ions, two sets of experiments were performed: *(i)* ED treatment of ROC to reduce the $Cl^-$ concentration, using a five-compartment reactor at a fixed applied current of 60 mA (Type C, Figure 3); and *(ii)* anodic oxidation of electrodialysed ROC ($ROC_{ED}$) at Ti/Pt-$IrO_2$, Ti/$SnO_2$-Sb and Si/BDD anodes, I=510 mA, pH 7, with the addition of 0.05 M $NaNO_3$ or 0.05 M $Na_2SO_4$. In the control experiment, 0.05 M NaCl was re-added to $ROC_{ED}$ in order to simulate the original concentration of $Cl^-$ in the ROC, having the same background matrix as in the case of $ROC_{ED}$ with $NaNO_3$ or $Na_2SO_4$ electrolytes. Details of the experimental procedure are described in Appendix F.

### 4.6.2. Results and Discussion

Besides Cl- ions, the concentration of other anions (e.g. $SO_4^{2-}$, $NO_3^-$) was also decreased during electrodialysis (Figure 21). After 8 days of electrodialysis of 10 L ROC ($Q$ = 1.15 Ah $L^{-1}$), the initial $Cl^-$ concentration (i.e. 1526 mg $L^{-1}$) was lowered for 90%, reaching 142 mg $L^{-1}$ in the final $ROC_{ED}$ used in the following oxidation experiments. Furthermore, decrease in COD, DOC and colour of 17%,

12% and 52%, respectively, was also observed due to the limited selectivity of the employed AEM for $Cl^-$, and thus electrodialysis of the charged organic compounds and other non-targeted ions. The electrodialysed organics are likely of low MW, since molar mass plays an important role in the transport of organic ions by the electrical field in ED [44]. Therefore, the concentration of COD, DOC and colour in the $ROC_{ED}$ was 145 mg $L^{-1}$, 46 mg $L^{-1}$ and 132 mg Pt-Co $L^{-1}$, respectively, while the conductivity was decreased to 1.4 mS $cm^{-1}$.

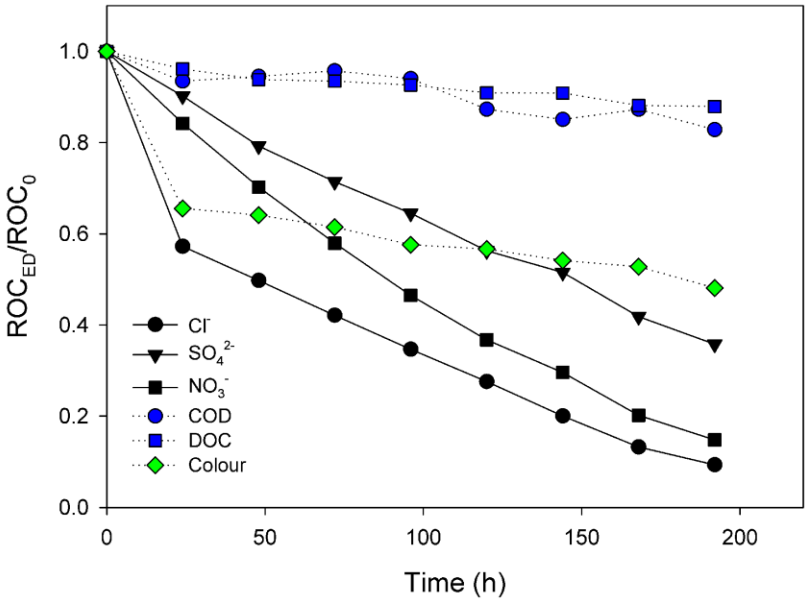


**Figure 21. Removal of COD, DOC, colour and chloride, nitrate and sulfate anions observed during electrodialysis of ROC.**

Table 6 summarises the results of the performance on electrochemical oxidation of 1 L $ROC_{ED}$ with the addition of NaCl, $NaNO_3$ or $Na_2SO_4$ at Ti/Pt-$IrO_2$, Ti/$SnO_2$-Sb and Si/BDD anodes, after $Q$ = 5.6 Ah $L^{-1}$. In electrochemical oxidation of $ROC_{ED}$+NaCl, the COD removal obtained by Ti/Pt-$IrO_2$ was lower than in the case of non-active anodes, i.e. 87%, vs. 93% and 100% for Ti/$SnO_2$-Sb and Si/BDD, respectively. The $CE_{COD}$ calculated for Ti/Pt-$IrO_2$, Ti/$SnO_2$-Sb and Si/BDD was 8.3, 8.9 and 9.5 %, respectively, at the end of electrolysis. However, the corresponding DOC removal achieved was limited to only 40% for Si/BDD, while lower DOC removal was obtained for Ti/$SnO_2$-Sb and Ti/Pt-$IrO_2$, i.e. 31% and 28%, respectively. The remaining organics measured as DOC could be attributed to the oxidation by-products which could not be oxidised by the dichromates in the COD analysis. These results support our earlier findings that electrochlorination plays an important role in the overall oxidation of organics at all electrodes, while in the case of Ti/$SnO_2$-Sb and Si/BDD, enhanced participation of $OH^{\bullet}$/ROS may be expected compared to Ti/Pt-$IrO_2$.

In the presence of 142 mg $L^{-1}$ of $Cl^-$ ions, Ti/Pt-$IrO_2$ exhibited the lowest COD and DOC removal in the presence of either $NO_3^-$ or $SO_4^{2-}$, i.e. 6-22% and 9-12% at $Q$ = 5.6 Ah $L^{-1}$, respectively. This result confirmed that electro-oxidation at active MMO electrodes mainly relies on the chlorine-mediated electrolysis [88]. The $CE_{COD}$ calculated in oxidation of $ROC_{ED}$+$NaNO_3$ at Ti/Pt-$IrO_2$ was only 2.2%, nearly four times lower than in the case of $ROC_{ED}$+NaCl, i.e. 8.3%.

**Table 6. The removal of COD, DOC, colour and tTHMs and tHAAs byproducts in electrochemical oxidation of $ROC_{ED}$ on Ti/Pt-$IrO_2$, Ti/$SnO_2$-Sb and Si/BDD anodes in the presence of NaCl, $NaNO_3$ or $Na_2SO_4$, observed after $Q$ = 5.6 Ah $L^{-1}$.**

| Measured parameter | $ROC_{ED}$ + NaCl | | | $ROC_{ED}$ + $NaNO_3$ | | | $ROC_{ED}$ + $Na_2SO_4$ | | |
|---|---|---|---|---|---|---|---|---|---|
| | Ti/Pt-$IrO_2$ | Ti/$SnO_2$-Sb | Si/BDD | Ti/Pt-$IrO_2$ | Ti/$SnO_2$-Sb | Si/BDD | Ti/Pt-$IrO_2$ | Ti/$SnO_2$-Sb | Si/BDD |
| COD (% removal) | 87 | 93 | 100 | 22 | 37 | 60 | 6 | 44 | 74 |
| DOC (% removal) | 28 | 31 | 40 | 12 | 23 | 41 | 9 | 21 | 51 |
| Colour (% removal) | 98 | 96 | 98 | 92 | 98 | 97 | 88 | 93 | 97 |
| tTHMs (μM) | 5.6 | 8.9 | 9.1 | 3.3 | 5.9 | 0.2 | 5.1 | 6.0 | 1.9 |
| tHAAs (μM) | 27.4 | 34.2 | 62.4 | 8.9 | 15 | 1.1 | 12.4 | 21.8 | 13.6 |

In the case of non-active Ti/$SnO_2$-Sb anode, 37-44% of COD and 21-23% of DOC was removed in the presence of $NO_3^-$ and $SO_4^{2-}$. The $SnO_2$-Sb coating exhibits lower adsorption of $OH^•$, leading to an enhanced oxidative degradation of $ROC_{ED}$. In the presence of low $Cl^-$ concentration the decolourisation seemed to be slower, although 88% removal was obtained at the end of electrolysis. Furthermore, faster decolourisation was observed for $ROC_{ED}$+$NaNO_3$ than for $ROC_{ED}$+$Na_2SO_4$ at the beginning of electrooxidation, possibly due to the slower generation of active chlorine in the latter case. Both $SO_4^{2-}$ and $NO_3^-$ ions compete with the remaining $Cl^-$ in the $ROC_{ED}$ for electroactive sites at the anode surface. Higher molar conductivity and larger hydrated ionic radius of $SO_4^{2-}$ [45] may limit more the oxidation of $Cl^-$ than $NO_3^-$ ions. Therefore, lower production of chlorine in the presence of $Na_2SO_4$ than in the presence of $NaNO_3$ was likely a consequence of the faster adsorption of divalent $SO_4^{2-}$ than monovalent $NO_3^-$ at the surface of the electrode. This, in turn, led to a lower colour and COD removal in the presence for $ROC_{ED}$+$Na_2SO_4$. Similarly, in the case of Ti/Pt-$IrO_2$ electrode higher COD removal was observed in the presence of $NO_3^-$ than in the presence of $SO_4^{2-}$.

Si/BDD exhibited superior performances over the other two anodes, and for $ROC_{ED}$+$NaNO_3$, 60% of COD and 41% of DOC removal was achieved at 5.6 Ah $L^{-1}$. An inert $NaNO_3$ allows a higher participation of $OH^•$ and other ROS in electrochemical oxidation. Compared to Ti/$SnO_2$-Sb where the generated $OH^•$ will be partially adsorbed at the anode surface, BDD is capable of producing quasi free $OH^•$ [10, 135]. Nevertheless, the highest COD and DOC removal, i.e. 74% and 51%, respectively, was obtained in $ROC_{ED}$+$Na_2SO_4$ oxidation at Si/BDD. Previous studies have reported higher mineralisation in anodic oxidation of model compounds on BDD in the chloride-free media, and particularly in the presence of $SO_4^{2-}$ [139, 140]. In the case of BDD/$Na_2SO_4$ electro-oxidation, long-lived $S_2O_8^{2-}$ oxidants are formed via direct electron transfer and/or via reaction with the generated $OH^•$, forming $SO_4^{•-}$ as intermediates [141-143]. Once strong oxidant $SO_4^{•-}$ is formed at the anode surface, it can rapidly attack oxidisable compounds present in the vicinity of the anode surface. The organic matter can also be oxidised by $S_2O_8^{2-}$, which is capable of diffusing away from the electrode surface into the bulk liquid [135, 140]. Therefore, both $S_2O_8^{2-}$ and $SO_4^{•-}$ were likely responsible for an enhanced oxidation of $ROC_{ED}$+$Na_2SO_4$ at Si/BDD electrode.

The concentration of tTHMs and tHAAs was higher for $ROC_{ED}$+NaCl at all three anodes investigated, consistent with the increasing concentration of chloride ions (Figure 22). In this case, the highest formation of both tTHMs and tHAAs were observed for Si/BDD, i.e. 9.1 and 62.4 μM, respectively at $Q$ = 5.6 Ah $L^{-1}$, although the most efficient anode for chlorine production was noted for Ti/Pt-$IrO_2$. This could be explained by the formation of radical RHS, e.g. $ClO^•$ and $Cl_2^{•-}$ [144, 145]. The formation of THMs and HAAs was successfully decreased as the concentration of chloride ions was lowered to 142 mg $L^{-1}$ in $ROC_{ED}$. In the presence of either $NaNO_3$ or $Na_2SO_4$, Ti/$SnO_2$-Sb showed the highest concentration of tTHMs and tHAAs, followed by Ti/Pt-$IrO_2$ and Si/BDD anodes. At the latter anode, the measured tTHMs and tHAAs concentrations were 1.9 and 13.6 μM in $ROC_{ED}$+$Na_2SO_4$, higher than in the case of $ROC_{ED}$+$NaNO_3$, i.e. and 0.2 and 1.1 μM, respectively. The enhanced formation of THMs and HAAs at BDD in the presence of $SO_4^{2-}$ than in the presence of inert $NO_3^-$ ions could be a

consequence of the bulk oxidation of $Cl^-$ to reactive chloro-species by $S_2O_8^{2-}$ ions, and/or in the vicinity of the electrode surface by $SO_4^{\bullet-}$ radicals [141, 146]. These additional pathways of formation of chloro-species would enhance the electro-chlorination and thus the formation of THMs and HAAs. On the other hand, since Ti/$SnO_2$-Sb and Ti/Pt-$IrO_2$ anodes are not capable of further oxidising $SO_4^{2-}$, an enhanced formation of THMs and HAAs for $ROC_{ED}$+$Na_2SO_4$ was not observed.

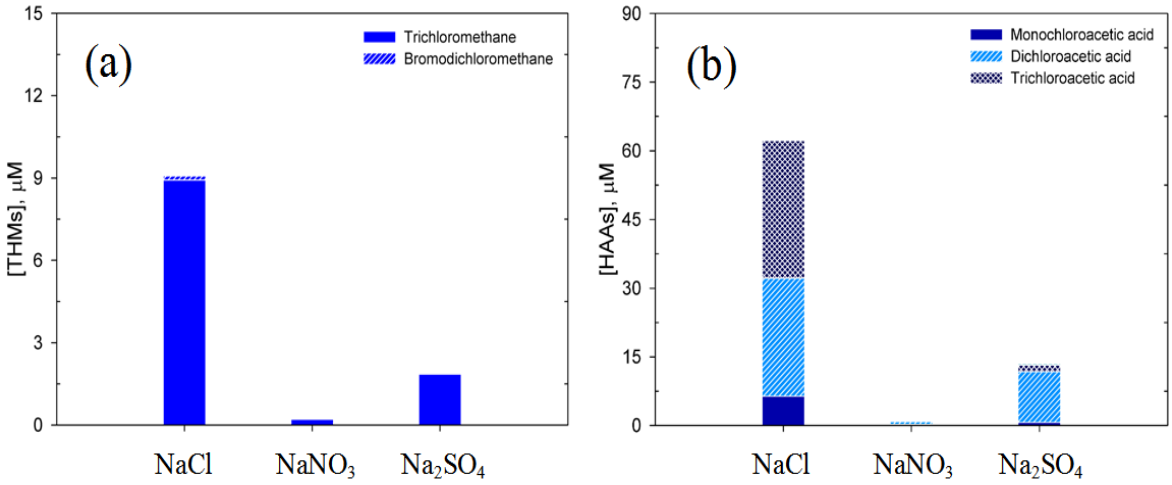


**Figure 22. Concentration of THMs A) and HAAs B) species measured in the last sample, i.e. after *Q* = 5.6 Ah $L^{-1}$ of the electrochemical oxidation of electrodialysed ROC with the addition of NaCl, $NaNO_3$ and $Na_2SO_4$. TBM and DBCM were detected at concentrations <0.01 µM, while brominated HAAs were detected at concentrations <0.12 µM.**

In the case of $ROC_{ED}$+NaCl, high concentration of chloride ions lead to the generation of poly-chlorinated by-products, i.e. TCM, TCAA and DCAA as the dominant THM and HAA species measured for all three anodes tested. On the other hand DCAA and TCM were the dominant species measured for both $ROC_{ED}$+$NaNO_3$ and $ROC_{ED}$+$Na_2SO_4$. For example, as represented in Figure 22, the TCM concentration was 8.9 µM in $ROC_{ED}$+NaCl, while in the case of $ROC_{ED}$+$NaNO_3$ and $ROC_{ED}$+$Na_2SO_4$, it was 0.2 and 1.9 µM, respectively. Similarly, DCAA concentration for $ROC_{ED}$+NaCl was decreased from 25.8 µM to 0.6 and 11 µM in $ROC_{ED}$+$NaNO_3$ and $ROC_{ED}$+$Na_2SO_4$, respectively. Furthermore, brominated HAAs and THMs were detected at low concentrations of maximum 0.12 and 0.01 µM, respectively, as the concentration of bromide ions was also lowered during the ED.

### 4.6.3. Conclusions

The most efficient COD removal was achieved in the presence of a high chloride ions concentration. When the concentration of the chloride ions was decreased and inert nitrate anions added to the electrodialysed ROC, superior performance of Si/BDD was observed, capable of generating quasi-free $OH^{\bullet}$/ROS, and leading to not only enhanced mineralisation (up to 51% DOC removal), but also a minimised formation of HAAs and THMs (i.e. from 62.4 to 1.1-13.6 µM of total HAAs and from 9.1 to 0.2-1.9 µM of total THMs). Although COD removal at BDD was worsened upon decreasing the $Cl^-$ concentration, this electrode was capable of achieving the same oxidative degradation (i.e. DOC removal) of the organic matter as in the case of chlorine-mediated oxidation. In the presence of sulphate ions, the performance of BDD anodes in terms of COD and DOC removal was enhanced from 60% to 74%, and 41% to 51%, respectively, compared to nitrate electrolyte, due to the participation of $S_2O_8^{2-}$ and $SO_4^{\bullet-}$ species in oxidation mechanisms. On the other hand, oxidation at Ti/Pt-$IrO_2$ and Ti/$SnO_2$-Sb appears to rely on HClO/$ClO^-$ species.

Considering the expected high energy demand of a combined electrodialysis and electrochemical oxidation process, anion exchange membranes selective for monovalent anions should be used. Since electrodialysed brine has a lowered conductivity, improved reactor design (e.g. column-type reactors, bipolar BDD electrodes) is required in order to reduce the energy investment of electrooxidation at high BDD anodic potentials.

## 4.7. Electrochemical oxidation in a Non-Divided Electrolytic Cell

### 4.7.1. Experimental Set-Up

In the beginning of the project, the preliminary experiments of the electrochemical oxidation of ROC were performed in a non-divided electrolytic cell. However, fast passivation of the stainless steel cathode surface occurred rapidly in all experiments, due to the local pH increase and precipitation of $Ca(OH)_2$. The $E_{cell}$ was then drastically increased due to the higher ohmic resistance in the system, leading to the experiment failure. Thus, all experiments were performed in a divided electrolytic cell, which allowed using different catholyte and anolyte solutions. In order to prevent the precipitation at the cathode, 0.1 M HCl was used as a catholyte. Anolyte used was ROC sampled at the AWTP Bundamba.

However, when operating the electrolytic cell using BDD electrode as both anode and cathode, the formation of the precipitate seemed to be limited to the non-active (i.e. silicon surface) of the cathode, whereas the coated side of the electrode was not fouled. Thus, experiments were performed in a non-divided cell (Type D reactor, Figure 3) equipped with two BDD electrodes (inter-electrode gap 1 cm). The process performance was estimated in terms of COD, DOC and colour removal, as well as free chlorine production (determined by the DPD method).

### 4.7.2. Results and Discussion

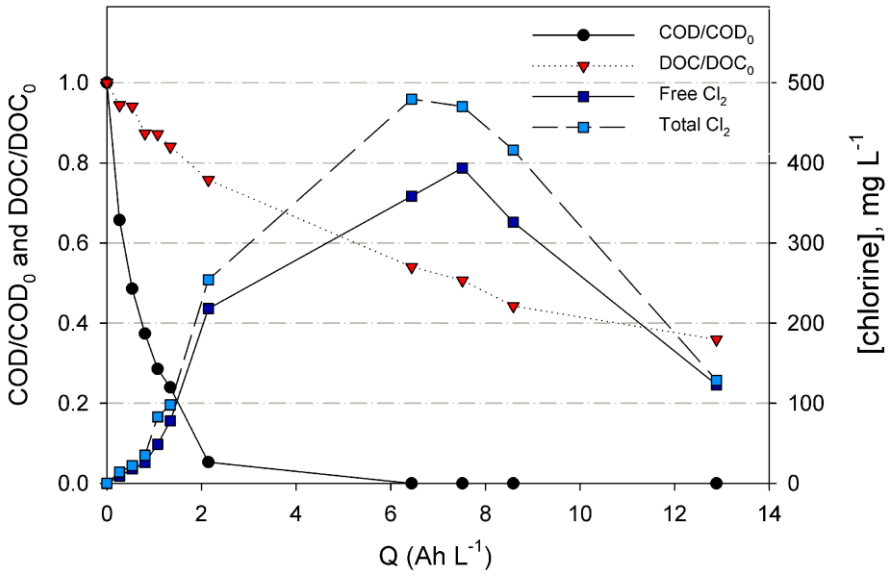


**Figure 23. Removal of COD and DOC, and accumulation of free and total chlorine, during electrochemical oxidation of ROC in a non-divided electrolytic cell (anode: BDD electrode, cathode: BDD electrode).**

Figure 23 illustrates the removal of COD and DOC, as well as the determined active and total chlorine in electrochemical oxidation of ROC using a non-divided cell. The results obtained are very similar to the performance of electro-oxidation of ROC at BDD anode in a divided electrolytic cell (Figure 18). COD and DOC removal was similar, e.g. ~40% of DOC removal was achieved after 10.5 Ah $L^{-1}$ of specific electrical charge applied. The accumulated active chlorine reached a maximum concentration of 393.7 mg $L^{-1}$ (measured at 7.5 Ah $L^{-1}$ of applied specific electrical charge), similar to the value determined for a divided cell (i.e. 442.6 mg $L^{-1}$ measured at 5.2 Ah $L^{-1}$). This indicated that the extent of electro-chlorination of the organic matter and formation of more toxic chlorinated by-products was likely similar to the one observed in electro-oxidation at BDD using a divided electrolytic cell (results presented in the section 4.5).

### 4.7.3. Conclusions

The preliminary results obtained for the non-divided electrolytic cell reveal similar process performance in terms of COD and DOC removal as the one observed for a divided cell (section 4.5). High accumulation of residual active chlorine suggests fast oxidation of chloride ions to chlorine at the anode, and possible electro-chlorination of the organics. However, the toxicity of the oxidised ROC, and/or the formation of AOX should be further studied for this configuration of electrolytic cell.

# APPENDIX A - Multi-Residue Method for the Analysis of Trace Organic Contaminants

## Target Trace Organic Contaminants

The target analytes were selected based on their consumption data, ubiquity in treated sewage effluent and detected concentrations in the analysed ROC from the AWTP Bundamba, and with the intention of enclosing the compounds with varying physio-chemical properties and belonging to different therapeutic groups (Table A 1). The target trace organic contaminants were 21 pharmaceuticals: anti-inflammatory drugs acetaminophen (ACTP), ibuprofen (IBP) and diclofenac (DCF), analgesic drug tramadol (TML), stimulant drug caffeine (CAFF), diuretic hydrochlorothiazide (HCT), antibiotics enrofloxacin (ENR), norfloxacin (NFL), roxythromycin (ROX), lincomycin (LNC), trimethoprim (TMP) and sulfadiazine (SDZ), anticonvulsant drugs phenytoin (PNT) and carbamazepine (CBZ), antidepressants sertraline (SRL), citalopram (CTP) and venlafaxine (VNF), lipid regulator gemfibrozil (GMF), antihistamine drug ranitidine (RNT), X-ray agent iopromide (IPM), and β-blocker metoprolol (MTP); also, 7 frequently encountered pesticides were included in the method: diuron (DIU), diazinon (DZN), triclopyr (TPR), atrazin (ATZ), 2,4-dichlorophenoxyacetic acid (2,4-D), *N*,*N*-diethyl-*meta*-toluamide (DEET) and metolachlor (MET).

**Table A 1. Target analytes with their molecular structures, molecular weights (MWs), acid dissociation constants (pKas) and octanol-water partition coefficients (log KOWs).**

| Compound | MW (g mol$^{-1}$) | pKa[a] | log $K_{OW}$[a] |
|---|---|---|---|
| 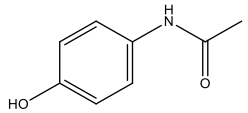 **Acetaminophen (ACTP)** | 151.16 | 9.38 | 0.46 |
| 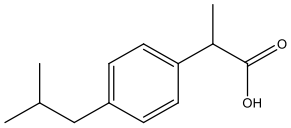 **Ibuprofen (IBU)** | 206.23 | 4.91 | 3.97 |
| 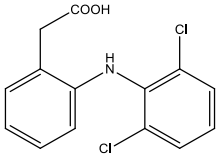 **Diclofenac (DCF)** | 296.15 | 4.2[b] | 4.6[c] |
| 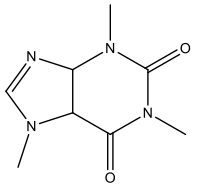 **Caffeine (CAFF)** | 194.20 | 10.40[d] | -0.07[d] |
| 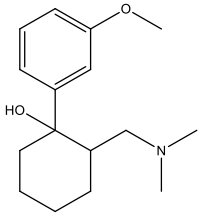 **Tramadol (TML)** | 263.38 | 9.44[e] | 2.31[f] |

| Compound | MW (g mol$^{-1}$) | pKa[a] | log $K_{OW}$[a] |
|---|---|---|---|
| 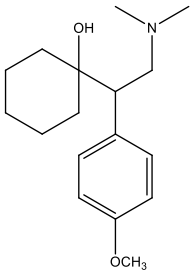 **Venlafaxine (VNF)** | 277.40 | 9.4[g] | 2.91[h] |
| 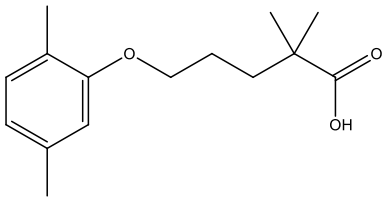 **Gemfibrozil (GMF)** | 250.33 | 4.43 | 4.77 |
| 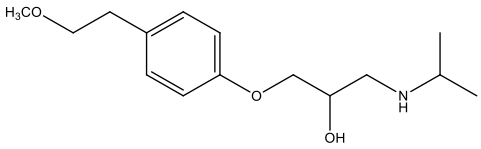 **Metoprolol (MTP)** | 267.36 | 9.68 | 1.88 |
| 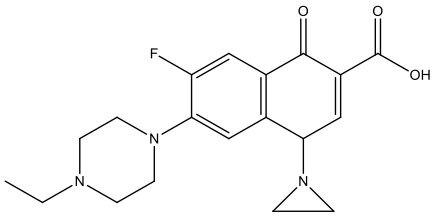 **Enrofloxacin (ENR)** | 359.40 | 5.94; 8.70[j] | 0.70 |
| 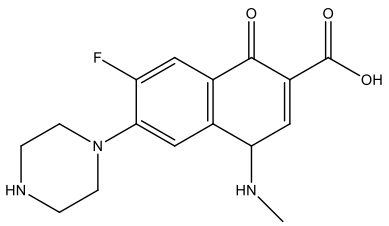 **Norfloxacin (NFL)** | 319.34 | 6.34; 8.75[k] | -1.03 |
| 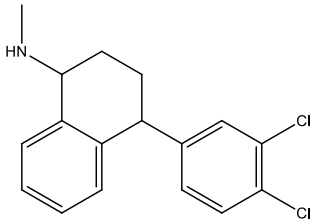 **Sertraline (SRL)** | 306.24 | 9.5[k] | 5.29 |
| 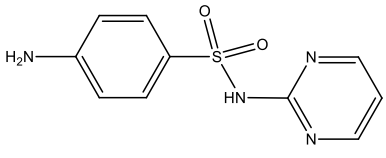 **Sulfadiazine (SDZ)** | 250.28 | 1.8; 6.36 | -0.09 |

| Compound | MW (g mol$^{-1}$) | pKa[a] | log $K_{OW}$[a] |
|---|---|---|---|
| 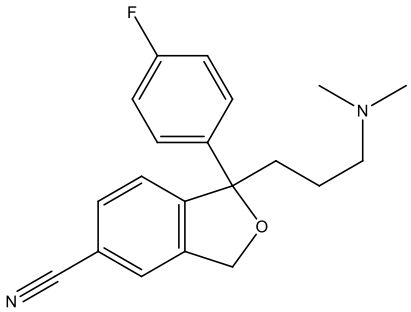 **Citalopram (CTP)** | 324.40 | 9.59[k] | 3.74 |
| 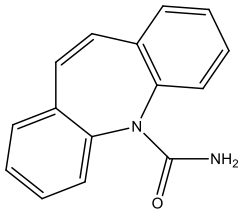 **Carbamazepine (CBZ)** | 236.27 | 1; 13.9 | 2.45 |
| 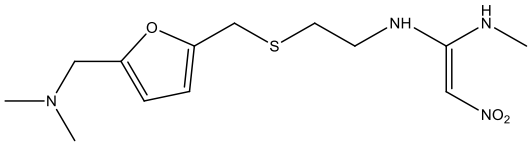 **Ranitidine (RNT)** | 314.41 | 2.7; 8.2 | 0.27 |
| 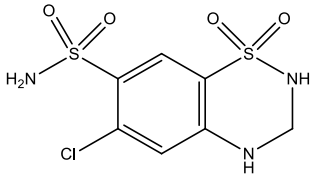 **Hydrochlorothiazide (HCT)** | 297.74 | 7.9 | -0.07 |
| 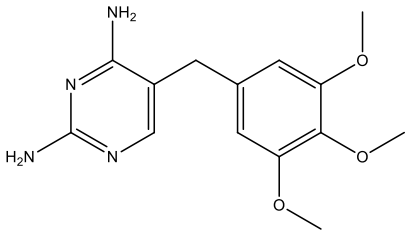 **Trimethoprim (TMP)** | 290.32 | 3.2; 7.1 | 0.91 |
| 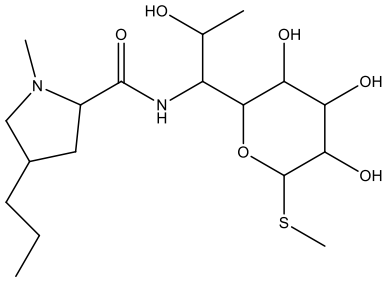 **Lincomycin (LNC)** | 406.54 | 7.6 | 0.56 |

| Compound | MW (g mol$^{-1}$) | pKa[a] | log $K_{OW}$[a] |
|---|---|---|---|
| 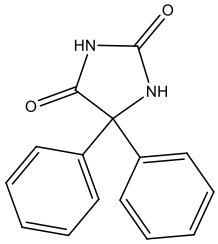 **Phenytoin (PNT)** | 252.28 | 8.33 | 2.47 |
| 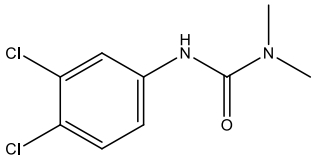 **Diuron (DIU)** | 233.10 | na | 2.68 |
| 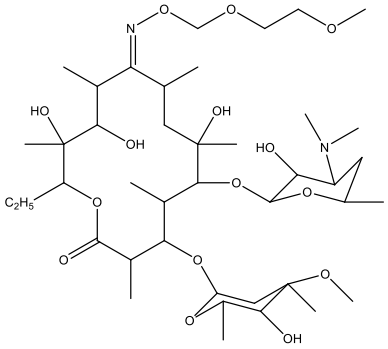 **Roxithromycin (ROX)** | 837.07 | 8.8[l] | 2.75 |
| 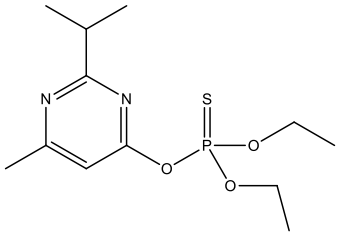 **Diazinon (DZN)** | 304.35 | 2.4[m] | 3.81 |
| 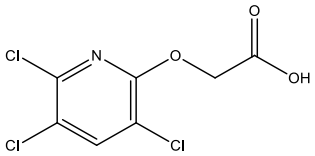 **Triclopyr (TPR)** | 256.46 | 3.97[n] | -0.45[n] |
| 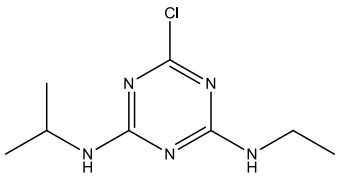 **Atrazin (ATZ)** | 215.69 | 1.7 | 2.61 |

| Compound | MW (g mol$^{-1}$) | pKa[a] | log $K_{OW}$[a] |
|---|---|---|---|
| 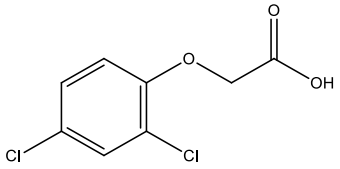 **2,4-D** | 221.04 | 2.73 | 2.81 |
| 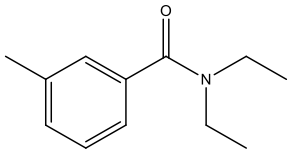 **DEET** | 191.28 | na | 2.18 |
| 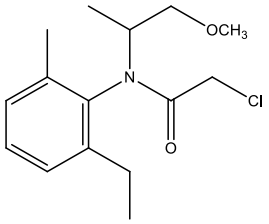 **Metolachlor (MET)** | 283.80 | na | 3.13 |
| 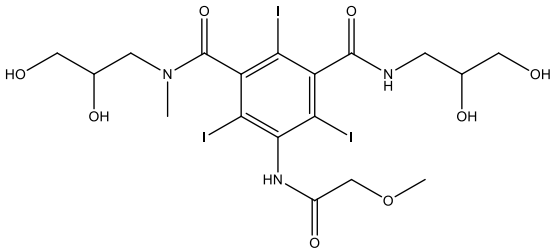 **Iopromide (IPM)** | 790.87 | 0 | na |

[a] pKa and log $K_{OW}$ values retrieved from PhysProp Database Demo, Syracuse Research Corporation, 2008 (www.syrres.com/esc/physdemo.htm)
[b] Jones *et al.*, 2002, Wat. Res. 26, 5013-5022.
[c] Hansch *et al.*, 1995. In: Heller, S.R. (Ed.) Exploring QSAR, American Chemical Society, Washington DC.
[d] EPI Suite™ v4.0
[e] Pospisilova *et al.*, 1998, J. Pharm. Biomed, Anal, 18, 777-783.
[f] Craig, P.N., 1990. In: Hansch, C., Sammes, P.G., Taylor, J.B. (Eds.). Comprehensive Medicinal Chemistry, Vol. 6. Pergamon Press, Oxford.
[g] Ellingrod *et al.*, 1994, Am. J. Hosp. Pharm. 51 (24), 3033-3046.
[h] Hasemann *et al.*, 2007, Electrophoresis 28, 1779–1787.
[i] McLean MJ. 1995. In: Levy R, Mattson R, Meldrum B. (Eds.) Antiepileptic Drugs. Raven Press Ltd, New York.
[j] Lizondo *et al.*, 1997, J. Pharm. Biomed. Anal. **15,** 1845-1849.
[k] The Merck Index
[l] Huber *et al.*, 2003, Environ. Sci. Technol. 37, 1016-1024.
[m] Ku *et al.*, 1998 Wat. Air Soil Poll. 108 , 445-456.
[n] Tran *et al.*, 2007, Environ. Toxicol. Chem. 26, 435–443.

## Multi-Residue Method Description

For the analysis in negative ionisation (NI) mode, eluent A was a mixture of acetonitrile/methanol (1:1, v/v) and eluent B was HPLC grade water at a flow rate of 1 mL $min^{-1}$. The elution gradient started with 5% eluent A, increasing to 90% of A in 7 min, held isocratically for 3 min, increased to raising to 100% of A in 2 min and held at 100% of A for 3 min before returning to the initial conditions. The column was re-equilibrated for 5 min before another injection with a total time for chromatographic analysis of 21 min. The analysis in positive ionisation (PI) mode was performed using acetonitrile with 0.1% formic acid as eluent A, and HPLC grade water with 0.1% formic acid as eluent B. The elution gradient started with 5% eluent A, increasing to 60% in 5 min, raising to 90% in the following 8 min, further increasing to 100% of A in the next 2 min. Next, the gradient was isocratically held at 100% of A for 2 min before returning to the initial conditions and re-equilibrating the column for 5 min. Chromatographic analysis lasted for 23 min.

The MS parameters were optimised for target pharmaceuticals and pesticides. In the analysis of estrone, ethynyl estradiol and bisphenol A problems with sensitivity occurred, and further work needs to be done on the inclusion of these three compounds in the multi-residue method. To the list of target analytes two pharmaceuticals were added, gabapentin and iopromide, in order to attempt the extraction of these two very polar and persistent compounds.

Settings for source-dependent parameters, common in both NI and PI modes, were determined by Flow Injection Analysis (FIA) and are as follows: curtain gas (CUR), 30V; nitrogen collision gas (CAD) high; source temperature (TEM) was 700 °C, and ion source gases GS1 and GS2 were set at 62 and 55V in NI and PI modes, respectively. Conversely, the ion spray voltages in NI and PI modes were set at -4500 and 5500V, respectively. To achieve higher sensitivity, resolution at the first quadrupole (Q1) is fixed at low while the resolution at the third quadrupole (Q3) was set to unit.

The optimisation of compound dependent MS parameters (declustering potential (DP), entrance potential (EP), collision energy (CE) and cell exit potential (CXP)) for each transition was performed by infusing standards of each individual compound at 100 $\mu g\,L^{-1}$ to the mass spectrometer. Optimum parameters are summarised Table A 1 and Table A 2 for the analysis of target analytes in the NI and PI mode, respectively.

**Table A 2: Optimised QqLIT-MS parameters for the analysis of target analytes in the negative ion (NI) mode. SRM-selected reaction monitoring transition. DP-declustering potential, CE-collision energy, CXP-cell exit potential, tR-retention time.**

| Compound | Precursor ion, m/z | SRM 1 | DP-CE-CXP (V) | SRM 2 | DP-CE-CXP (V) | $t_R$, min |
|---|---|---|---|---|---|---|
| Acetaminophen | 150.0 | 106.9 | 60-26-7 | 107.8 | 60-22-5 | 6.07 |
| Acetaminophen-$d_4$ | 154.0 | 111.1 | 60-26-7 | 120.9 | 60-42-5 | 6.07 |
| Hydrochlorothiazide | 296.0 | 268.8 | 90-26-13 | 204.9 | 90-30-17 | 6.38 |
| Hydrochlorothiazide$^{13}C_3$ | 299.0 | 269.9 | 90-28-5 | 78.0 | 90-50-3 | 6.35 |
| Ibuprofen | 205.0 | 161.0 | 52-11-10 | - | - | 10.78 |
| Ibuprofen-$d_3$ | 208.0 | 163.9 | 45-10-11 | 161.3 | 45-10-5 | 10.78 |
| Gemfibrozil | 249.0 | 121.0 | 85-20-7 | 127.0 | 85-14-5 | 11.49 |
| Gemfibrozil-$d_6$ | 255.1 | 121.0 | 60-28-7 | 133.0 | 60-14-9 | 11.45 |
| Diclofenac | 293.9 | 250.0 | 40-16-1 | 214.0 | 40-30-15 | 10.56 |
| Diclofenac-$d_4$ | 298.0 | 253.9 | 60-16-1 | 216.9 | 60-30-12 | 10.54 |
| Diuron | 230.9 | 185.8 | 65-26-15 | 149.9 | 65-36-9 | 9.69 |
| 2,4-D | 218.8 | 160.9 | 45-18-5 | 124.9 | 45-40-9 | 9.73 |
| Triclopyr | 256.0 | 198.0 | 55-30-5 | - | - | 9.93 |
| Triclopyr | 254.0 | - | - | 196.0 | 55-30-5 | 9.93 |

**Table A 3: Optimised QqLIT-MS parameters for the analysis of target analytes in the positive ion (PI) mode. SRM-selected reaction monitoring transition.**

| Compound | Precursor ion, m/z | SRM 1 | DP-CE-CXP (V) | SRM 2 | DP-CE-CXP (V) | $t_R$, min |
|---|---|---|---|---|---|---|
| DEET | 192.2 | 119.1 | 61-25-8 | 91.2 | 61-45-6 | 10.15 |
| DEET-$d_6$ | 198.3 | 116.1 | 68-27-8 | 91.1 | 68-45-6 | 10.09 |
| Caffeine | 195.1 | 138.1 | 71-28-8 | 110.0 | 71-32-8 | 6.21 |
| Caffeine$^{13}C_3$ | 198.1 | 140.2 | 36-29-12 | 112.1 | 36-27-12 | 6.20 |
| Carbamazepine | 237.2 | 194.2 | 61-27-16 | 193.3 | 61-47-12 | 8.53 |
| Carbamazepine-$d_{10}$ | 247.2 | 204.2 | 81-31-12 | 202.2 | 81-50-14 | 8.47 |
| Atrazin | 216.1 | 174.2 | 81-27-10 | 68.0 | 81-53-12 | 10.05 |
| Atrazin-$d_5$ | 221.1 | 179.3 | 71-27-12 | 101.2 | 71-35-6 | 10.0 |
| Sulfadiazine | 251.1 | 92.1 | 66-39-6 | 65.1 | 66-63-4 | 6.33 |
| Sulfadiazine-$d_4$ | 255.0 | 160.1 | 71-23-12 | 96.2 | 71-39-6 | 6.29 |
| Phenytoin | 253.1 | 182.2 | 61-27-10 | 104.1 | 61-51-8 | 8.28 |
| Diazinon | 305.2 | 169.2 | 81-31-14 | 153.2 | 81-29-8 | 14.56 |
| Metolachlor | 285.1 | 253.2 | 61-25-16 | 177.3 | 61-37-16 | 13.02 |
| Tramadol | 264.4 | 58.1 | 45-44-8 | 42.2 | 45-125-3 | 6.32 |
| Tramadol-$d_6$ | 270.2 | 64.2 | 61-39-2 | 45.2 | 61-113-8 | 6.30 |
| Metoprolol | 268.2 | 116.2 | 76-27-8 | 121.1 | 76-35-8 | 6.26 |
| Venlafaxine | 278.2 | 58.1 | 61-41-10 | 260.3 | 61-19-6 | 6.63 |
| Venlafaxine-$d_6$ | 284.3 | 58.2 | 61-59-8 | 266.3 | 61-19-20 | 6.59 |
| Trimethoprim | 291.2 | 230.3 | 86-10-4 | 261.2 | 86-37-6 | 5.85 |
| Trimethoprim$^{13}C_3$ | 294.2 | 233.2 | 96-33-12 | 126.1 | 96-34-9 | 5.85 |
| Sertraline | 306.1 | 159.1 | 56-39-12 | 275.1 | 56-19-18 | 7.59 |
| Ranitidine | 315.3 | 176.1 | 61-25-14 | 102.2 | 61-51-16 | 5.25 |
| Ranitidine-$d_6$ | 321.3 | 176.2 | 51-25-16 | 102.2 | 51-47-8 | 5.25 |
| Norfloxacin | 320.2 | 276.2 | 70-26-14 | 233.2 | 70-35-14 | 5.82 |
| Enrofloxacin | 360.2 | 316.2 | 81-29-12 | 245.2 | 81-39-20 | 6.10 |
| Enrofloxacin-$d_5$ | 365.2 | 321.2 | 86-33-18 | 245.2 | 86-35-22 | 6.09 |
| Citalopram | 325.3 | 109.1 | 70-38-4 | 262.2 | 70-28-4 | 6.97 |
| Lincomycin | 407.3 | 126.2 | 91-39-10 | 359.3 | 91-27-10 | 5.55 |
| Roxithromycin | 837.6 | 679.5 | 96-31-12 | 158.0 | 96-49-12 | 7.50 |
| Iopromide | 791.88 | 773.87 | 120-35-10 | 572.9 | 125-54-10 | 5.32 |

## Optimisation of the Sample Pre-Treatment

In order to optimise a unique sample pre-treatment method for all target analytes, several extraction methods were tested using two types of cartridges: Oasis HLB (200 mg) and Evolute ABN (200 mg), at circumneutral pH (i.e. pH of the sample, ~7.7) and acidic pH (pH 3). Additionally, sequential extraction using two cartridges was investigated, with Oasis HLB at neutral pH placed on top, and Evolute ABN at pH 3 below. In all methods, cartridges were preconditioned with 10 mL of methanol and 20 mL of Milli-Q water (acidified to pH 3 for the extraction at acidic pH). ROC sample volume used for the extraction was 100 mL. Prior to sample concentration, aqueous solution of $Na_2EDTA$ was added to the sample (5%) and left to react during 30 min, in order to improve the extraction efficiency of fluoroquinolone antibiotics (soluble metals are bound to the chelating agent, increasing the extraction efficiency of antibiotics) [147]. In the case of acidic extraction, sample was acidified with HCl (18%) to pH 3. Next, the samples were spiked with a mixture of labelled standards in methanol to a final concentration of 1 µg/L. For the solid phase extraction (SPE) a Baker vacuum system (J.T. Baker) was used. After sample concentration, cartridges were rinsed with 5 mL of Milli-Q water and dried under vacuum for 2 h to remove excess water. Elution was performed using 10 mL of methanol and 10 mL of mixture of hexane/acetone (1/1, v/v). Extracts were evaporated to a very low volume under a gentle nitrogen stream, reconstituted with 1 mL of methanol/water (25:75, v/v) and analysed at ultra fast liquid chromatography (UFLC) coupled to quadrupole linear ion trap mass spectrometry (QqLIT-MS).

Recoveries of the method were determined as follows: ROC samples were spiked in triplicate with a standard mixture of target analytes to a final concentration of 1 µg/L. These triplicates as well as blank samples were also spiked with a mixture of labelled compounds (i.e. internal standards) to a final concentration of 1 µg/L, in order to account for the possible losses during extraction and matrix interferences. Spiked samples together with a blank sample were analysed at UFLC-QqLIT-MS, and the recoveries were determined by substraction of the blank concentrations from the ones measured in the samples, and comparison with the initial spiking level. Concentrations of target analytes were determined using internal standards (i.e. labelled compounds spiked prior to the sample concentration) and matrix-matched calibration curves for quantification.

**Table A 4: Recoveries (R) expressed as mean values with their standard deviations (SDs), and method quantification limits (MQLs) of the target analytes.**

| Compound | $R_1$ (ROC-1) ± SD,% | $R_2$ (ROC-2) ± SD,% | MQL (ROC-1,2), ng $L^{-1}$ |
|---|---|---|---|
| **DEET** | 125.0±2.3 | 117.4±4.2 | 2.8 |
| **Caffeine** | 85.4±21.8 | 72.4±7.9 | 7.9 |
| **Carbamazepine** | 59.2±10.5 | 56.1±15.5 | 7.2 |
| **Atrazine** | 98.4±16.4 | 75.2±9.6 | 34.6 |
| **Sulfadiazine** | 49.1±4.9 | 52.2±1.0 | 4.8 |
| **Phenytoin** | 64.5±21.4 | 71.8±14.4 | 74.3 |
| **Diazinon** | 115.0±0.3 | 102.0±2.9 | 1.9 |
| **Metolachlor** | 68.5±25.1 | 61.5±17.0 | 3.8 |
| **Tramadol** | 119.2±7.2 | 92.3±2.7 | 2.2 |
| **Metoprolol** | 89.5±33.8 | 99.3±8.2 | 1.5 |
| **Venlafaxine** | 62.0±22.6 | 82.3±19.3 | 1.8 |
| **Trimethoprim** | 115.0±14.8 | 90.3±2.7 | 3.7 |
| **Sertraline** | 42.2±2.8 | 57.5±8.4 | 42.1 |
| **Ranitidine** | 68.6±21.2 | 70.0±16.3 | 2.0 |
| **Norfloxacin** | 134.0±12.4 | 125.0±5.8 | 17.5 |
| **Enrofloxacin** | 164.4±5.9 | 142.6±11.3 | 19.1 |
| **Citalopram** | 71.9±23.1 | 66.0±20.9 | 34.1 |
| **Lincomycin** | 80.4±10.8 | 87.1±3.4 | 12.3 |
| **Roxithromycin** | 121.8±2.9 | 103.2±12.5 | 46.7 |
| **Iopromide** | 123.1±38.3 | 102.1±13.0 | 31.0 |
| **Acetaminophen** | 72.1±6.2 | 52.0±7.8 | 32.0 |
| **Hydrochlorothiazide** | 78.9±3.2 | 68.5±10.4 | 7.2 |
| **Gemfibrozil** | 98.2±12.0 | 87.8±1.5 | 10.5 |
| **Diclofenac** | 40.1±0.6 | 50.6±4.1 | 43.7 |
| **Diuron** | 47.1±3.1 | 45.7±4.3 | 86.7 |
| **2,4-D** | 80.5±22.8 | 71.4±12.3 | 4.5 |
| **Triclopyr** | 61.4±3.3 | 72.8±9.1 | 8.6 |
| **Ibuprofen** | 77.8±23.5 | 76.9±15.6 | 61.2 |

It was found that the performances of the two investigated SPE cartridges were quite similar. Overall, Oasis HLB cartridges showed better performance at circumneutral pH, whereas Evolute ABN cartridges were more efficient in extracting the target analytes at acidic pH. Gabapentin was extracted only at acidic pH. For several compounds (i.e. ß-blockers, sulfadiazine, carbamazepine) acceptable recoveries (i.e. >50%) were obtained only at neutral pH. Sequential extraction showed an improved performance and efficient extraction of all analytes. However, considering the increased cost of the analysis per sample in sequential extraction, and the fact that, except in the case of diclofenac, no significant increase in extraction recoveries of other compounds was noted by lowering the pH, the extraction protocol at circumneutral pH using Oasis HLB was adopted for further analysis. The recoveries of the target analytes determined for two sample batches of ROC from the AWTP Bundamba, together with their method quantification limits (MQLs) are summarised in Table A 3.

# APPENDIX B - Supporting Information for Chapter 4.1. Impact of Mixed Metal Oxide (MMO) Coating on the Performance of Electrochemical Oxidation

Synthetic ROC matrix was synthetised using inorganic salts (i.e. NaCl, $(NH_4)_2SO_4$, $NaHSO_3$, $KH_2PO_4$, $CaCO_3$, $Mg(NO_3)_2$), humic acid, melanoidin (glucose, glycine), polysaccharides (cellulose, carboxymethyl cellulose, and hydroxypropyl cellulose) and peptones. Characteristics of the synthetic ROC and ROC samples at the AWTP Bundamba are summarised in Table B 1.

**Table B 1. Characteristics of synthetic ROC, and ROC from AWTP Bundamba**

| Parameter | Unit | Real ROC | Synthetic ROC |
|---|---|---|---|
| pH | | 7.8 ± 0.2 | 7.5 ± 0.3 |
| COD | mg $O_2$ $L^{-1}$ | 166 ± 3 | 213 ± 19 |
| Colour | mg Pt-Co $L^{-1}$ | 161 ± 5 | 248 ± 43 |
| $UV_{254}$ | $cm^{-1}$ | 1.4 ± 0.3 | 0.5 ± 0.1 |

In electrochemical oxidation of synthetic ROC and AWTP Bundamba ROC using Ti/$RuIrO_2$ anode, the two samples showed significant differences in the oxidation performance (Table B 2).

**Table B 2. Performance of electro-oxidation of synthetic vs AWTP Bundamba ROC using Ti/$RuIrO_2$ anode (supplied specific electrical charge, Q=0.67 A h $L^{-1}$).**

| % Removal | Real ROC | Synthetic ROC |
|---|---|---|
| COD (%R) | 17 | 10 |
| Colour (%R) | 98 | 84 |
| $UV_{254}$ (%R) | 34 | 18 |

Difference observed between the initial $UV_{254}$ absorbance for the synthetic and real ROC, as well as different performance of the electrochemical treatment observed led to the conclusion that the composition of the existing synthetic ROC is not similar enough to the real ROC. All further experiments were performed using batches of ROC sampled at the AWTP Bundamba.

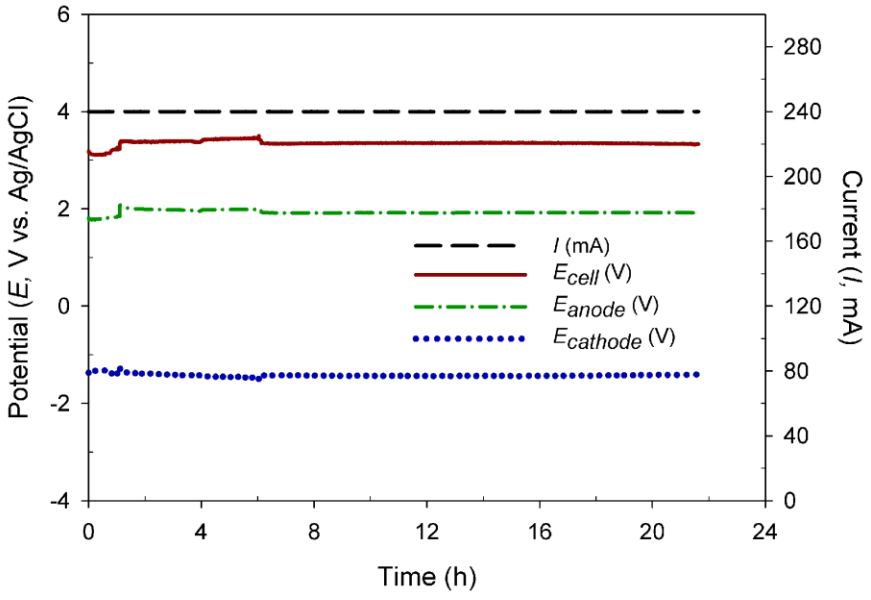


**Figure B 1. Chronovoltammetric profiles of anodic, cathodic and cell potentials recorded during the electrochemical oxidation of ROC at Ti/$RuIrO_2$.**

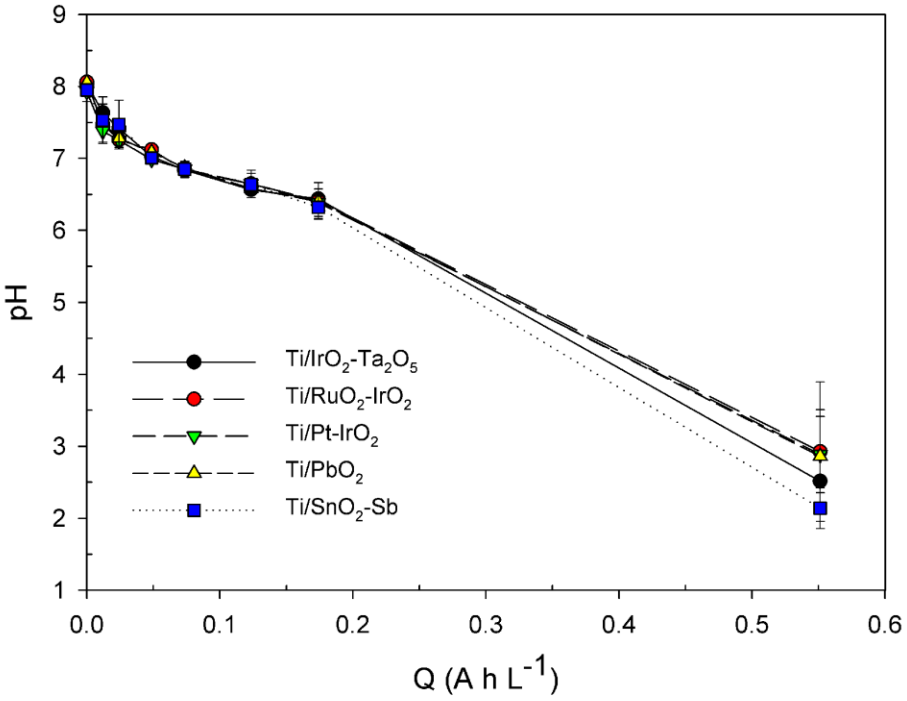


**Figure B 2. Decrease in pH observed at mixed metal oxide (MMO) anodes during electrochemical oxidation of reverse osmosis concentrate (ROC).**

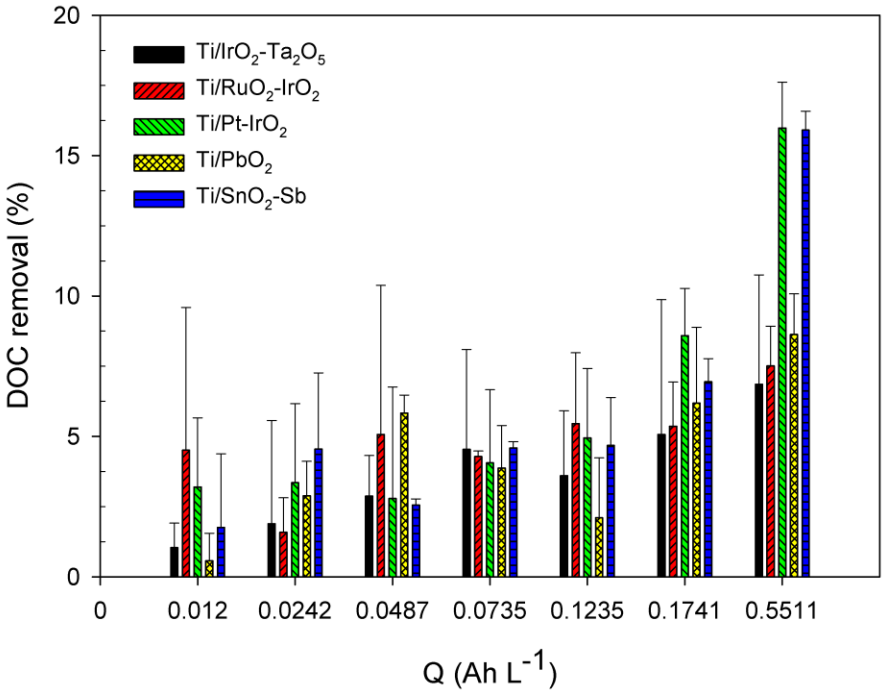


**Figure B 3. Removal of DOC versus *Q* for the different electrode materials tested.**

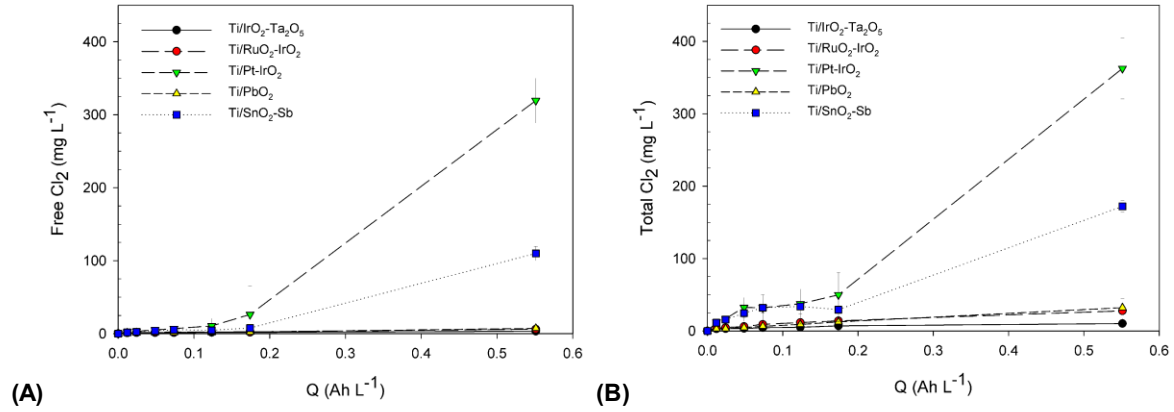


**Figure B 4. Evolution of: A) free $Cl_2$, and B) total $Cl_2$, as determined by the DPD method for each electrode material tested, versus Q.**

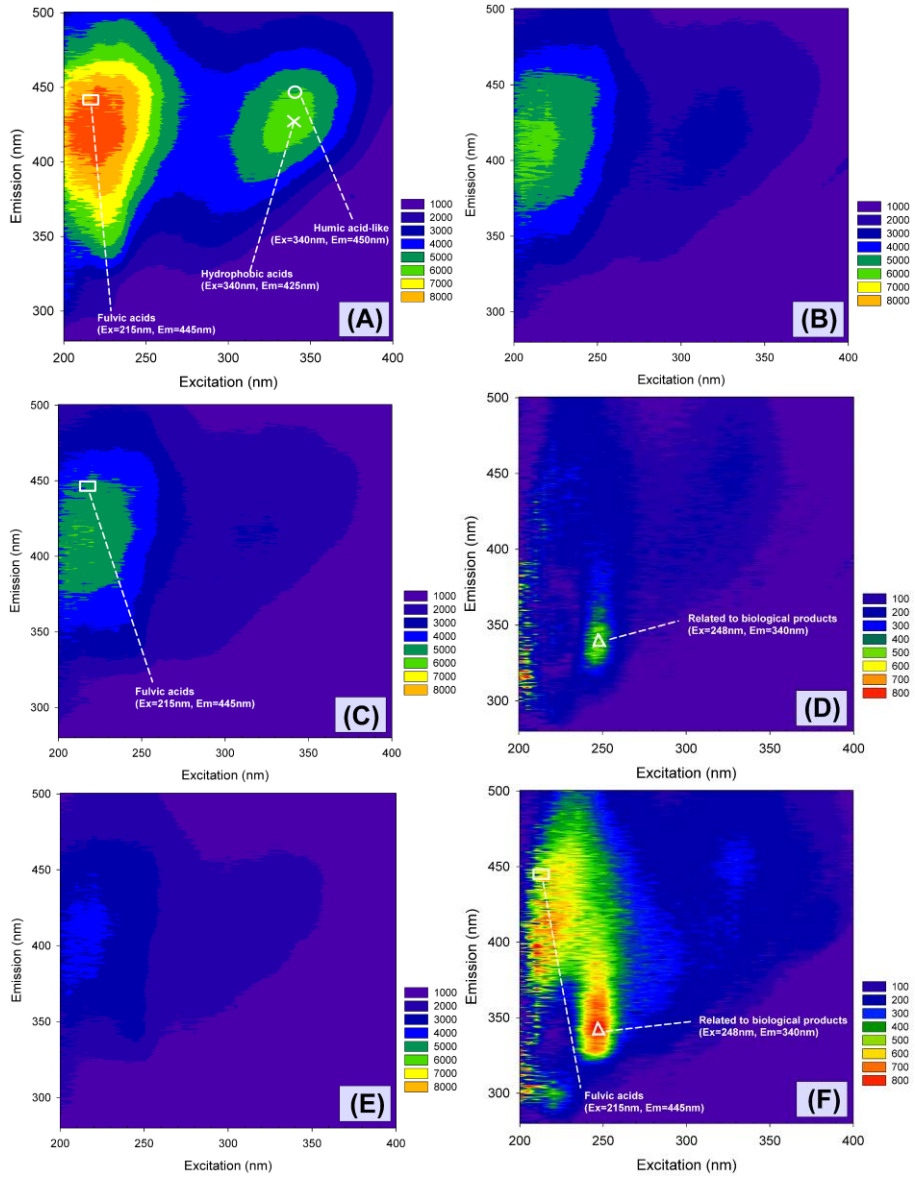


**Figure B 5. Identification of organics as indicated by EEM for: A) untreated ROC, and remaining compounds after treatment ($Q$ = 0.55 Ah $L^{-1}$) by: B) Ti/$IrO_2$-$Ta_2O_5$, C) Ti/$RuO_2$-$IrO_2$, D) Ti/Pt-$IrO_2$, E) Ti/$PbO_2$, and F) Ti/$SnO_2$-Sb. The EEM in Ti/Pt-$IrO_2$ and Ti/$SnO_2$-Sb was plotted in higher scale (ten times lower fluorescence intensities than the others).**

# APPENDIX C - Supporting Information for Chapter 4.2. Electrochemical Oxidation at Ruiro2–Coated Titanium Electrode

## Experimental Set-Up

In the continuous experiments two different ROC samples were used, collected at the abovementioned AWTP within a one month time span and marked as ROC-1 and ROC-2 (physico-chemical characteristics of ROC-1 and ROC-2 are given in Table C1), while in batch experiments only ROC-1 was used.

**Table C 1. Main characteristics of the two ROC samples used in the experiments.**

| Measures | ROC-1 | ROC-2 |
|---|---|---|
| pH | 7.5 | 7.7 |
| Conductivity, mS $cm^{-1}$ | 4.25 | 3.97 |
| Colour, mg Pt-Co $L^{-1}$ | 104.6 | 174.9 |
| SUVA, L $mg^{-1}$ $m^{-1}$ | 1.6 | 2.3 |
| DOC, mg $L^{-1}$ | 57.1 | 57.2 |
| $Cl^-$, mg $L^{-1}$ | 1.5 | 1.2 |
| $Fe^{2+}$, mg $L^{-1}$ | 0.22 | 0.35 |
| $Mn^{2+}$, mg $L^{-1}$ | 227 | 234 |
| $SO_4^{2-}$, mg $L^{-1}$ | 241 | 239 |

The experiments were performed at constant liquid flow-rate at room temperature (25 ± 1 °C), with galvanostatic control in: i) continuous mode, with step-wise increase in current density ($J$ = 1, 10, 30, 50, 100, 150, 200 and 250 A $m^{-2}$) (Figure C 1), and samples taken after 75 min of operation at each current density, and ii) batch mode at $J$ = 250 A $m^{-2}$, and samples taken after 2, 4, 7 and 23.5 h. In the continuous mode experiments, the system was operated at a hydraulic retention time (HRT) of 8.8 min (i.e. flow-rate of 13 mL $min^{-1}$). In order to maintain well-mixed conditions and avoid concentration gradients, both anolyte and catholyte were recirculated internally at a rate of 162 mL $min^{-1}$. In order to avoid gas trapping inside the anodic and cathodic compartment and enable stable potentials and ambient pressure, two degassers were installed as illustrated in Figure C 1. The volume of ROC in the degassers was maintained at 100 mL, providing a ratio of active and total volume, $V_{ACT}/V_{TOT}$ of 0.51 in the continuous mode.

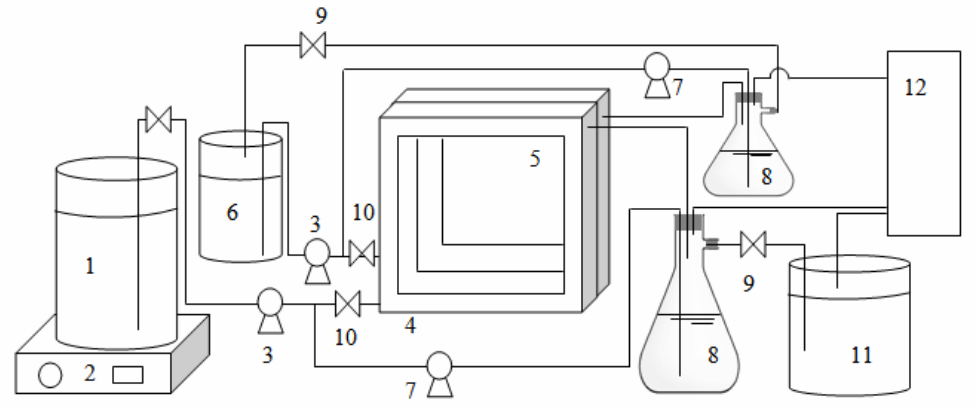


**Figure C 1. Scheme of laboratory-scale electrochemical reactor operating in the continuous mode. 1-anode feed tank, 2-magnetic stirrer, 3-feed pump, 4-anode cell, 5-cathode cell, 6-cathode feed tank, 7-recycling pump, 8-holding vessel for gas release, 9-effluent sampling point, 12-gass collector (suction tube).**

Preparative continuous oxidation experiments were carried out in order to establish the time required to reach steady state. In the batch mode experiments, anolyte and catholyte were recirculated at a rate of 162 mL $min^{-1}$. The volume of ROC used in batch experiments was 10 L, hence the ratio of $V_{ACT}/V_{TOT}$ was 0.011. The results of each experimental condition are given as the means of triplicates, with their corresponding standard deviations (SDs).

**Table C 2. Concentrations of target analytes measured in the ROC samples after the spiking.**

| Compound | $c_1$ (ROC-1), µg $L^{-1}$ | $c_2$ (ROC-b), µg $L^{-1}$ |
|---|---|---|
| DEET | 8.3 | 8.6 |
| Caffeine (CAFF) | 15.7 | 18.3 |
| Carbamazepine (CBZ) | 7.8 | 8.1 |
| Atrazine (ATZ) | 9.9 | 9.8 |
| Sulfadiazine (SDZ) | 18.6 | 22.5 |
| Phenytoin (PNT) | 19.9 | 29.2 |
| Diazinon (DZN) | 13.6 | 14.1 |
| Metolachlor (MET) | 13.3 | 15.4 |
| Tramadol (TML) | 13.5 | 14.0 |
| Metoprolol (MTP) | 18.2 | 14.6 |
| Venlafaxine (VNF) | 16.8 | 17.1 |
| Trimethoprim (TMP) | 25.6 | 26.3 |
| Sertraline (SRL) | 15.7 | 22.9 |
| Ranitidine (RNT) | 25.4 | 12.8 |
| Norfloxacin (NFL) | 10.5 | 12.6 |
| Enrofloxacin (ENR) | 14.7 | 15.4 |
| Citalopram (CTP) | 13.3 | 13.6 |
| Lincomycin (LNC) | 8.6 | 8.7 |
| Roxithromycin (ROX) | 14.5 | 14.4 |
| Iopromide (IPM) | 37.4 | 33.7 |
| Acetaminophen (ACTP) | 14.1 | 14.7 |
| Hydrochlorothiazide (HCT) | 13.4 | 18.5 |
| Gemfibrozil (GMF) | 14.3 | 17.0 |
| Diclofenac (DCF) | 15.5 | 15.4 |
| Diuron (DIU) | 11.5 | 11.3 |
| 2,4-D | 13.6 | 12.9 |
| Triclopyr (TPR) | 10.1 | 9.2 |
| Ibuprofen (IBU) | 20.7 | 21.2 |

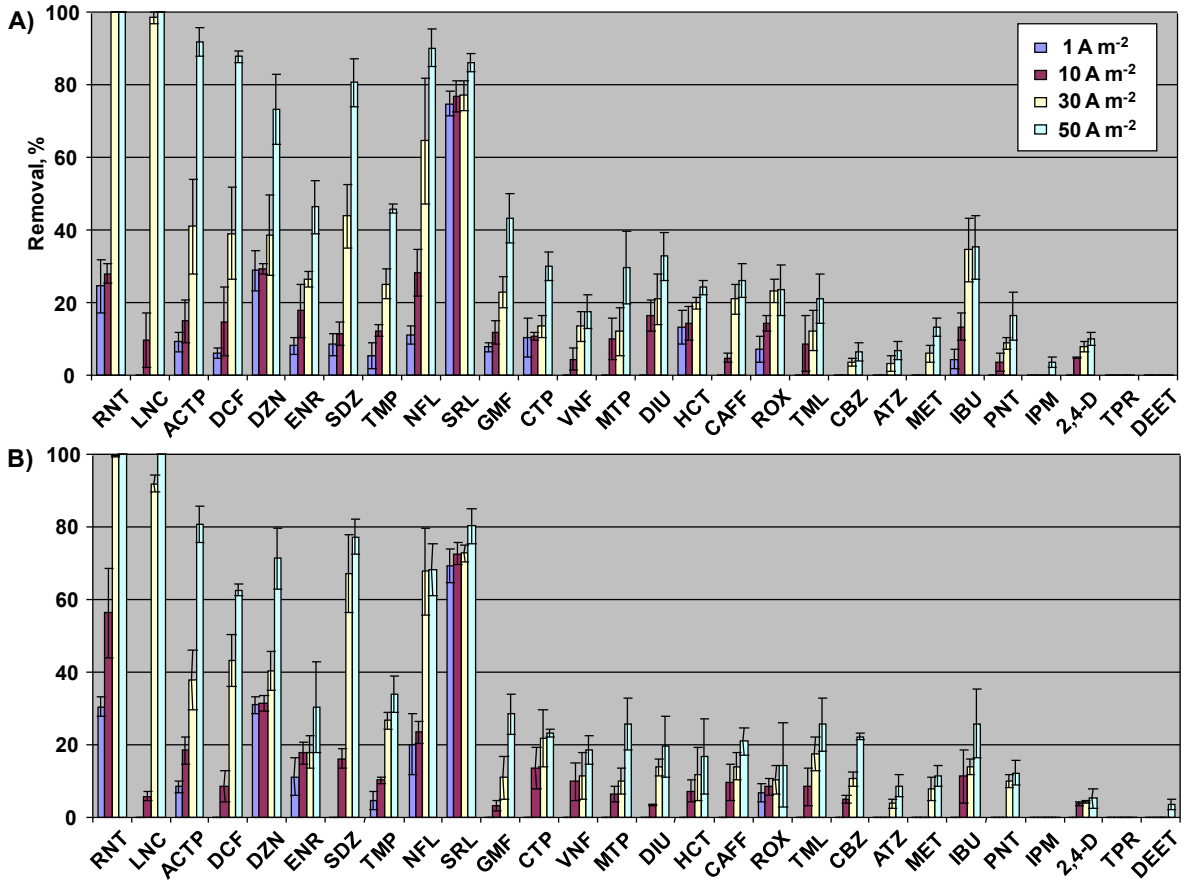


**Figure C 2. Removals of target analytes during anodic oxidation in continuous mode, with stepwise increase in current density (J=1-50 A $m^{-2}$) of: a) ROC-1, and b) ROC-2, spiked with the trace organic contaminants. Values are expressed as mean with their SDs.**

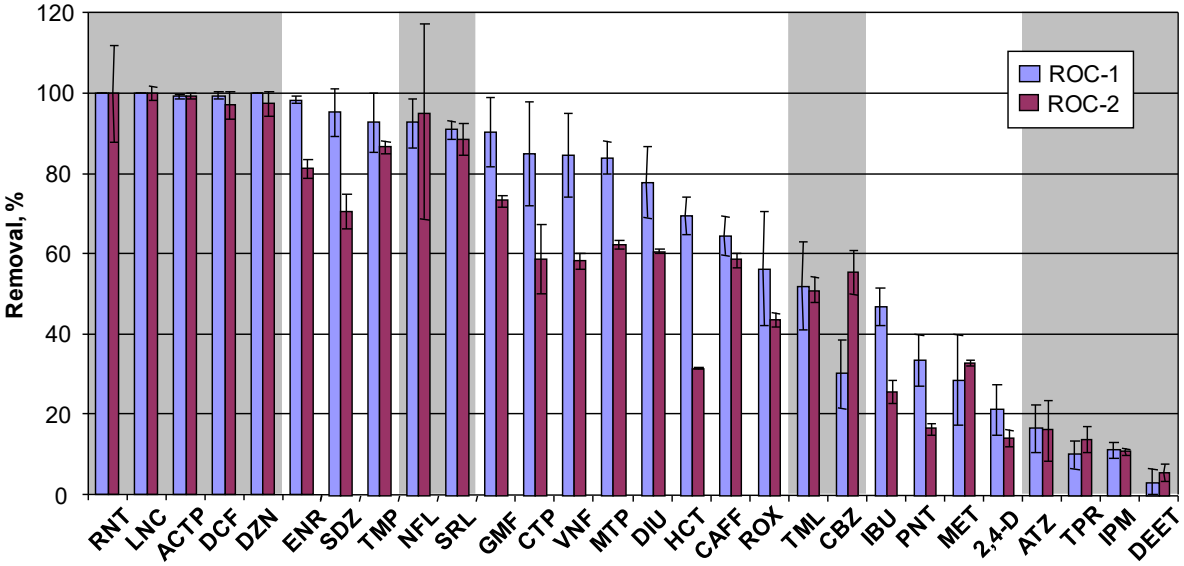


**Figure C 3. Removal of target contaminants in electrochemical oxidation of ROC-1 and ROC-2 at Ti/RuIrO2 anode at J=100 A $m^{-2}$.**

# APPENDIX D - Supporting Information for Chapter 4.3. Comparison of Electrochemical Oxidation Pathways and By-Products at Ti/Ruiro2 and Ti/Sno2–Sb Electrodes

## Experimental Set-Up

To investigate the electrochemical oxidation pathways of metoprolol (MTP), 1 L of ROC collected prior to the nitrification stage at AWTP Bundamba was amended with the target compound dissolved in water to a final concentration of MTP of 50 µM. The spiked ROC was then recirculated over the electrochemical cell over a period of 3 h, at current densities $J = 100$ and 250 A m$^{-2}$ using Ti/$Ru_{0.7}Ir_{0.3}O_2$ or a Ti/$SnO_2$-Sb electrode. The system was operated in batch mode, with 1 mL samples taken every 5–15 min during the 3 h experiment.

The measured anode potentials ($E_{AN}$) of Ti/$RuIrO_2$ and Ti/$SnO_2$-Sb were 1.77 ± 0.1 and 2.25 ± 0.06 V vs Ag/AgCl, respectively. No electrode passivation was observed in any of the experiments conducted. The anolyte pH decreased from the initial pH 7.75 ± 0.1 to pH 3.4 ± 0.15 ($J = 100$ A m$^{-2}$) and 2.4 ± 0.1 ($J = 250$ A m$^{-2}$) using Ti/$RuIrO_2$ anode, and to pH 2.7 ± 0.2 ($J = 100$ A m$^{-2}$) and 2.2 ± 0.1 ($J = 250$ A m$^{-2}$) using Ti/$SnO_2$–Sb anode.

To determine the toxicity of formed by-products relative to the parent compound, 10 L of the same ROC matrix containing MTP (50 µM) was oxidised in batch mode using the same reactor and the Ti/$SnO_2$-Sb anode, at $J = 250$ A m$^{-2}$. 100 mL samples were taken after 2, 4, 6, 8, 10 and 24 h and extracted by a previously optimised SPE method. Analysis of sample extracts used in bioassays enabled assignment of the observed ecotoxic effect to a mixture of specific, newly identified by-products. All experiments were performed in duplicate under galvanostatic control, at room temperature (25 ± 1 °C).

## Qualitative Analysis of MTP By-Products

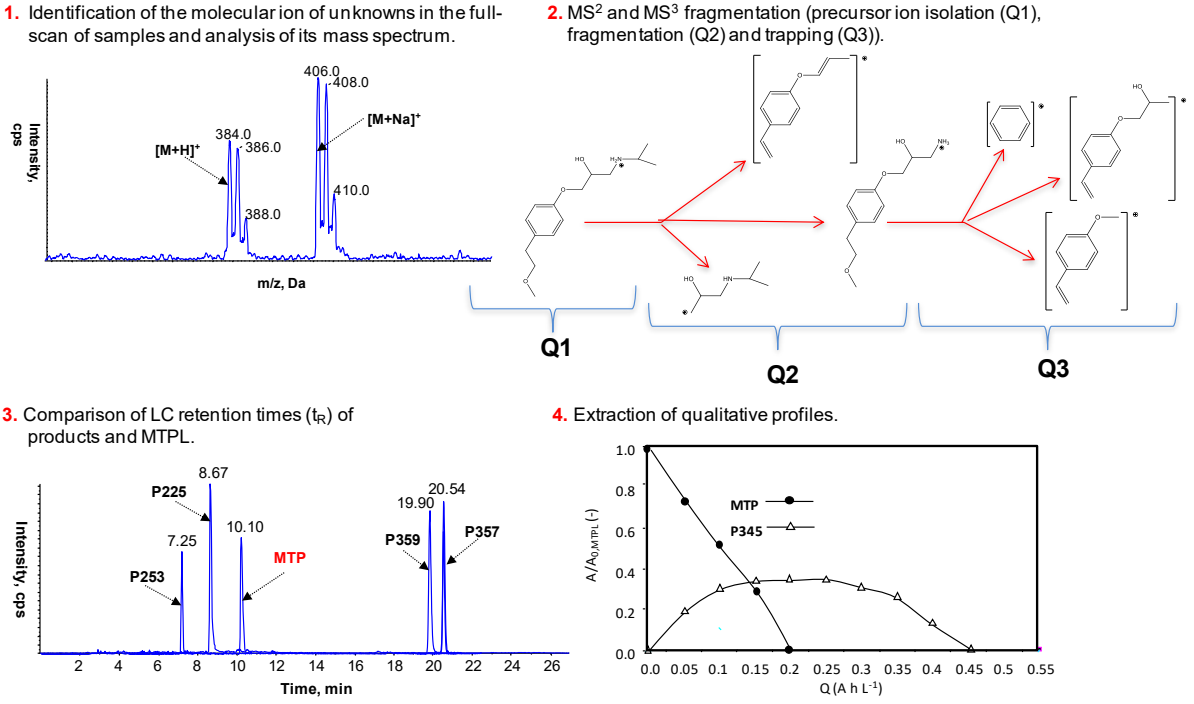


**Figure D 1. The main steps in qualitative analysis of unknown by-products using QTRAP-MS.**

The main steps in qualitative analysis using QLIT-MS are: *i)* full-scan mode experiments with optimised chromatographic conditions, in order to detect the peaks of unknown by-products, *ii)* $MS^2$ fragmentation of the identified molecular ions of the unknown by-products, *iii)* $MS^3$ fragmentation of the molecular ions of unknowns in order to confirm the proposed structure, *iv)* comparison of chromatographic retention times ($t_R$) obtained with $t_R$ of the parent compound, and *v)* extraction of qualitative profiles of the postulated by-products and comparison with the profiled of parent compound and other related by-products (Figure D 1). Figure D 2 illustrates $MS^2$ and $MS^3$ spectra of two structurally similar by-products, P349 (hydroxylated form) and P347 (keto form), as well as the MS spectra of the molecular ion, sodium and potassium adducts of product P347. The same approach was applied for all other by-products (data can be found in the Supporting Information of [113]). Extracted ion chromatograms of MTP and its by-products are illustrated in Figure D 3.

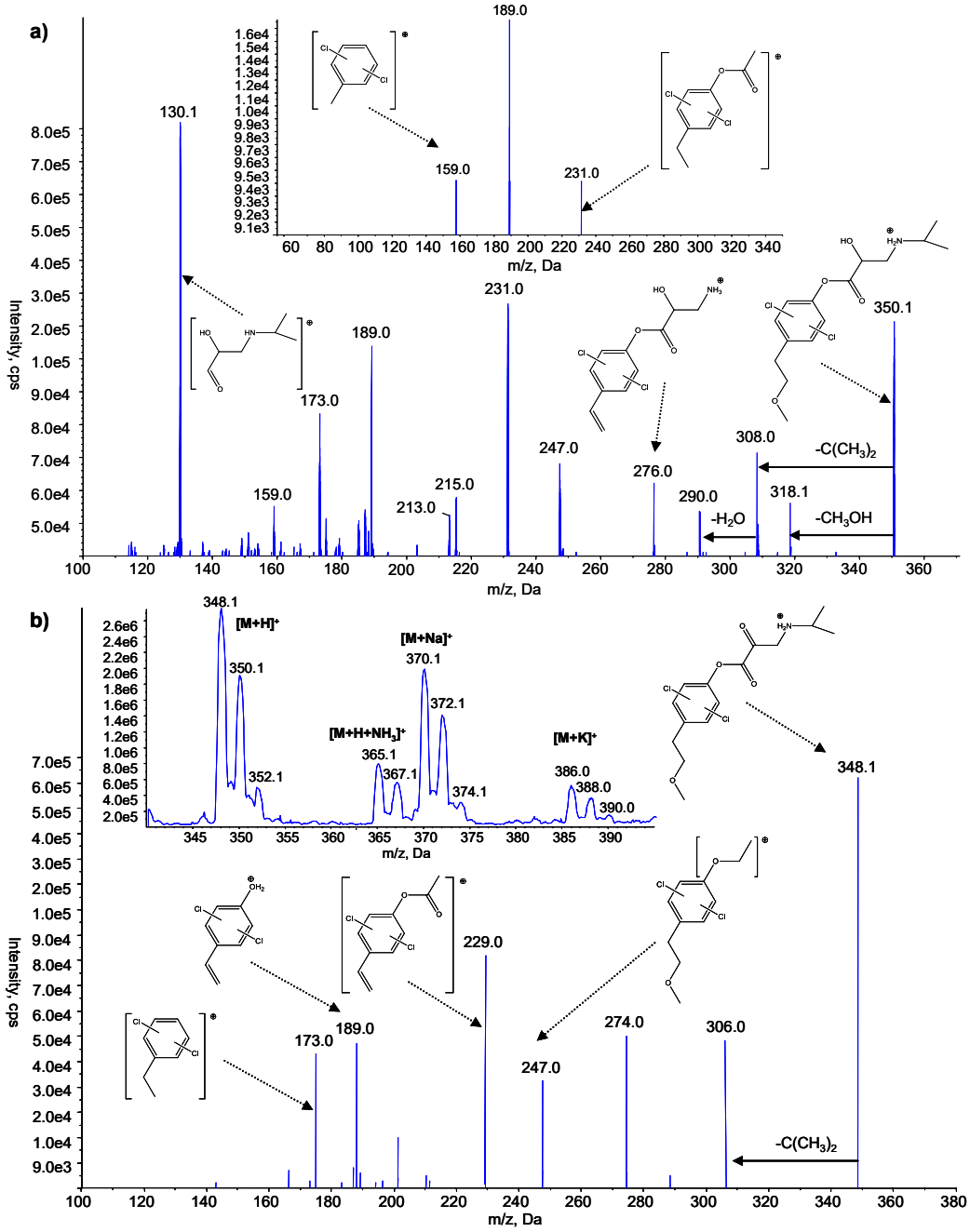


**Figure D 2. A) (+)ESI-QqLIT-MS2 spectrum of P349; insert: (+)ESI-QqLIT-MS3 spectrum: m/z 350→m/z 276, B) (+)ESI-QqLIT-MS2 spectrum of P347; insert: (+)ESI-QqLIT-MS spectrum of P347, [M+H]+ at m/z 348.1, [M+H+NH3]+ at m/z 365.1. [M+Na]+ at m/z 370.1 and [M+K]+ at 386.0.**

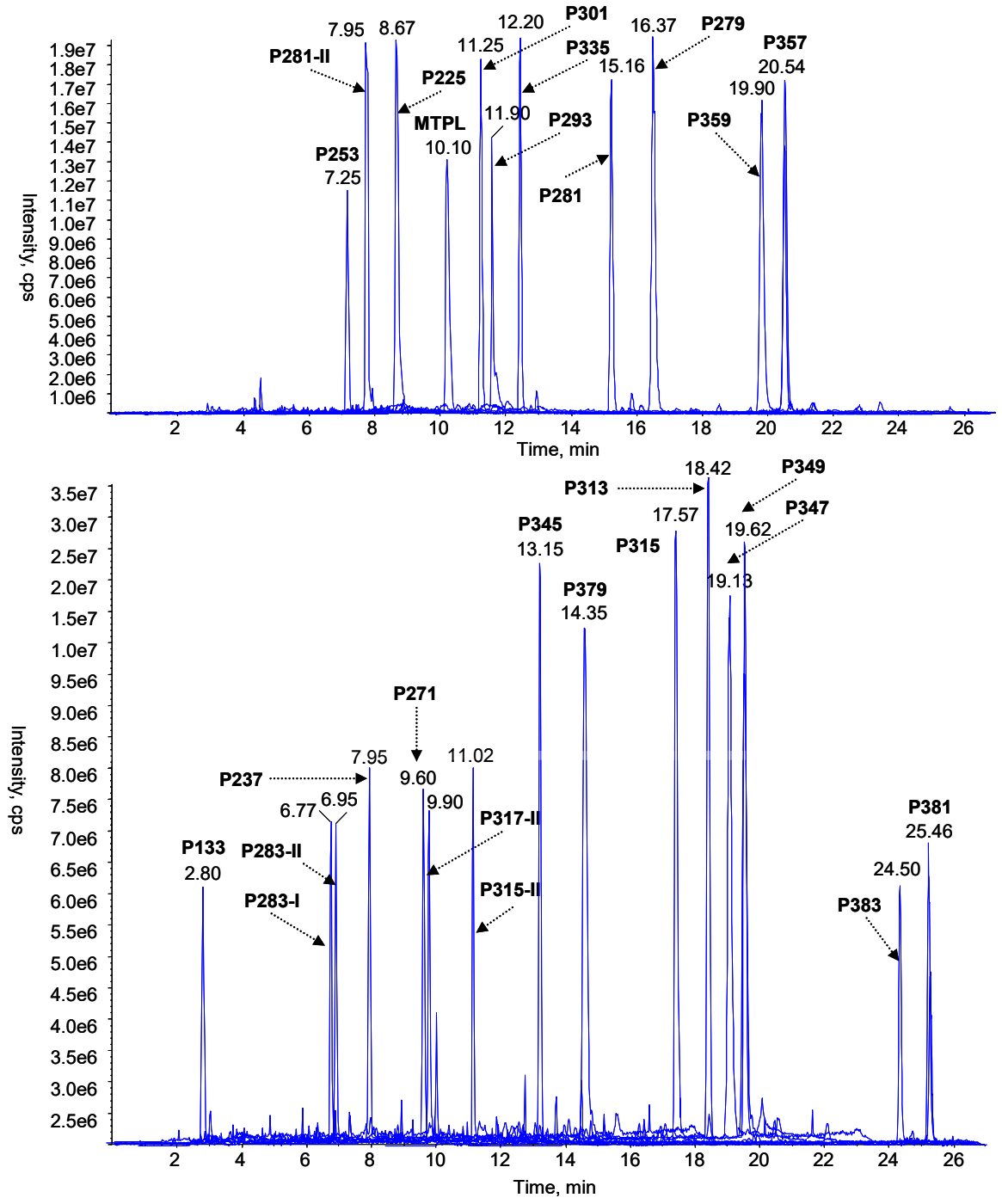


**Figure D 3. Extracted ion chromatograms of MTP and its identified electrochemical products, obtained at UFLC-(+)ESI-QqLIT-MS.**

**Table D 1. Identified electrochemical oxidation products of MTP in ROC.**

| Compound | Molecular Formula | MW | $t_R$ (min) | Proposed Structure |
|---|---|---|---|---|
| **MTP** | $C_{15}H_{25}NO_3$ | 267.18 | 10.10 | 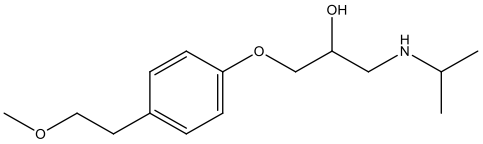 |
| **P133** | $C_6H_{15}NO_2$ | 133.11 | 2.80 | 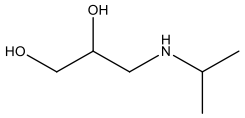 |
| **P283-I** | $C_{15}H_{25}NO_4$ | 283.18 | 6.15 | 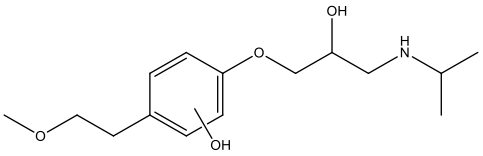 |
| **P253** | $C_{14}H_{23}NO_3$ | 253.17 | 7.25 | 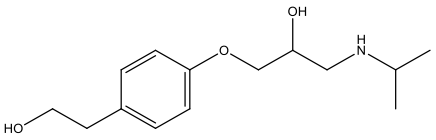 |
| **P283-II** | $C_{15}H_{25}NO_4$ | 283.18 | 6.77 | 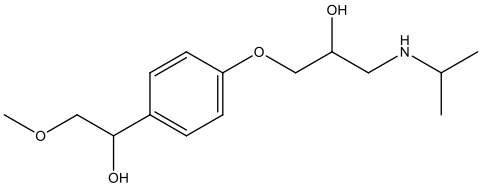 |
| **P237** | $C_{14}H_{23}NO_2$ | 237.17 | 7.95 | 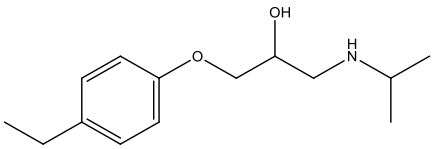 |
| **P281-II** | $C_{15}H_{23}NO_4$ | 281.17 | 6.95 | 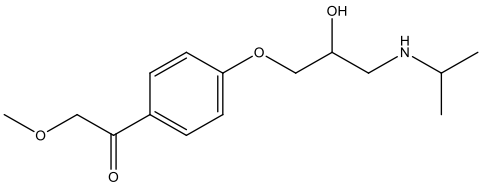 |
| **P225** | $C_{12}H_{19}NO_3$ | 225.14 | 8.70 | 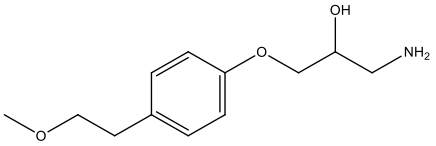 |
| **P271** | $C_{14}H_{22}ClNO_2$ | 271.13 | 9.60 | 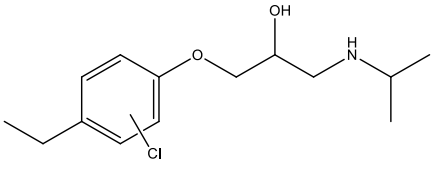 |

| Compound | Molecular Formula | MW | $t_R$ (min) | Proposed Structure |
|---|---|---|---|---|
| **P317-II** | $C_{15}H_{24}ClNO_4$ | 317.14 | 9.90 | 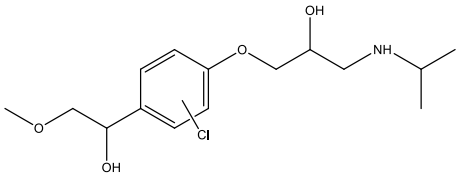 |
| **P293** | $C_{12}H_{17}Cl_2NO_3$ | 293.06 | 11.90 | 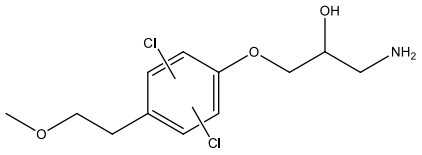 |
| **P315-II** | $C_{15}H_{22}ClNO_4$ | 315.12 | 11.02 | 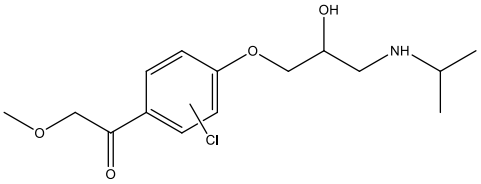 |
| **P301** | $C_{15}H_{24}ClNO_3$ | 301.14 | 11.25 | 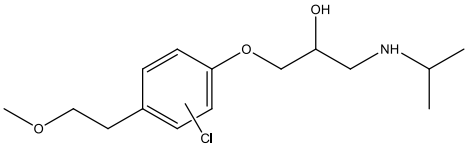 |
| **P345** | $C_{15}H_{24}BrNO_3$ | 345.10 | 13.15 | 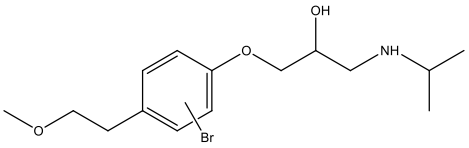 |
| **P335** | $C_{15}H_{23}Cl_2NO_3$ | 335.10 | 12.2 | 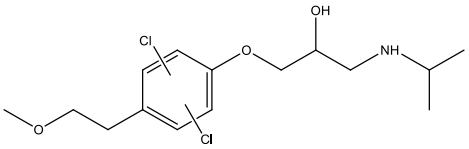 |
| **P379** | $C_{15}H_{23}ClBrNO_3$ | 14.35 | 379.05 | 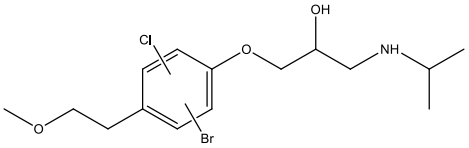 |
| **P281** | $C_{15}H_{23}NO_4$ | 281.16 | 15.16 | 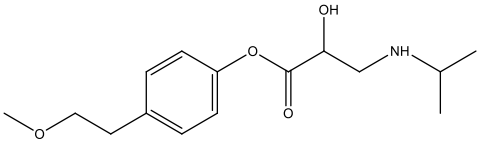 |
| **P279** | $C_{15}H_{21}NO_4$ | 279.15 | 16.37 | 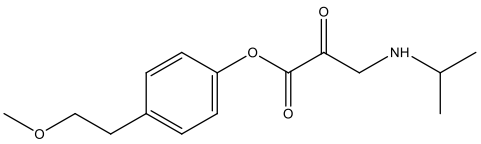 |
| **P315** | $C_{15}H_{22}ClNO_4$ | 315.12 | 17.57 | 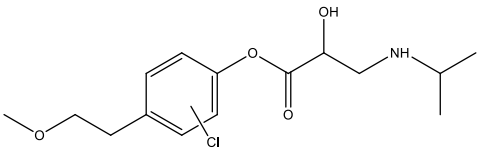 |

| Compound | Molecular Formula | MW | $t_R$ (min) | Proposed Structure |
|---|---|---|---|---|
| **P313** | $C_{15}H_{20}ClNO_4$ | 313.11 | 18.42 | 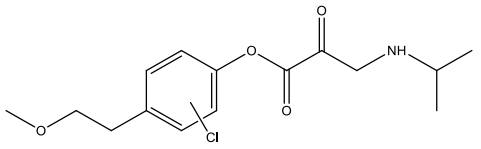 |
| **P349** | $C_{15}H_{21}Cl_2NO_4$ | 349.08 | 19.13 | 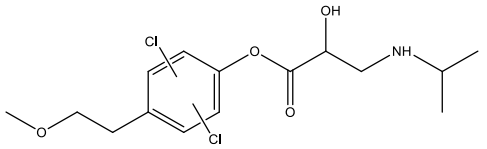 |
| **P347** | $C_{15}H_{19}Cl_2NO_4$ | 347.07 | 19.62 | 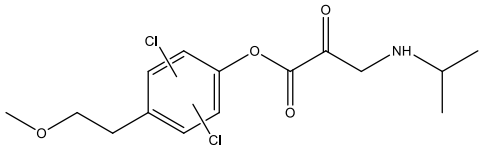 |
| **P359** | $C_{15}H_{22}BrNO_4$ | 359.07 | 19.90 | 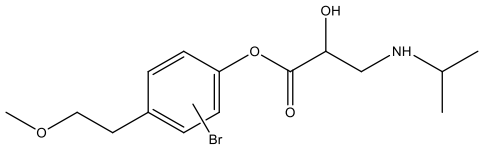 |
| **P357** | $C_{15}H_{20}BrNO_4$ | 357.06 | 20.54 | 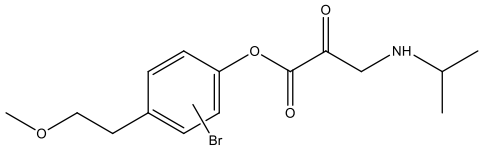 |
| **P383** | $C_{15}H_{20}Cl_3NO_4$ | 383.05 | 24.50 | 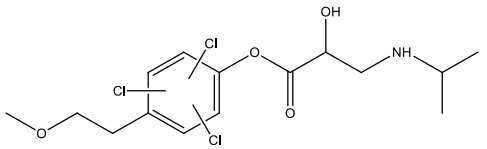 |
| **P381** | $C_{15}H_{18}Cl_3NO_4$ | 381.03 | 25.46 | 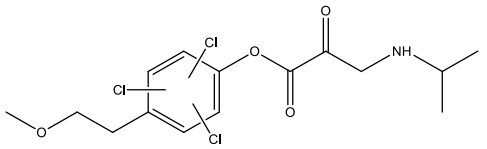 |

Due to the lack of analytical standards, the newly identified by-products could not be quantified. Figure D 4 and Figure D 5 illustrate the qualitative profiles of MTP and its halogenated derivatives, determined by the peak area in full-scan (+)ESI experiments with non-extracted samples, and normalised to the initial peak area of MTP ($t$ = 0 min), plotted versus specific electrical charge consumed (Q, Ah $L^{-1}$).

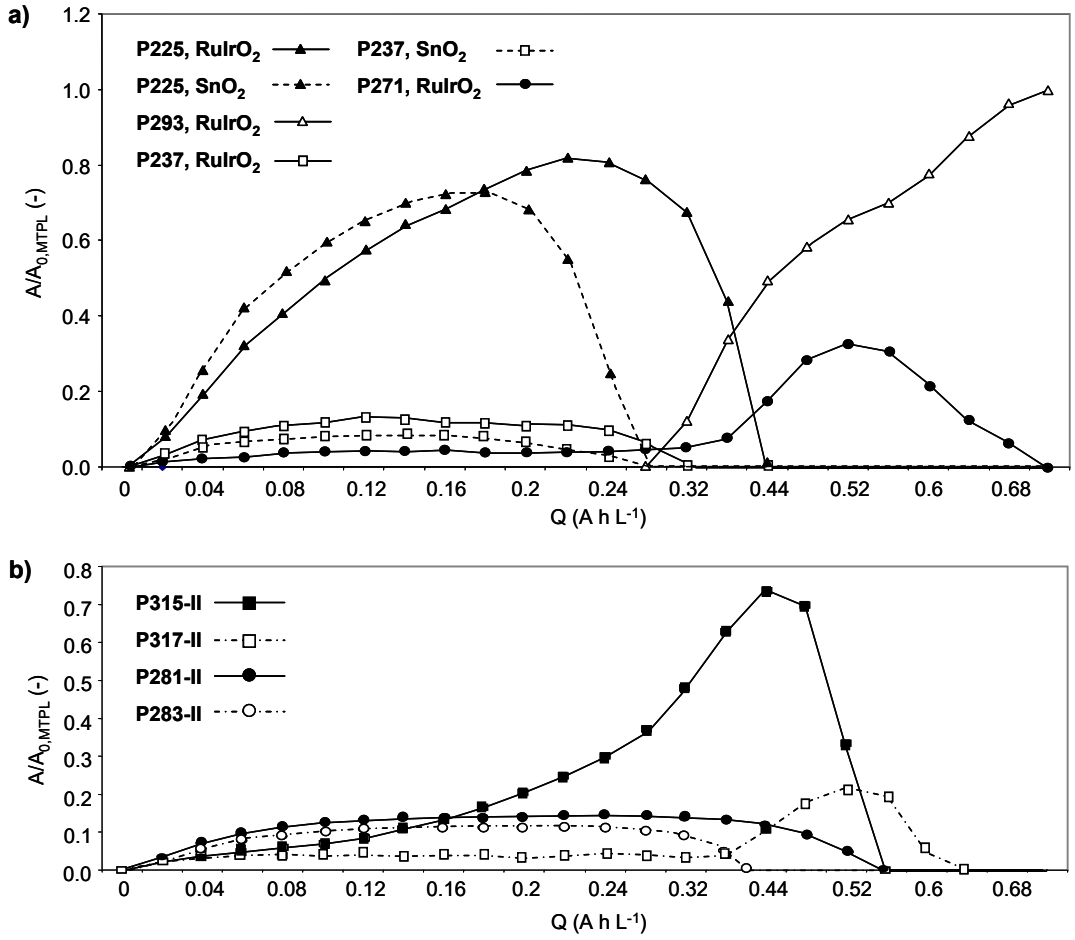


**Figure D 4. The peak areas of products P225, P237, P271 and P293, formed during electrochemical oxidation, normalised to the initial value of the peak area of MTP (t=0) presented vs. Q (A h $L^{-1}$): A) $Ti/Ru_{0.3}Ir_{0.7}O_2$ and $Ti/SnO_2$-$Sb_2O_5$, J=100 A $m^{-2}$ and B) $Ti/Ru_{0.3}Ir_{0.7}O_2$, J=100 A $m^{-2}$.**

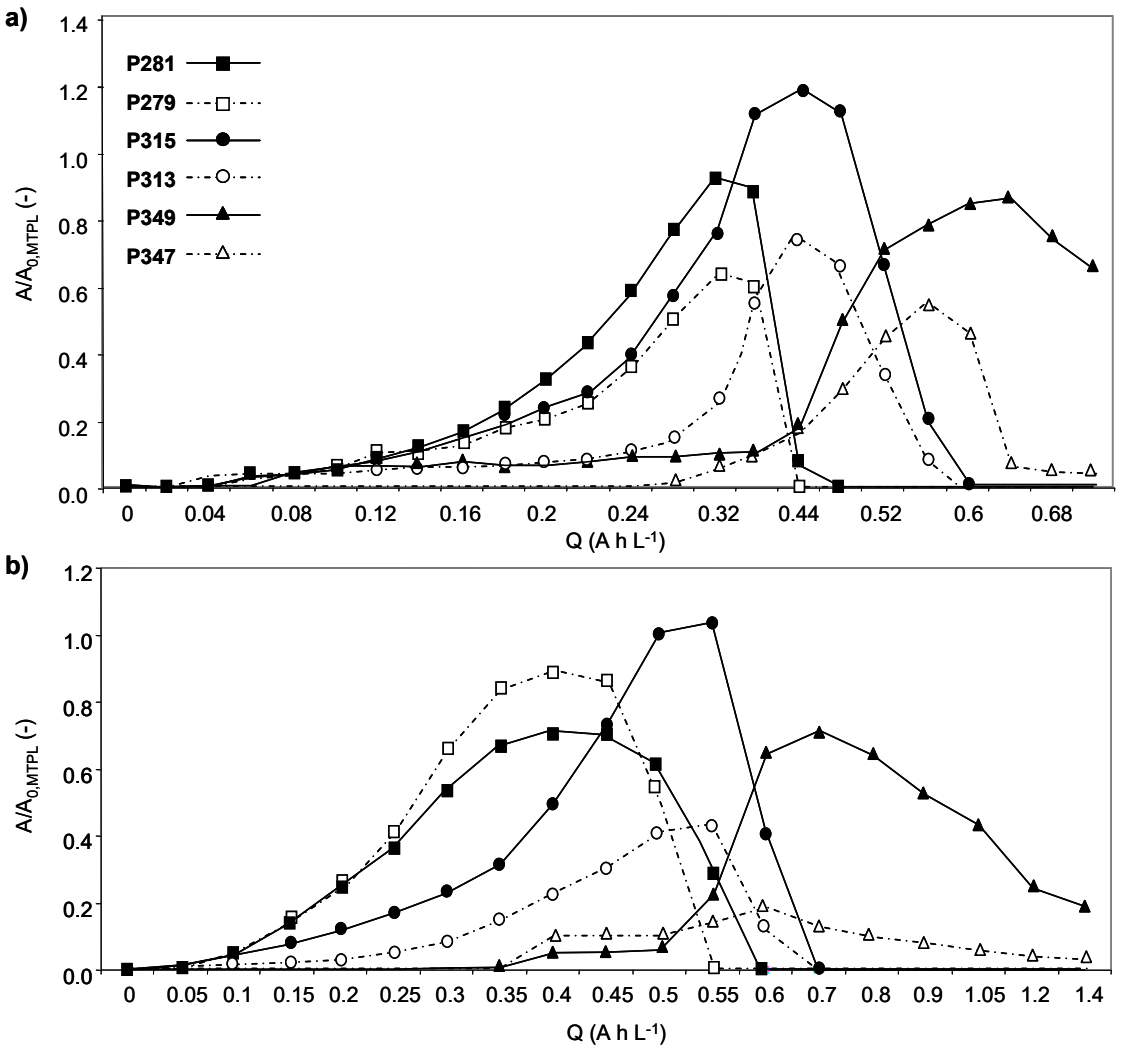


**Figure D 5. The peak areas of products P279, P281, P313, P315, P347 and P349, formed during electrochemical oxidation, normalised to the initial value of the peak area of MTP (t=0) presented vs. Q (A h $L^{-1}$): a) $Ti/Ru_{0.3}Ir_{0.7}O_2$, J=100 A $m^{-2}$ and b) $Ti/Ru_{0.3}Ir_{0.7}O_2$, J=250 A $m^{-2}$.**

In Figure D 6 are presented qualitative profiles of products that were detected in the sample extracts. As illustrated in, 17 out of the 25 identified products were retained and detected in the SPE sample extracts used for the bioassay analyses under these conditions. The toxicity experiment had to be performed with a larger volume of the reaction mixture due to the need for larger sample volumes for the bioassays. Since the ratio of total (i.e.$V_T$=10 L) vs. active anolyte volume (i.e. $V_{ACT}$=114 mL) was augmented relative to the first experiment performed (i.e. $V_T$=1 L), qualitative profiles of MTPL and its products were shifted towards higher values of specific electrical charge, and rates of formation and degradation of oxidation by-products were decreased. Thus, in the last sample taken, the concentration of halogenated by-products was still significant, and the experiment would have to be run for significantly longer time in order to observe a decrease in their concentration.

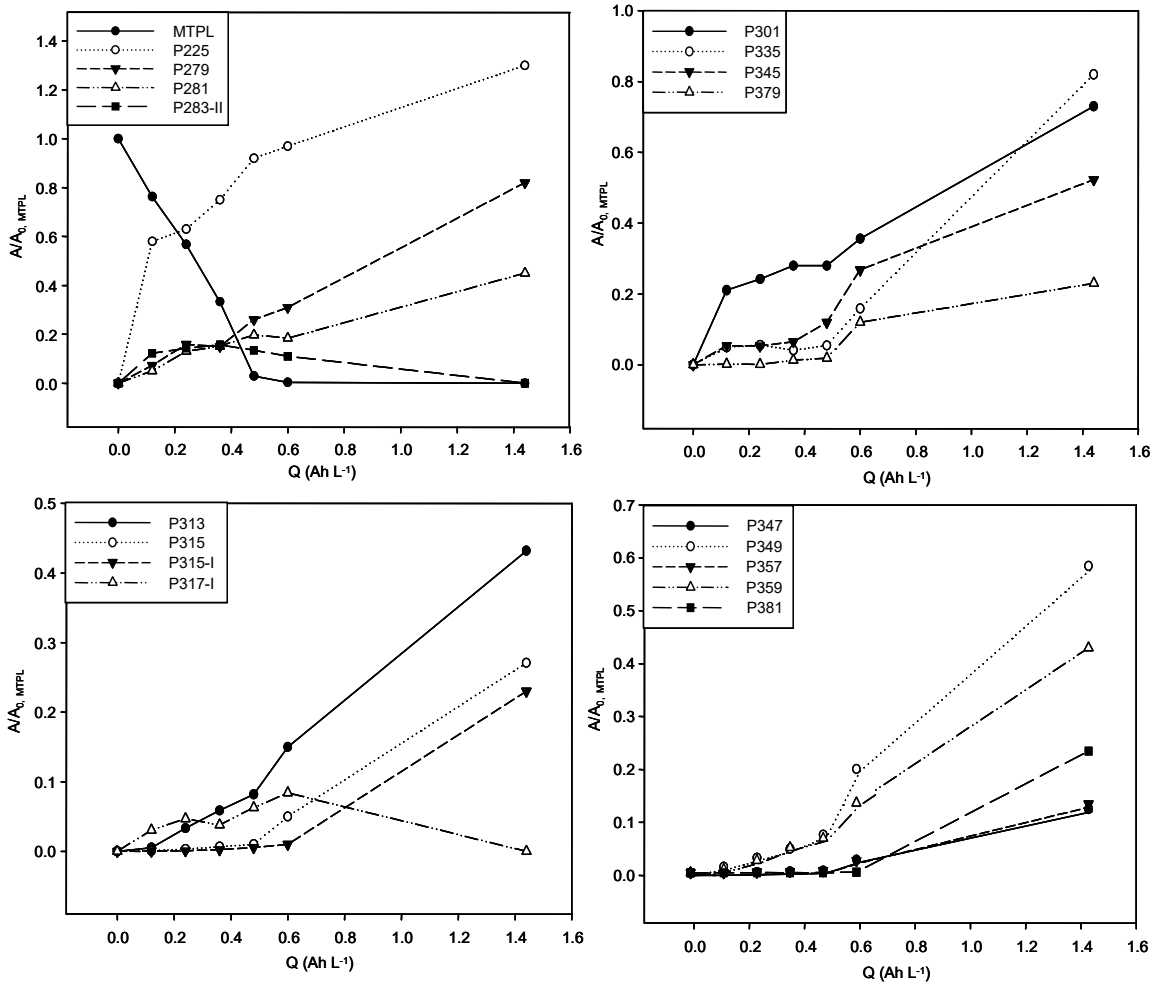


**Figure D 6. The peak areas of MTP and its electrochemical oxidation products generated at Ti/$SnO_2$-Sb anode ($V_T$=10 L, $V_{ACT}$=114 mL, J=250 A $m^{-2}$) normalised to the initial value of the peak area of MTP (t=0) presented vs. Q (A h $L^{-1}$), determined for the sample extracts (i.e. SPE treated samples) used for bioassay analyses. All peak areas were obtained from extracted ion chromatograms in full-scan experiments in (+)ESI-QqLIT-MS. Because of very high concentration of MTPL and its products, 1:5 dilutions of sample extracts were applied before scanning the samples.**

The toxicity of the samples increased with ongoing electrochemical oxidation as the shift of the concentration effect curves in the Microtox assay towards lower concentrations (expressed as relative enrichment factors REF) demonstrates (Figure D 7). A logREF of 0 represents the original sample, lower logREF refer to diluted, higher logREF to enriched samples. All endpoints in the combined algae test showed the same pattern (data not shown).

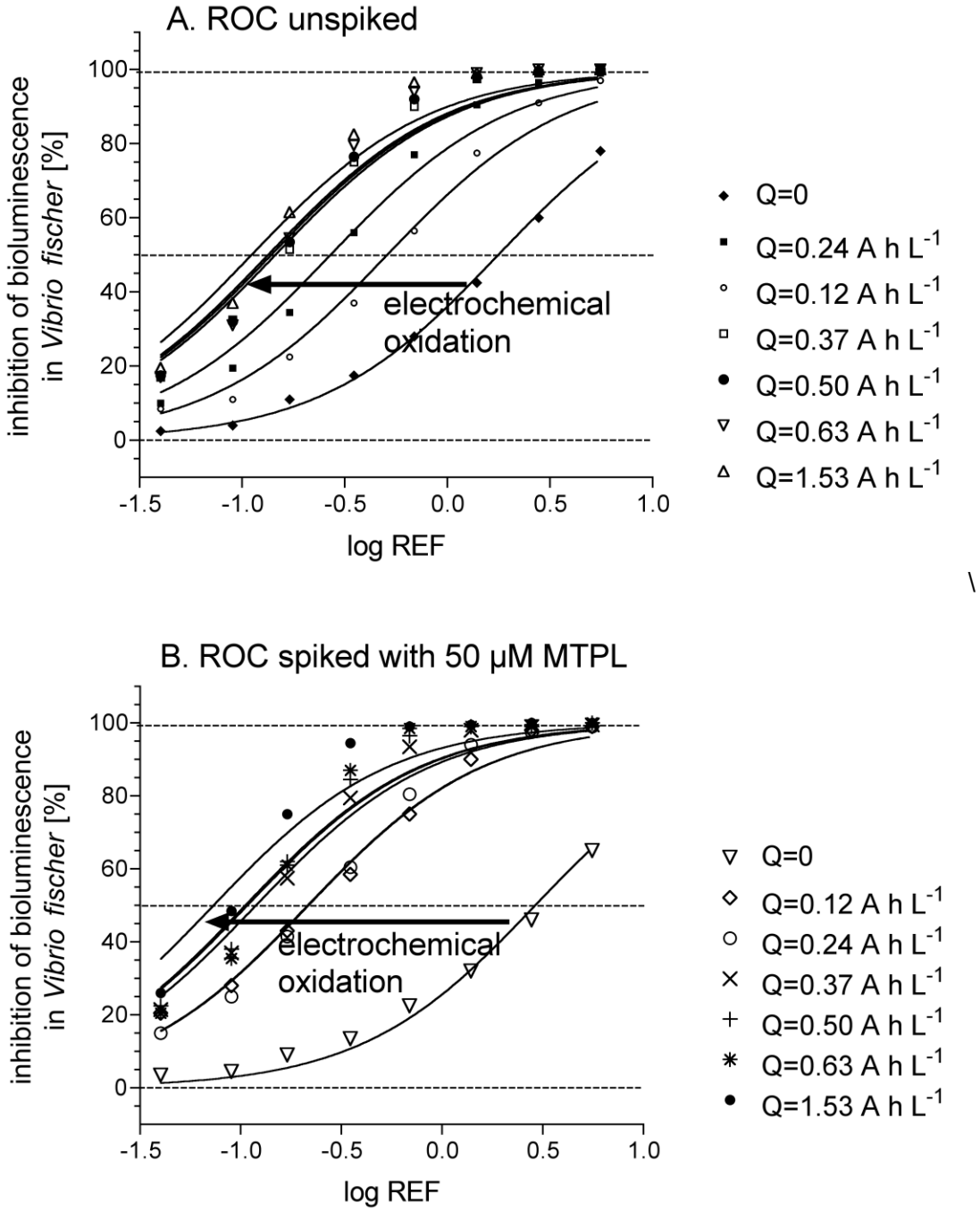


**Figure D 7. Concentration-effect curves of A. ROC unspiked and B. ROC spiked with 50 µM MTPL in the Microtox assay.**

The $1/EC_{50}$ values (inverse value to associate a high number with a high toxicity and vice versa) were then plotted as a function of the specific electrical charged consumed. Figure D 8 depicts $1/EC_{50}$ values for all endpoints of the combined algae test. MTP shows highest sensitivity for 24h IPAM, closely followed by 24h growth rate and 2h IPAM. For most baseline toxicants, the 24h IPAM and the growth rate endpoint were very similar typically the growth rate exceeding slightly the toxicity of 24h IPAM. Thus the pattern of MTP is the pattern of a baseline toxicant. At the beginning of the electrochemical oxidation experiment the samples showed an endpoint pattern influenced by herbicides, with 24h IPAM only slightly more toxic than 2h IPAM and the growth endpoint was seven

times less sensitive than direct inhibition of photosynthesis. This is an indication that the ROC contained a significant portion of herbicides, which dominated the mixture toxicity. This picture changes immediately with onset of the electrochemical oxidation- the ability to inhibit photosynthesis after 2h of exposure decreased proportionally with increasing charge applied and the non-specific toxicity detected by the 24h IPAM and growth endpoints dominated the picture. It is interesting to note that MTP itself had no contribution to the mixture toxicity at 50 µM concentration but its transformation products formed must contribute substantially as the toxicity increased more in the spiked sample than in the raw ROC. Given that the ROC reaction mixture is dominated by non-specific toxicity, we can compare the $EC_{50}$ values directly with those of the Microtox assay (Figure D 9). As is evident from Figure D 9, the $EC_{50}$ values are lower in the Microtox assay, i.e. it is the more sensitive assay for the same samples, presumably because of matrix interferences, which are known to be more problematic for the Microtox assay, but the relative trends over the course of the oxidation experiments are very similar, indicating that both assays respond in a similar fashion to the transformation products.

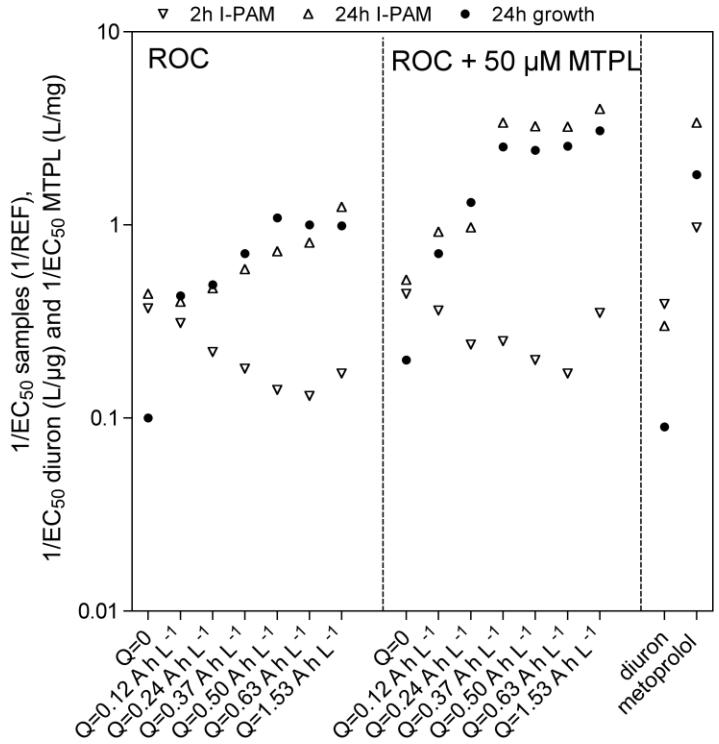


**Figure D 8. $1/EC_{50}$ values for all endpoints of the combined algae test.**

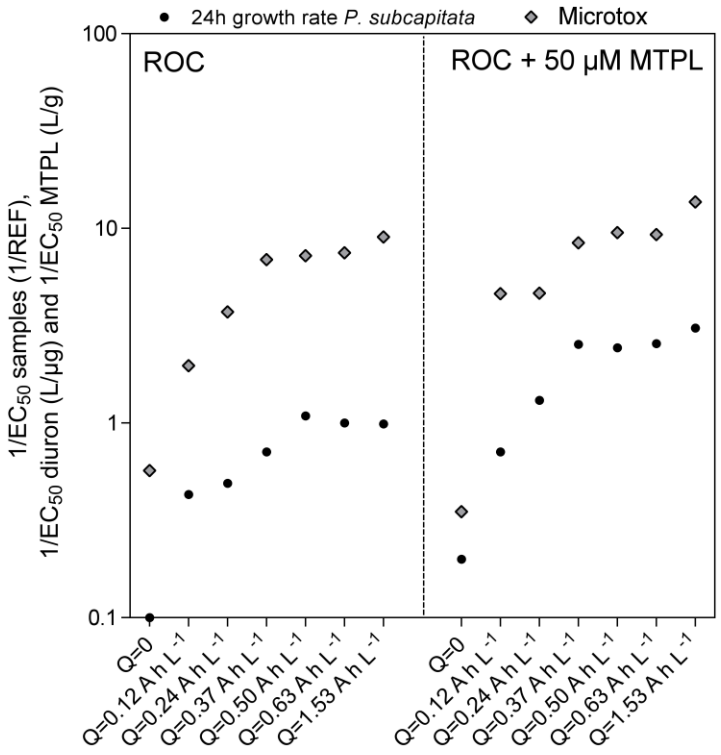


**Figure D 9. Baseline-TEQ derived from the $EC_{50}$ values of the Microtox assay and of the 24h growth endpoint of the combined algae test.**

As nonspecific toxicity dominates the algal 24h growth rate inhibition, it is justified to convert the $EC_{50}$ values of the 24h growth rate to baseline-TEQ. As baseline toxicity is concentration-additive in mixtures, i.e. the baseline-TEQ are additive, we can subtract the baseline-TEQ of the ROC samples from the baseline-TEQ of the ROC samples spiked with MTPL to obtain the contribution of the transformation products to the mixture toxicity at any given Q. The resulting Δbaseline-TEQ agree well between *Vibrio fischeri* and algae and they show a linear relationship with the applied charge Q (Figure D 10).

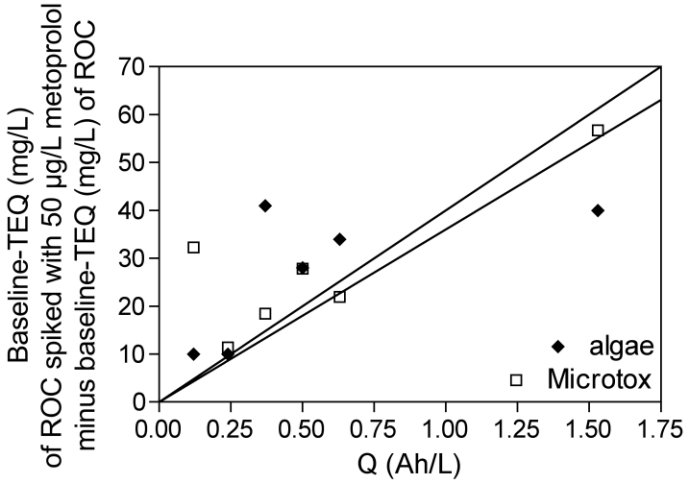


**Figure D 10. Contribution to the formed products from MTPL to the increase in toxicity, expressed as baseline-TEQ of spiked ROC minus ROC, during electrochemical oxidation.**

While the transformation products were not quantified due to lack of standards but just their relative peak area, the total sum of the peak area of the transformation products may provide a first measure of the total amount of products formed. As we do not have the octanol-water partition coefficients $K_{ow}$ available for all transformation products, their baseline toxicity cannot be estimated. Since the $K_{ow}$ is proportional to the retention time of the reverse phase HPLC, we can at least weigh the peak areas by their relative hydrophobicity relative to MTPL ($t_R$/ $t_{R,MTPL}$) to get an approximate measure of the baseline-TEQ caused by the identified products. This measure (sum($A/A_{0,MTPL}*t_R/t_{R,MTPL}$)) correlated linearly with the experimental baseline-TEQ of ROC spiked with 50 µM MTPL minus baseline-TEQ (mg/L) of ROC (Figure D 11), thus confirming the relevance of the toxicity of the transformation products formed during electrochemical oxidation.

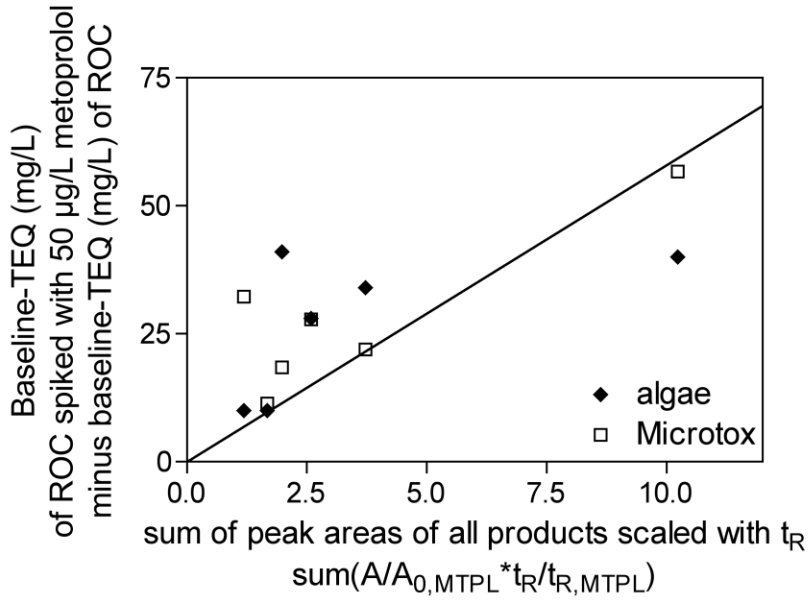


**Figure D 11. Relationship between baseline-TEQ of spiked ROC minus ROC, and sum of peak areas of the identified products (see Figure S22), scaled with the retention times in the HPLC to account for toxicity differences due to hydrophobicity.**

# APPENDIX E - Supporting Information for Chapter 4.5. Electrochemical Oxidation at Boron Doped Diamond Electrodes

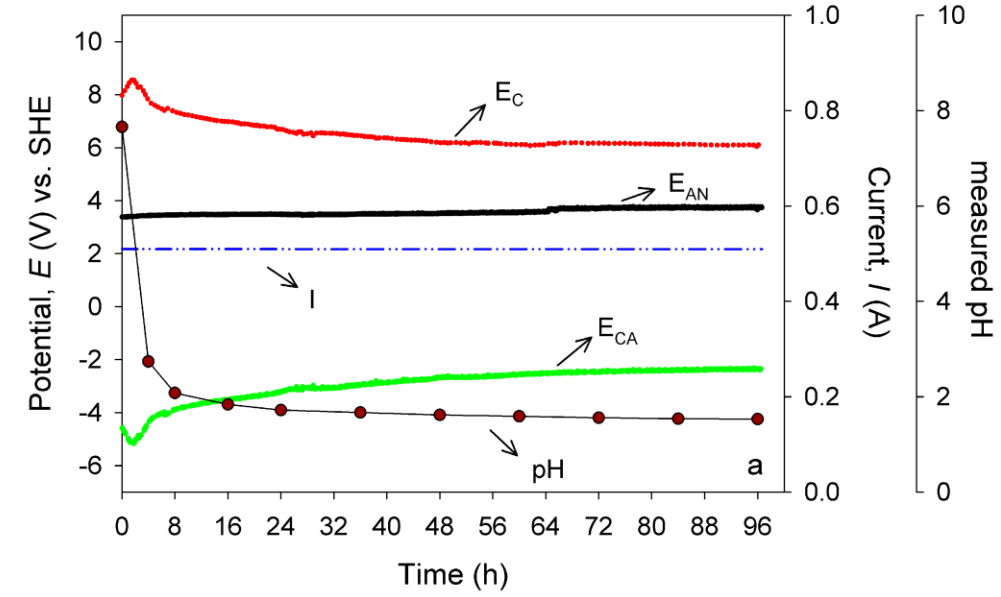


(A)

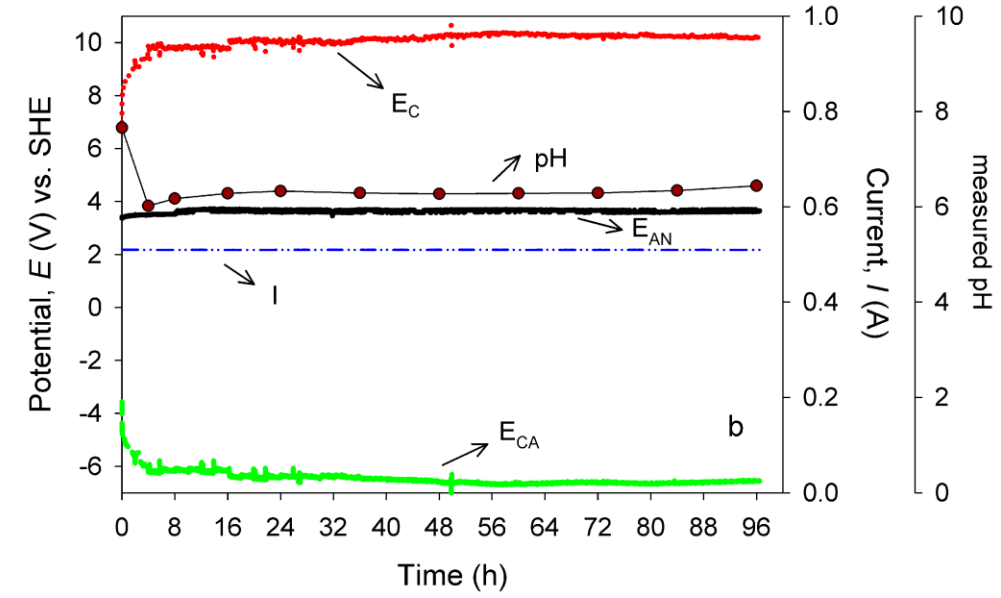


(B)

**Figure E 1. Chronovoltammetric response of the BDD electrode at I= 510 mA for electrochemical oxidation of ROC at: A) acidic pH, and B) circumneutral pH.**

**Table E 1. THMs and HAAs measured in electrochemical oxidation of ROC using BDD anode after *Q* = 5.2 and 10.9 Ah $L^{-1}$ in pH 1-2 and pH 6-7 (J = 12.5 mA $cm^{-2}$).**

| DBPs | Compound | Concentration (μM) at Q (Ah $L^{-1}$) | | | | |
|---|---|---|---|---|---|---|
| | | 0 - initial (pH = 7.66) | 5.2 (pH 1.62) | 10.9 (pH = 1.53) | 5.2 (pH 6.27) | 10.9 (pH = 6.44) |
| HAAs | Monochloroacetic Acid | 0.19 | 3.66 | 1.47 | 3.49 | 2.92 |
| | Dichloroacetic Acid | 0.63 | 4.43 | 2.87 | 12.30 | 9.17 |
| | Trichloroacetic Acid | 0.06 | 12.88 | 7.69 | 11.86 | 9.78 |
| | Bromochloroacetic Acid | 0.19 | 0.70 | 0.28 | 1.09 | 0.39 |
| | Monobromoacetic Acid | 0.04 | 0.15 | 0.09 | 0.12 | 0.04 |
| | Dibromoacetic Acid | 0.06 | 0.13 | 0.02 | 0.15 | 0.02 |
| | Total HAAs | 1.17 | 21.96 | 12.42 | 29.00 | 22.32 |
| THMs | Chloroform | 0.65 | 2.62 | 0.91 | 11.11 | 3.85 |
| | Bromodichloromethane | 0.16 | 0.33 | 0.09 | 1.49 | 0.51 |
| | Dibromochloromethane | 0.07 | 0.12 | 0.04 | 0.27 | 0.09 |
| | Bromoform | 0.03 | 0.02 | 0.01 | 0.03 | 0.01 |
| | Total THMs | 0.92 | 3.10 | 1.05 | 12.91 | 4.47 |

# APPENDIX F - Supporting Information for Chapter 4.6. Electrochemical Oxidation of Electrodialysed Reverse Osmosis Concentrate

## Experimental Set-Up

Electrodialysis was performed in Type C reactor (Figure 3). Electrochemical oxidation experiments were performed in the cation exchange membrane (CEM) divided electrochemical cell, Type-A reactor, in batch mode at a constant current of 510 mA (anodic current density, $J = 12.5$ mA cm$^{-2}$). In order to maintain well-mixed conditions and avoid concentration gradients, both anolyte (i.e. total volume, $V_{TOT} = 5$ L of ROC) and catholyte (i.e. 0.5 M $H_2SO_4$ solution, 2 L) were continuously recirculated through the anode and cathode half-cells, respectively, during 96 h at a rate of 120 mL min$^{-1}$ with vigorous magnetic stirring in each electrolyte vessel. The experiments were performed at two operating pH values: (i) acidic pH (i.e. pH 1–2) where no pH adjustment was applied during electrolysis, and (ii) controlled, circumneutral pH, where aliquots of a 3 M NaOH solution were automatically added by a dosing system to keep the pH in the range of pH 6–7 during electrolysis. The pH and temperature values were monitored using a pH transmitter (CPM 223, Endress + Hauser) with the probe placed in the holding vessel. In the case of controlled pH conditions, a peristaltic pump was connected to the pH transmitter for the automatic dosing (flow rate: 4–5 mL h$^{-1}$) into the anodic compartment.

In order to determine the effect of pH on chlorine and oxygen evolution at the BDD electrode used in this study, linear sweep voltammetry (LSV) experiments were performed in electrolyte solutions of the same ionic strength (i.e. $\mu = 0.5$) at pH 7 (0.5 M NaCl solution and 0.16 M $Na_2SO_4$ solution) and at pH ≤ 1 (0.5 M HCl solution + 0.25 M $NaNO_3$ solution and 0.25 M $H_2SO_4$ solution). 55 mL samples of the oxidised ROC were taken after 0, 4, 8, 16, 24, 36, 48, 60, 72, 84 and 96 h of electrolysis and filtered using a 0.22 µm Millipore syringe unit prior to further analyses. After determining free and available chlorine in the samples, the remaining amount of samples was then quenched by adding a specific volume of 0.24, 0.48, or 0.71 M $Na_2SO_3$ solution in order to eliminate further reaction of active chlorine. Quenching agent was added in 120% excess of the molar concentration of FAC, i.e. 1.2 mol of sulphite per mol of HClO, assuming all chlorine was in HClO form. The volume of the quenching agent solution added was kept to a minimum of no more than 2 mL of $Na_2SO_3$ solutions.

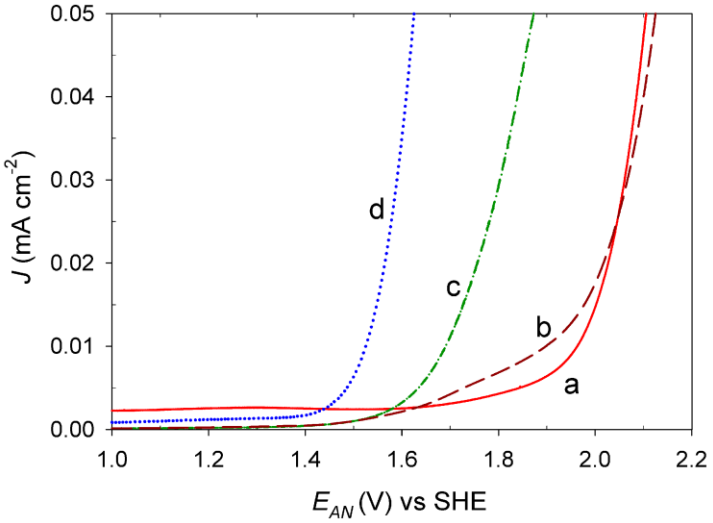


**Figure F 1. Linear sweep voltammograms (LSVs) of BDD anode in aqueous solution: A) 0.25 M H2SO4 solution (pH 0.5), B) 0.5 M HCl + 0.25 M NaNO3 solutions (pH 0.5), and C) 0.16 M Na2SO4 solution (pH 7) and (d) 0.5 M NaCl solution (pH 7). Scan rate: 10 mV s-1.**

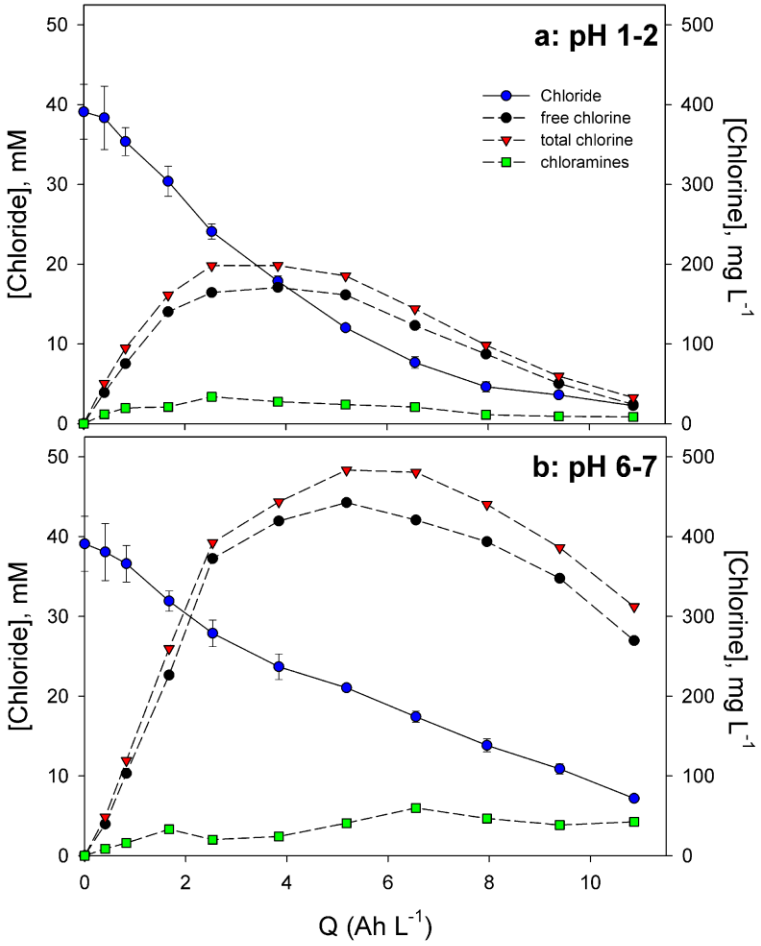


**Figure F 2. Depletion of chloride ions and profile of formed chlorine species (chlorine and chloramines) measured vs. Q during electrochemical oxidation of ROC at A) acidic pH, and B) circumneutral pH conditions. Error value is the average deviation of duplicate analyses.**

# LIST OF PUBLICATIONS

The following publications have been delivered from this research:

J Radjenović, A Bagastyo, D Batstone, J Keller. Electrochemical treatment of reverse osmosis concentrates. In **Encyclopedia of Applied Electrochemistry**. Eds: R. F. Savinell, K-i Ota, G. Kreysa. In press. 2013. Springer, Berlin, Germany.

AY Bagastyo, DJ Batstone, K Rabaey, J Radjenović. 2012. Electrochemical oxidation of electrodialysed reverse osmosis concentrate on Ti/Pt-$IrO_2$, Ti/$SnO_2$-Sb and boron-doped diamond electrodes. **Water Research**. Submitted. 2012.

AY Bagastyo, DJ Batstone, I Kristiana, W Gernjak, C Joll, J Radjenović. Electrochemical oxidation of reverse osmosis concentrate on boron-doped diamond anodes at circumneutral and acidic pH. **Water Research**. 46 (18) (2012) 6104-6112, 2012.

AY Bagastyo, DJ Batstone, W Gernjak, K Rabaey, J Radjenović. Electrochemical Treatment of Reverse Osmosis Concentrate: Strategies to Minimise the Formation of Halogenated By-Products. Platform Presentation and Conference Paper. Eds: D Begbie, W Sharon. In: **4th UWSRA Science Forum**. June, 2012. Brisbane Australia.

AY Bagastyo, DJ Batstone, I Kristiana, Y Mu, W Gernjak, C Joll, J Radjenović. Electrochemical oxidation of reverse osmosis concentrates on boron-doped diamond electrodes. Platform Presentation. **9th IWA Leading-Edge Technology (LET) Conference on Water and Wastewater Technologies**. June 2012. Brisbane, Australia.

AY Bagastyo, J Radjenović, Y Mu, RA Rozendal, DJ Batstone, K Rabaey. Electrochemical oxidation of reverse osmosis membrane concentrates on mixed metal oxide (MMO) titanium coated electrodes. **Water Research**. 45 (16) (2011) 4951-4959.

AY Bagastyo, J Radjenović, I Kristiana, Y Mu, DJ Batstone, W Gernjak, C Joll, K Rabaey. Electrochemical treatment of problematic reverse osmosis concentrates. Eds: D Begbie, W Sharon. In: **3rd UWSRA Science Forum.** September, 2011. Brisbane, Australia.

J Radjenović, M Macova, AY Bagastyo, B Escher, K Rabaey. Electrochemical oxidation for the removal of organic micropollutants. Platform Presentation. **7th IWA Micropol and Ecohazard Conference**. July, 2011. Sydney, Australia.

J Radjenović, AY Bagastyo, K Rabaey. Electrochemical treatment of reverse osmosis concentrates. Platform Presentation. **8th IWA International Conference on Water Reclamation and Reuse**. September, 2011. Barcelona, Spain.

AY Bagastyo, J Radjenović, Y Mu, RA Rozendal, DJ Batstone, K Rabaey. Electrochemical treatment of reverse osmosis concentrates. Platform Presentation. **62nd ISE Electrochemistry Conference**. September, 2011. Niigata, Japan.

J Radjenović, B Escher, K Rabaey. Electrochemical degradation of the β-blocker metoprolol by Ti/$Ru_{0.7}Ir_{0.3}O_2$ and Ti/$SnO_2$-Sb electrodes. **Water Research**. 45 (10) (2011) 3205-3214.

J Radjenović, AY Bagastyo, RA Rozendal, Y Mu, J Keller, K Rabaey. Electrochemical oxidation of trace organic contaminants in reverse osmosis concentrate using $RuO_2$/$IrO_2$ coated titanium anodes. **Water Research**. 45 (4) (2011) 1579-1586.

AY Bagastyo, J Radjenović, Y Mu, RA Rozendal, DJ Batstone, K Rabaey. Influence of electrode materials on the electrochemical oxidation of reverse osmosis concentrates. Poster presentation. In: **2nd UWSRA Science Forum**. September, 2010. Brisbane, Australia.

J Radjenović, A Bagastyo, Y Mu, RA Rozendal, K Rabaey. Electrochemical Treatment of Reverse Osmosis Concentrate. Platform Presentation. **2nd Regional Symposium on Electrochemistry: South-East Europe**. June, 2010. Belgrade, Serbia.

# GLOSSARY

| | |
|---|---|
| ACTP | Acetaminophen |
| AEM | Anion Exchange Membrane |
| AOP | Advanced Oxidation Process |
| AOCl | Adsorbable Organic Chlorine |
| AOBr | Adsorbable Organic Bromine |
| AOI | Adsorbable Organic Iodine |
| AOX | Adsorbable Organic Halogen |
| ARC | Australian Research Council |
| ATZ | Atrazine |
| AWMC | Advanced Water Management Centre |
| AWTP | Advanced Water Treatment Plants |
| BAC | Biological Activated Carbon |
| BDCM | Bromodichloromethane |
| BDD | Boron Doped Diamond |
| BCAA | Bromochloroacetic Acid |
| CAFF | Caffeine |
| CBZ | Carbamazepine |
| CE | Coulombic (Current) Efficiency |
| CEM | Cation Exchange Membrane |
| CID | Collision Induced Dissociation |
| COD | Chemical Oxygen Demand |
| DBAA | Dibromoacetic Acid |
| DBCM | Dibromochloromethane |
| DBP | Disinfection By-Products |
| DCAA | Dichloroacetic Acid |
| DCF | Diclofenac |
| DEET | N,N-Diethyl-meta-toluamide |
| DIU | Diuron |
| DOC | Dissolved Organic Carbon |
| DON | Dissolved Organic Nitrogen |
| DPD | N-N-diethyl-p-phenylenediamine |
| DSA | Dimensionally Stable Anode |
| DZN | Diazinon |
| EEM | Excitation Emission Matrix |
| ED | Electrodialysis |
| EDC | Endocrine Disrupting Compound |
| ENR | Enrofloxacin |
| EPA | Environmental Protection Agency |
| FAC | Free Available Chlorine |
| GAC | Granular Activated Carbon |
| GC-ECD | Gas Chromatography-Electron Capture Detection |
| GC-MS | Gas Chromatography-Mass Spectrometry |
| GMF | Gemfibrozil |
| HA | Haloacetaldehyde |
| HAA | Haloacetic Acid |
| HAN | Haloacetonitrile |
| HCT | Hydrochlorothiazide |
| HER | Hydrogen Evolution Reaction |
| HPLC | High Performance Liquid Chromatography |
| HRT | Hydraulic Retention Time |
| IBU | Ibuprofen |
| ICE | Instantaneous Current Efficiency |
| ICP-OES | Inductively Coupled Plasma-Optical Emission Spectroscopy |
| LC-MS | Liquid Chromatography-Mass Spectrometry |
| LNC | Lincomycin |
| MBAA | Monobromoacetic Acid |
| MBBR | Moving Bed Biofilm Reactor |
| MCAA | Monochloroacetic Acid |
| MET | Metolachlor |
| MF | Micro Filtration |
| MIEX | Magnetic Ion Exchange |
| MMO | Mixed Metal Oxide |
| MTP | Metoprolol |
| MW | Molecular Weight |
| NDMA | N-nitrosodimethylamine |
| NF | Nanofiltration |
| NFL | Norfloxacin |
| NHE | Normal Hydrogen Electrode |
| NOM | Natural Organic Matter |
| NPOC | Non-Purgeable Organic Carbon |
| OER | Oxygen Evolution Reaction |
| PAC | Powdered Activated Carbon |
| PNT | Phenytoin |
| QHFSS | Queensland Health Forensic and Scientific Services |
| QqLIT-MS | Triple Quadrupole Linear Ion Trap-Mass Spectrometer |
| QSAR | Quantitative Structure Activity Relationship |
| RDE | Rotating Disk Electrode |
| REF | Relative Enrichment Factor |
| RHS | Reactive Halogen Species |
| RNT | Ranitidine |
| RO | Reverse Osmosis |
| ROC | Reverse Osmosis Concentrate |
| ROS | Reactive Oxygen Species |
| ROX | Roxythromycin |
| SDZ | Sulfadiazine |
| SEQ | South East Queensland |
| SHE | Standard Hydrogen Electrode |
| SMP | Soluble Microbial Product |
| SPE | Solid Phase Extraction |
| SRL | Sertraline |
| SUVA | Specific Ultraviolet Absorbance |
| TAN | Total Ammonia Nitrogen |
| TBM | Tribromomethane |
| TCAA | Trichloroacetic Acid |
| TCM | Trichloromethane |
| TDS | Total Dissolved Solids |
| TEA | Triethanolamine |
| TEQ | Toxicity Equivalent Concentration |
| tHAAs | total HAAs |
| THM | Trihalomethane |
| TKN | Total Kjeldahl Nitrogen |
| TML | Tramadol |
| TMP | Trimethoprim |
| TOC | Total Organic Carbon |
| tTHMs | total THMs |
| UF | Ultrafiltration |
| UFLC | Ultra Fast Liquid Chromatography |
| UQ | The University of Queensland |
| UVA | Ultraviolet Absorbance |
| UWSRA | Urban Water Security Research Alliance |
| VNF | Venlafaxine |
| WCRWP | Western Corridor Recycled Water Project |
| WWTP | Wastewater Treatment Plant |
| ZLD | Zero Liquid Discharge |

# REFERENCES


1. Le-Minh, N.; Khan, S. J.; Drewes, J. E.; Stuetz, R. M., Fate of antibiotics during municipal water recycling treatment processes. *Water Research* **2010,** *44*, (15), 4295-4323.
2. Köck-Schulmeyer, M.; Ginebreda, A.; Postigo, C.; López-Serna, R.; Pérez, S.; Brix, R.; Llorca, M.; Alda, M. L. D.; Petrović, M.; Munné, A.; Tirapu, L.; Barceló, D., Wastewater reuse in Mediterranean semi-arid areas: The impact of discharges of tertiary treated sewage on the load of polar micro pollutants in the Llobregat river (NE Spain). *Chemosphere* **2011,** *82*, (5), 670-678.
3. Dialynas, E.; Mantzavinos, D.; Diamadopoulos, E., Advanced treatment of the reverse osmosis concentrate produced during reclamation of municipal wastewater. *Water Research* **2008,** *42*, (18), 4603-4608.
4. Lee, L. Y.; Ng, H. Y.; Ong, S. L.; Hu, J. Y.; Tao, G.; Kekre, K.; Viswanath, B.; Lay, W.; Seah, H., Ozone-biological activated carbon as a pretreatment process for reverse osmosis brine treatment and recovery. *Water Research* **2009,** *43*, (16), 3948-3955.
5. Benner, J.; Salhi, E.; Ternes, T.; von Gunten, U., Ozonation of reverse osmosis concentrate: Kinetics and efficiency of beta blocker oxidation. *Water Research* **2008,** *42*, (12), 3003-3012.
6. Anglada, Ã.; Urtiaga, A.; Ortiz, I., Contributions of electrochemical oxidation to waste-water treatment: Fundamentals and review of applications. *Journal of Chemical Technology and Biotechnology* **2009,** *84*, (12), 1747-1755.
7. Cong, Y. Q.; Wu, Z. C.; Tan, T. E., Dechlorination by combined electrochemical reduction and oxidation. *Journal of Zhejiang University: Science* **2005,** *6 B*, (6), 563-568.
8. Malpass, G. R. P.; Miwa, D. W.; Machado, S. A. S.; Olivi, P.; Motheo, A. J., Oxidation of the pesticide atrazine at DSA® electrodes. *Journal of Hazardous Materials* **2006,** *B137*, 565–572.
9. Carlesi Jara, C.; Fino, D.; Specchia, V.; Saracco, G.; Spinelli, P., Electrochemical removal of antibiotics from wastewaters. *Applied Catalysis B: Environmental* **2007,** *70*, (1-4), 479-487.
10. Bejan, D.; Guinea, E.; Bunce, N. J., On the nature of the hydroxyl radicals produced at boron-doped diamond and Ebonex® anodes. *Electrochimica Acta* **2012,** *69*, 275-281.
11. Traves, W. H.; Gardner, E. A.; Dennien, B.; Spiller, D., Towards indirect potable reuse in South East Queensland. *Water Science and Technology* **2008,** *58*, (1), 153-161.
12. Poussade, Y.; Roux, A.; Walker, T.; Zavlanos, V., Advanced oxidation for indirect potable reuse: a practical application in Australia. *Water Science and Technology* **2009,** *60*, (9), 2419-2424.
13. Khan, S. J.; Murchland, D.; Rhodes, M.; Waite, T. D., Management of concentrated waste streams from high-pressure membrane water treatment systems. *Critical Reviews in Environmental Science and Technology* **2009,** *39*, (5), 367-415.
14. Solley, D.; Gronow, C.; Tait, S.; Bates, J.; Buchanan, A., Managing the reverse osmosis concentrate from the Western Corridor Recycled Water Scheme. *Water Practice and Technology* **2010,** *5*, (1).
15. Vargas, C.; Buchanan, A., Monitoring ecotoxicity and nutrients load in the reverse osmosis concentrate from bundamba advanced water treatment plant, Queensland Australia. *Water Practice and Technology* **2011,** *6*, (1).
16. Macova, M.; Escher, B. I.; Mueller, J. F.; Toze, S. *Bioanalytical Tools to Evaluate Micropollutants across the Seven Barriers of the Indirect Potable Reuse Scheme*; 2010.
17. Liu, K.; Roddick, F. A.; Fan, L., Impact of salinity and pH on the UVC/H 2O 2 treatment of reverse osmosis concentrate produced from municipal wastewater reclamation. *Water Research* **2012,** *46*, (10), 3229-3239.
18. Westerhoff, P.; Moon, H.; Minakata, D.; Crittenden, J., Oxidation of organics in retentates from reverse osmosis wastewater reuse facilities. *Water Research* **2009,** *43*, (16), 3992-3998.
19. Pérez-González, A.; Urtiaga, A. M.; Ibáñez, R.; Ortiz, I., State of the art and review on the treatment technologies of water reverse osmosis concentrates. *Water Research* **2012,** *46*, (2), 267-283.
20. Van Hege, K.; Verhaege, M.; Verstraete, W., Indirect electrochemical oxidation of reverse osmosis membrane concentrates at boron-doped diamond electrodes. *Electrochemistry Communications* **2002,** *4*, (4), 296-300.
21. Van Hege, K.; Verhaege, M.; Verstraete, W., Electro-oxidative abatement of low-salinity reverse osmosis membrane concentrates. *Water Research* **2004,** *38*, (6), 1550-1558.
22. Chelme-Ayala, P.; Smith, D. W.; El-Din, M. G., Membrane concentrate management options: a comprehensive critical review. *Canadian Journal of Civil Engineering* **2009,** *36*, 1107-1119.
23. Greenlee, L. F.; Lawler, D. F.; Freeman, B. D.; Marrot, B.; Moulin, P., Reverse osmosis desalination: Water sources, technology and today's challenges. *Water Research* **2009,** *43*, 2317-2348.
24. Van der Bruggen, B.; Lejon, L.; Vandecasteele, C., Reuse, treatment, and discharge of the concentrate of pressure-driven membrane processes. *Environmental Science and Technology* **2003,** *37*, (17), 3733-3738.

25. Khan, S. J.; Murchland, D.; Rhodes, M.; Waite, T. D., Management of concentrated waste streams from high-pressure membrane water treatment systems. *Critical Reviews in Environmental Science and Technology* **2009,** *39*, 367–415.
26. Drewes, J. E.; Bellona, C.; Oedekoven, M.; Xu, P.; Kim, T.-U.; Amy, G., Rejection of Wastewater-Derived Micropollutants in High-Pressure Membrane Applications Leading to Indirect Potable Reuse. *Environmental Progress* **2005,** *24*, 400-409.
27. Goosen, M. F. A.; Sablani, S. S.; Al-Hinai, H.; Al-Obeidani, S.; Al-Belushi, R.; Jackson, D., Fouling of Reverse Osmosis and Ultrafiltration Membranes: A Critical Review. *Separation Science and Technology* **2004,** *39*, (10), 2261-2297.
28. Lopez-Ramirez, J. A.; Sahuquillo, S.; Sales, D.; Quiroga, J. M., Pre-treatment optimisation studies for secondaryeffluent reclamation with reverse osmosis. *Water Research* **2003,** *37*, 1177-1184.
29. Qin, J. J.; Wai, M. N.; Oo, M. H.; Kekre, K. A.; Seah, H., Impact of anti-scalant on fouling of reverse osmosis membranes in reclamation of secondary effluent. *Water Science and Technology* **2009,** *60*, (11), 2767-2774.
30. Bagastyo, A. Y.; Keller, J.; Poussade, Y.; Batstone, D. J., Characterisation and removal of recalcitrants in reverse osmosis concentrates from water reclamation plants. *Water Research* **2011,** *45*, (7), 2415-2427.
31. Radjenovic, J.; Petrovic, M.; Ventura, F.; Barcelo, D., Rejection of pharmaceuticals in nanofiltration and reverse osmosis membrane drinking water treatment. *Water Research* **2008,** *42*, (14), 3601-3610.
32. Snyder, S. A.; Adham, S.; Redding, A. M.; Cannon, F. S.; DeCarolis, J.; Oppenheimer, J.; Wert, E. C.; Yoon, Y., Role of membranes and activated carbon in the removal of endocrine disruptors and pharmaceuticals. *Desalination* **2007,** *202*, (1-3), 156-181.
33. Plakas, K. V.; Karabelas, A. J., Removal of pesticides from water by NF and RO membranes - A review. *Desalination* **2012,** *287*, 255-265.
34. Squire, D., Reverse osmosis concentrate disposal in the UK. *Desalination* **2000,** *132*, 47-54.
35. Shon, H. K.; Vigneswaran, S.; Snyder, S. A., Effluent organic matter (EfOM) in wastewater: Constituents, effects, and treatment. *Critical Reviews in Environmental Science and Technology* **2006,** *36*, (4), 327-374.
36. Escher, B. I.; Lawrence, M.; Macova, M.; Mueller, J. F.; Poussade, Y.; Robillot, C.; Roux, A.; Gernjak, W., Evaluation of Contaminant Removal of Reverse Osmosis and Advanced Oxidation in Full-Scale Operation by Combining Passive Sampling with Chemical Analysis and Bioanalytical Tools. *Environmental Science and Technology* **2011,** *45*, (12), 5387-5394.
37. Arnal, J. M.; Sancho, M.; Iborra, I.; Gozalvez, J. M.; Santafe, A.; Lora, J., Concentration of brines from RO desalination plants by natural evaporation. *Desalination* **2005,** *182*, 435-439.
38. Ahmed, M.; Shayya, W. H.; Hoey, D.; Al-Handaly, J., Brine disposal from reverse osmosis desalination plants in Oman and the United Arab Emirates. *Desalination* **2001,** *133*, (2), 135-147.
39. Miri, R.; Chouikhi, A., Ecotoxicological marine impacts from seawater desalination plants. *Desalination* **2005,** *182*, 403–410.
40. Mohammadesmaeili, F.; Badr, M. K.; Abbaszadegan, M.; Fox, P., Mineral recovery from inland reverse osmosis concentrate using isothermal evaporation. *Water Research* **2010,** *44*, 6021-6030.
41. Perez-Gonzalez, A.; Urtiaga, A. M.; Ibanez, R.; Ortiz, I., State of the art and review on the treatment technologies of water reverse osmosis concentrates. *Water Research* **2011,** *46*, (2), 267-283.
42. Ji, X.; Curcio, E.; Obaidani, S. A.; Profio, G. D.; Fontananova, E.; Drioli, E., Membrane distillation-crystallization of seawater reverse osmosis brines. *Separation and Purification Technology* **2010,** *71*, 76-82.
43. Kumar, M.; Badruzzaman, M.; Adham, S.; Oppenheimer, J., Beneficial phosphate recovery from reverse osmosis (RO) concentrate of an integrated membrane system using polymeric ligand exchanger (PLE). *Water Research* **2007,** *411*, 2211-2219.
44. Zhang, Y.; Van Der Bruggen, B.; Pinoy, L.; Meesschaert, B., Separation of nutrient ions and organic compounds from salts in RO concentrates by standard and monovalent selective ion-exchange membranes used in electrodialysis. *Journal of Membrane Science* **2009,** *332*, 104–112.
45. Zhang, Y.; Ghyselbrecht, K.; Meesschaert, B.; Pinoy, L.; Van der Bruggen, B., Electrodialysis on RO concentrate to improve water recovery in wastewater reclamation. *Journal of Membrane Science* **2011,** *378*, 101– 110.
46. Korngold, E.; Aronov, L.; Daltrophe, N., Electrodialysis of brine solutions discharged from an RO plant. *Desalination* **2009,** *242*, 215-227.
47. Badruzzaman, M.; Oppenheimer, J.; Adham, S.; Kumar, M., Innovative beneficial reuse of reverse osmosis concentrate using bipolar membrane electrodialysis and eletrochlorination processes. *Journal of Membrane Science* **2009,** *326*, 392-399.
48. Zhao, C.; Gu, P.; Cui, H.; Zhang, G., Reverse osmosis concentrate treatment via a PAC-MF accumulative countercurrent adsorption process. *Water Research* **2012,** *46*, 218-226.
49. Zhou, T.; Lim, T.-T.; Chin, S.-S.; Fane, A. G., Treatment of organics in reverse osmosis concentrate from a municipal wastewater reclamation plant: Feasibility test of advanced oxidation processes with/without pretreatment. *Chemical Engineering Journal* **2011,** *166*, 932-939.

50. Alexander, J. T.; Hai, F. I.; Al-aboud, T. M., Chemical coagulation-based processes for trace organic contaminant removal: Current state and future potential. *Journal of Environmental Management* **2012,** *111*, (0), 195-207.
51. Drikas, M.; Chow, C. W. K.; Cook, D., The impact of recalcitrant organic character on disinfection stability, trihalomethane formation and bacterial regrowth: An evaluation of magnetic ion exchange resin (MIEX) and alum coagulation. *Journal of Water Supply: Research and Technology-AQUA* **2003,** *52*, (7), 475-487.
52. Fearing, D. A.; Banks, J.; Guyetand, S.; Eroles, C. M.; Jefferson, B.; WIlson, D.; Hillis, P.; Campbell, A. T.; Parsons, S. A., Combination of ferric and MIEX for the treatment of a humic rich water *Water Research* **2004,** *38*, 2551-2558.
53. Mergen, M. R. D.; Jefferson, B.; Parsons, S. A.; Jarvis, P., Magnetic ion-exchange resin treatment: Impact of water type and resin use. *Water Research* **2008,** *42*, 1977-1988.
54. Warton, B.; Heitz, A.; Zappia, L. R.; Franzmann, P. D.; Masters, D.; Joll, C. A.; Alessandrino, M.; Allpike, B.; O'Leary, B.; Kagi, R. I., Magnetic ion exchange drinking water treatment in a large-scale facility. *American Water Works Association Journal* **2007,** *99*, (1), 89-94.
55. Boyer, T. H.; Graf, K. C.; Comstock, S. E. H.; Townsend, T. G., Magnetic ion exchange treatment of stabilized landfill leachate. *Chemosphere* **2011,** *83*, 1220-1227.
56. Ng, H. Y.; Lee, L. Y.; Ong, S. L.; Tao, G.; Viawanath, B.; Kekre, K.; Lay, W.; Seah, H., Treatment of RO brine-towards sustainable water reclamation practice. *Water science and technology* **2008,** *58*, (4), 931-936.
57. Lee, L. Y.; Ng, H. Y.; Ong, S. L.; Hu, J. Y.; Tao, G.; Kekre, K.; Viswanath, B.; Lay, W.; Seah, H., Ozone-biological activated carbon as a pretreatment process for reverse osmosis brine treatment and recovery. *Water research* **2009,** *43*, 3948-3955.
58. Liu, K.; Roddick, F. A.; Fan, L., Impact of salinity and pH on the UVC/$H_2O_2$ treatment of reverse osmosis concentrate produced from municipal wastewater reclamation. *Water Research* **2012,** *46*, (10), 3229-3239.
59. Westerhoff, P.; Mash, H., Dissolved organic nitrogen in drinking water supplies: a review. *Journal of Water Supply: Research and Technology* **2002,** *51*, (8), 415-448.
60. Panizza, M., Importance of electrode material in the electrochemical treatment of wastewater containing organic pollutants. In *Electrochemistry for the Environment*, Comninellis, C.; Chen, G., Eds. Springer Science+Business Media: 2010.
61. Kapalka, A.; Foti, G.; Comninellis, C., Basic principles of the electrochemical mineralization of organic pollutants for wastewater treatment. In *Electrochemistry for the environment*, Comninellis, C.; Chen, G., Eds. Springer Science+Business Media: 2010.
62. Parsons, S., *Advanced Oxidation Processes for Water and Wastewater Treatment*. IWA Publishing: 2004.
63. Chen, G., Electrochemical technologies in wastewater treatment. *Separation and Purification Technology* **2004,** *38*, 11-41.
64. Konstantinov, A.; Bejan, D.; Bunce, N. J.; Chittim, B.; McCrindle, R.; Potter, D.; Tashiro, C., Electrolytic debromination of PBDEs in DE-83TM technical decabromodiphenyl ether. *Chemosphere* **2008,** *72*, (8), 1159-1162.
65. Zwiener, C.; Glauner, T.; Sturm, J.; Wörner, M.; Frimmel, F., Electrochemical reduction of the iodinated contrast medium iomeprol: iodine mass balance and identification of transformation products. *Analytical and Bioanalytical Chemistry* **2009,** *395*, (6), 1885-1892.
66. Zhu, K.; Baig, S. A.; Xu, J.; Sheng, T.; Xu, X., Electrochemical reductive dechlorination of 2,4-dichlorophenoxyacetic acid using a palladium/nickel foam electrode. *Electrochimica Acta* **2012,** *69*, (0), 389-396.
67. Meenakshisundaram, D. *Electrochemical Reduction of Nitro-aromatic Compouncs: Product Studies and Mathematical Modeling*; 1999; 69.
68. Rondinini, S.; Vertova, A., Electroreduction of Halogenated Organic Compounds Electrochemistry for the Environment. In Comninellis, C.; Chen, G., Eds. Springer New York: 2010; 279-306.
69. Comninellis, C.; Chen, G., *Electrochemistry for the Environment*. Springer: 2010.
70. Comninellis, C., Electrocatalysis in the electrochemical conversion/combustion of organic pollutants for waste water treatment. *Electrochimica Acta* **1994,** *39*, (11-12), 1857-1862.
71. Panizza, M.; Cerisola, G., Application of diamond electrodes to electrochemical processes. *Electrochimica Acta* **2005,** *51*, (2), 191-199.
72. Lawrence K. Wang; Hung, Y.-T.; Shammas, N. K., *Advanced physicochemical treatment technologies*. Springer: 2007.
73. Panizza, M.; Bocca, C.; Cerisola, G., Electrochemical treatment of wastewater containing polyaromatic organic pollutants. *Water Research* **2000,** *34*, (9), 2601-2605.
74. Silverstein, R. M. C.; Bassler, G. C.; Morrill, T. C., *Spectrophotometric identification of organic compounds*. John Wiley and Sons: New York, 1991.

75. Chaplin, B. P.; Schrader, G.; Farrell, J., Electrochemical destruction of N -Nitrosodimethylamine in reverse osmosis concentrates using boron-doped diamond film electrodes. *Environmental Science and Technology* **2010,** *44*, (11), 4264-4269.
76. Zhou, M.; Liu, L.; Jiao, Y.; Wang, Q.; Tan, Q., Treatment of high-salinity reverse osmosis concentrate by electrochemical oxidation on BDD and DSA electrodes. *Desalination* **2011,** *277*, (1-3), 201-206.
77. Perez, G.; Fernandez-Alba, A. R.; Urtiaga, A. M.; Ortiz, I., Electro-oxidation of reverse osmosis concentrates generated in tertiary water treatment. *Water Research* **2010,** *44*, (9), 2763-2772.
78. Bergmann, M. E.; Rollin, J.; Iourtchouk, T., The occurrence of perchlorate during drinking water electrolysis using BDD anodes. *Electrochimica Acta* **2009,** *54*, 2102-2107.
79. Bergmann, M. E. H.; Iourtchouk, T.; Rollin, J., The occurrence of bromate and perbromate on BDD anodes during electrolysis of aqueous systems containing bromide: First systematic experimental studies. *Journal of Applied Electrochemistry* **2011,** *41*, (9), 1109-1123.
80. Radjenovic, J.; Keller, J., Electrochemical treatment of reverse osmosis concentrates. In *Encyclopedia of Applied Electrochemistry*, Savinell, R. F.; Ota, K.-i.; Kreysa, G., Eds. Springer: 2012.
81. Chaplin, B. P.; Schrader, G.; Farrell, J., Electrochemical Destruction of *N*-Nitrosodimethylamine in Reverse Osmosis Concentrates using Boron-doped Diamond Film Electrodes. *Environmental Science and Technology* **2010,** *44*, 4264–4269.
82. Szpyrkowicz, L.; Kaul, S. N.; Neti, R. N.; Satyanarayan, S., Influence of anode material on electrochemical oxidation for the treatment of tannery wastewater. *Water Research* **2005,** *39*, 1601-1613.
83. APHA, *Standard Methods for the Examination of Water and Wastewater, twentieth ed.* American Water Works Association (AWWA): Washington, DC, 1998.
84. Kristiana, I.; Gallard, H.; Joll, C.; Croue, J.-P., The formation of halogen-specific TOX from chlorination and chloramination of natural organic matter isolates. *Water research* **2009,** *43*, 4177-4186.
85. Escher, B. I.; Bramaz, N.; Mueller, J. F.; Quayle, P.; Rutishauser, S.; Vermeirssen, E. L. M., Toxic equivalent concentrations (TEQs) for baseline toxicity and specific modes of action as a tool to improve interpretation of ecotoxicity testing of environmental samples. *Journal Environmental Monitoring* **2008,** *10*, 612-621.
86. Chen, W.; Westerhoff, P.; Leenheer, J. A.; Booksh, K., Fluorescence excitation-emission matrix regional integration to quantify spectra for dissolved organic matter. *Environmental Science and Technology* **2003,** *37*, 5701-5710.
87. Baker, A.; Ward, D.; Lieten, S. H.; Periera, R.; Simpson, E. C.; Slater, M., Measurement of protein-like fluorescence in river and wastewater using a handled spectrophotometer. *Water Research* **2004,** *38*, 2934-2938.
88. Panizza, M.; Cerisola, G., Direct and mediated anodic oxidation of organic pollutants. *Chemical Reviews* **2009,** *109*, (12), 6541-6569.
89. Roccaro, P.; Vagliasindi, F. G. A.; Korshin, G. V., Changes in NOM fluorescence caused by chlorination and their associations with disinfection by-products formation. *Environmental science and technology* **2009,** *43*, (3), 724-729.
90. Gallard, H.; Pellizzari, F.; Croué, J. P.; Legube, B., Rate constants of reactions of bromine with phenols in aqueous solution *Water research* **2003,** *37*, (12), 2883-2892.
91. Lei, Y.; Shen, Z.; Huang, R.; Wang, W., Treatment of landfill leachate by combined aged-refuse bioreactor and electro-oxidation *Water research* **2007,** *41*, (11), 2417-2426.
92. Nurmi, J. T.; Tratnyek, P. G., Electrochemical Properties of Natural Organic Matter (NOM), Fractions of NOM, and Model Biogeochemical Electron Shuttles. *Environmental Science and Technology* **2002,** *36*, (4), 617-624.
93. Pillai, K. C.; Kwon, T. O.; Park, B. B.; Moon, I. S., Studies on process parameters for chlorine dioxide production using IrO2 anode in an un-divided electrochemical cell. *Journal of Hazardous Materials* **2009,** *164*, (2-3), 812-819.
94. Bergmann, M. E. H.; Koparal, A. S., Studies on electrochemical disinfectant production using anodes containing RuO<sub>2</sub>. *Journal of Applied Electrochemistry* **2005,** *35*, (12), 1321-1329.
95. Bedner, M.; MacCrehan, W. A., Transformation of acetaminophen by chlorination produces the toxicants 1,4-benzoquinone and N-acetyl-p-benzoquinone imine. *Environmental Science and Technology* **2006,** *40*, (2), 516-522.
96. Westerhoff, P.; Yoon, Y.; Snyder, S.; Wert, E., Fate of endocrine-disruptor, pharmaceutical, and personal care product chemicals during simulated drinking water treatment processes. *Environmental Science and Technology* **2005,** *39*, (17), 6649-6663.
97. Acero, J. L.; Benitez, F. J.; Real, F. J.; Gonzalez, M., Chlorination of organophosphorus pesticides in natural waters. *Journal of Hazardous Materials* **2008,** *153*, (1-2), 320-328.
98. Dodd, M. C.; Shah, A. D.; Von Gunten, U.; Huang, C. H., Interactions of fluoroquinolone antibacterial agents with aqueous chlorine: Reaction kinetics, mechanisms, and transformation pathways. *Environmental Science and Technology* **2005,** *39*, (18), 7065-7076.

99. Bedner, M.; MacCrehan, W. A., Reactions of the amine-containing drugs fluoxetine and metoprolol during chlorination and dechlorination processes used in wastewater treatment. *Chemosphere* **2006,** *65*, (11), 2130-2137.
100. Chen, W. H.; Young, T. M., NDMA formation during chlorination and chloramination of aqueous diuron solutions. *Environmental Science and Technology* **2008,** *42*, (4), 1072-1077.
101. Chamberlain, E.; Adams, C., Oxidation of sulfonamides, macrolides, and carbadox with free chlorine and monochloramine. *Water Research* **2006,** *40*, (13), 2517-2526.
102. Gould, J. P.; Richards, J. T., The kinetics and products of the chlorination of caffeine in aqueous solution. *Water Research* **1984,** *18*, (8), 1001-1009.
103. Huber, M. M.; Korhonen, S.; Ternes, T. A.; Von Gunten, U., Oxidation of pharmaceuticals during water treatment with chlorine dioxide. *Water Research* **2005,** *39*, (15), 3607-3617.
104. Panizza, M.; Barbucci, A.; Ricotti, R.; Cerisola, G., Electrochemical degradation of methylene blue. *Separation and Purification Technology* **2007,** *54*, (3), 382-387.
105. Malpass, G. R. P.; Miwa, D. W.; Machado, S. A. S.; Olivi, P.; Motheo, A. J., Oxidation of the pesticide atrazine at DSA® electrodes. *Journal of Hazardous Materials* **2006,** *137*, (1), 565-572.
106. Bonfatti, F.; Ferro, S.; Lavezzo, F.; Malacarne, M.; Lodi, G.; De Battisti, A., Electrochemical incineration of glucose as a model organic substrate II. Role of active chlorine mediation. *Journal of the Electrochemical Society* **2000,** *147*, (2), 592-596.
107. Panizza, M.; Cerisola, G., Electrochemical oxidation of 2-naphthol with in situ electrogenerated active chlorine. *Electrochimica Acta* **2003,** *48*, (11), 1515-1519.
108. Martínez-Huitle, C. A.; Brillas, E., Decontamination of wastewaters containing synthetic organic dyes by electrochemical methods: A general review. *Applied Catalysis B: Environmental* **2009,** *87*, (3-4), 105-145.
109. Comninellis, C.; Nerini, A., Anodic oxidation of phenol in the presence of NaCl for wastewater treatment. *Journal of Applied Electrochemistry* **1995,** *25*, (1), 23-28.
110. Gallard, H.; Leclercq, A.; Croué, J.-P., Chlorination of bisphenol A: kinetics and by-products formation. *Chemosphere* **2004,** *56*, (5), 465-473.
111. Kim, S.; Choi, S. K.; Yoon, B. Y.; Lim, S. K.; Park, H., Effects of electrolyte on the electrocatalytic activities of RuO2/Ti and Sb-SnO2/Ti anodes for water treatment. *Applied Catalysis B: Environmental* **2010,** *97*, (1-2), 135-141.
112. Wu, M.; Zhao, G.; Li, M.; Liu, L.; Li, D., Applicability of boron-doped diamond electrode to the degradation of chloride-mediated and chloride-free wastewaters. *Journal of Hazardous Materials* **2009,** *163*, (1), 26-31.
113. Radjenovic, J.; Escher, B. I.; Rabaey, K., Electrochemical degradation of the β-blocker metoprolol by Ti/Ru0.7Ir0.3O2 and Ti/SnO2-Sb electrodes. *Water Research* **2011,** *45*, (10), 3205-3214.
114. Radjenovic, J.; Bagastyo, A.; Rozendal, R. A.; Mu, Y.; Keller, J.; Rabaey, K., Electrochemical oxidation of trace organic contaminants in reverse osmosis concentrate using RuO2/IrO2-coated titanium anodes. *Water Research* **2011,** *45*, (4), 1579-1586.
115. Bagastyo, A. Y.; Radjenovic, J.; Mu, Y.; Rozendal, R. A.; Batstone, D. J.; Rabaey, K., Electrochemical oxidation of reverse osmosis concentrate on mixed metal oxide (MMO) titanium coated electrodes. *Water Research* **2011,** *45*, (16), 4951-4959.
116. Anglada, Á.; Urtiaga, A.; Ortiz, I.; Mantzavinos, D.; Diamadopoulos, E., Boron-doped diamond anodic treatment of landfill leachate: Evaluation of operating variables and formation of oxidation by-products. *Water Research* **2011,** *45*, (2), 828-838.
117. Hernando, M. D.; Gomez, M. J.; Aguera, A.; Fernandez-Alba, A. R., LC-MS analysis of basic pharmaceuticals (beta-blockers and anti-ulcer agents) in wastewater and surface water. *TrAC - Trends in Analytical Chemistry* **2007,** *26*, (6), 581-594.
118. Slegers, C.; Maquille, A.; Deridder, V.; Sonveaux, E.; Habib Jiwan, J. L.; Tilquin, B., LC-MS analysis in the e-beam and gamma radiolysis of metoprolol tartrate in aqueous solution: Structure elucidation and formation mechanism of radiolytic products. *Radiation Physics and Chemistry* **2006,** *75*, (9), 977-989.
119. Song, W.; Cooper, W. J.; Mezyk, S. P.; Greaves, J.; Peake, B. M., Free radical destruction of Î²-blockers in aqueous solution. *Environmental Science and Technology* **2008,** *42*, (4), 1256-1261.
120. Benner, J.; Ternes, T. A., Ozonation of metoprolol: Elucidation of oxidation pathways and major oxidation products. *Environmental Science and Technology* **2009,** *43*, (14), 5472-5480.
121. Grebel, J. E.; Pignatello, J. J.; Mitch, W. A., Effect of Halide Ions and Carbonates on Organic Contaminant Degradation by Hydroxyl Radical-Based Advanced Oxidation Processes in Saline Waters. *Environmental Science and Technology* **2010,** *44*, (17), 6822-6828.
122. Gallard, H.; Pellizzari, F.; Croue, J. P.; Legube, B., Rate constants of reactions of bromine with phenols in aqueous solution. *Water Research* **2003,** *37*, (12), 2883-2892.
123. Krasner, S. W.; Weinberg, H. S.; Richardson, S. D.; Pastor, S. J.; Chinn, R.; Sclimenti, M. J.; Onstad, G. D.; Thruston Jr, A. D., Occurrence of a new generation of disinfection byproducts. *Environmental Science and Technology* **2006,** *40*, (23), 7175-7185.

124. Deborde, M.; von Gunten, U., Reactions of chlorine with inorganic and organic compounds during water treatment-Kinetics and mechanisms: A critical review. *Water Research* **2008,** *42*, (1-2), 13-51.
125. Martínez-Huitle, C. A.; Ferro, S.; De Battisti, A., Electrochemical incineration in the presence of halides. *Electrochemical and Solid-State Letters* **2005,** *8*, (11), D35-D39.
126. Li, X. Y.; Cui, Y. H.; Feng, Y. J.; Xie, Z. M.; Gu, J. D., Reaction pathways and mechanisms of the electrochemical degradation of phenol on different electrodes. *Water Research* **2005,** *39*, (10), 1972-1981.
127. Panizza, M.; Sires, I.; Cerisola, G., Anodic oxidation of mecoprop herbicide at lead dioxide. *Journal of Applied Electrochemistry* **2008,** *38*, (7), 923-929.
128. Durante, C.; Isse, A. A.; Sandona, G.; Gennaro, A., Electrochemical hydrodehalogenation of polychloromethanes at silver and carbon electrodes. *Applied Catalysis B: Environmental* **2009,** *88*, 479–489.
129. Zou, L.; Morris, G.; Qi, D., Using activated carbon electrode in electrosorptive deionisation of brackish water. *Desalination* **2008,** *225*, 329-340.
130. Ramalho, A. M. Z.; Martínez-Huitle, C. A.; Silva, D. R. d., Application of electrochemical technology for removing petroleum hydrocarbons from produced water using a DSA-type anode at different flow rates. *Fuel* **2010,** *89*, (2), 531-534.
131. Boudreau, J.; Bejan, D.; Li, S.; Bunce, N. J., Competition between electrochemical advanced oxidation and electrochemical hypochlorination of sulfamethoxazole at a boron-doped diamond anode. *Industrial and Engineering Chemistry Research* **2010,** *49*, (6), 2537-2542.
132. Scialdone, O.; Randazzo, S.; Galia, A.; Silvestri, G., Electrochemical oxidation of organics in water: Role of operative parameters in the absence and in the presence of NaCl. *Water Research* **2009,** *43*, (8), 2260-2272.
133. Deborde, M.; Von Gunten, U., Reactions of chlorine with inorganic and organic compounds during water treatment - Kinetics and mechanisms: A critical review *Water Research* **2008,** *42*, 13-51.
134. De Laat, J.; Le, G. T.; Legube, B., A comparative study of the effects of chloride, sulfate, and nitrate ions on the rates of decomposition of $H_2O_2$ and organic compounds by Fe(II)/$H_2O_2$ and Fe(III)$H_2O_2$. *Chemosphere* **2004,** *55*, 715-723.
135. Zhu, X.; Tong, M.; Shi, S.; Zhao, H.; Ni, J., Essential Explanation of the Strong Mineralization Performance of Boron-Doped Diamond Electrodes. *Environmental science and technology* **2008,** *42*, 4914–4920.
136. Gallard, H. e.; Pellizzari, F.; Croue, J. P.; Legube, B., Rate constants of reactions of bromine with phenols in aqueous solution. *Water Research* **2003,** *37*, (12), 2883-2892.
137. Chen, B., Hydrolytic Stabilities of Halogenated Disinfection Byproducts: Review and Rate Constant Quantitative Structure–Property Relationship Analysis. *Environmental Engineering Science* **2011,** *28*, (6), 385-394.
138. Tang, W. Z.; Tassos, S., Oxidation kinetics and mechanisms of trihalomethanes by fenton's reagent *Water Research* **1997,** *31*, (5), 1117-1125.
139. Scialdone, O.; Randazzo, S.; Galia, A.; Silvestri, G., Electrochemical oxidation of organics in water: role of operative parameters in the absence and in the presence of NaCl. *Water Research* **2009,** *43*, 2260-2272.
140. Murugananthan, M.; Yoshihara, S.; Rakuma, T.; Shirakashi, T., Mineralization of bisphenol A (BPA) by anodic oxidation with boron-doped diamond (BDD) electrode. *Journal of Hazardous Materials* **2008,** *154*, 213-220.
141. Khamis, D.; Mahe, E.; Dardoize, F.; Devilliers, D., Peroxodisulfate generation on boron-doped diamond microelectrodes array and detection by scanning electrochemical microscopy. *Journal of Applied Electrochemistry* **2010,** *40*, 1829–1838.
142. Murugananthan, M.; Latha, S. S.; Bhaskar Raju, G.; Yoshihara, S., Role of electrolyte on anodic mineralization of atenolol at boron doped diamond and Pt electrodes. *Separation and Purification Technology* **2011,** *79*, 56-62.
143. Ozcan, A.; Sahin, Y.; Koparal, A. S.; Oturan, M. A., Propham mineralization in aqueous medium by anodic oxidation using boron-doped diamond anode: Influence of experimental parameters on degradation kinetics and mineralization efficiency. *Water Research* **2008,** *42*, 2889-2898.
144. Ferro, S.; Battisti, A. D.; Duo, I.; Comninellis, C.; W. Haenni; Perret, A., Chlorine Evolution at Highly Boron-Doped Diamond Electrodes. *Journal of The Electrochemical Society* **2000,** *147*, (7), 2614-2619.
145. Park, H.; Vecitis, C. D.; Hoffmann, M. R., Electrochemical Water Splitting Coupled with Organic Compound Oxidation: The Role of Active Chlorine Species. *Journal of Physical Chemistry C* **2009,** *113*, 7935–7945.
146. Provent, C.; Haenni, W.; Santoli, E.; Rychen, P., Boron-doped diamond electrodes and microelectrode-arrays for the measurement of sulfate and peroxodisulfate. *Electrochimica Acta* **2004,** *49*, 3737–3744.
147. Gros, M.; Petrović, M.; Barceló, D., Tracing pharmaceutical residues of different therapeutic classes in environmental waters by using liquid chromatography/quadrupole-linear ion trap mass spectrometry and automated library searching. *Analytical Chemistry* **2009,** *81*, (3), 898-912.